ORIGIN AND SIGNIFICANCE OF A QUARTZ-TOURMALINE BRECCIA ZONE WITHIN THE CENTRAL ANATOLIAN CRYSTALLINE COMPLEX, TURKEY

A THESIS SUBMITTED TO
THE GRADUATE SCHOOL OF NATURAL AND APPLIED SCIENCES
OF
MIDDLE EAST TECHNICAL UNIVERSITY

BY

SERHAT DEMİREL

IN PARTIAL FULFILLMENT OF THE REQUIREMENTS
FOR
THE DEGREE OF MASTER OF SCIENCE
IN
GEOLOGICAL ENGINEERING

SEPTEMBER 2004

Approval of the Graduate School of Natural and Applied Sciences.

Prof.Dr. Canan Özgen
Director

I certify that this thesis satisfies all the requirements as a thesis for the degree of Master of Science.

Prof.Dr. Asuman G. Türkmenoğlu
Head of Department

This is to certify that we have read this thesis and that in our opinion it is fully adequate, in scope and quality, as a thesis for the degree of Master of Science.

Prof.Dr. M. Cemal Göncüoğlu
Supervisor

Examining Committee Members

Prof.Dr. Asuman G. Türkmenoğlu	(METU, GEOE)	
Prof.Dr. M. Cemal Göncüoğlu	(METU, GEOE)	
Assoc.Prof.Dr. A.Taylan Lünel	(METU, GEOE)	
Assoc.Prof.Dr. Kadir Dirik	(HU, GEOE)	
Dr. Steven Mittwede	(Müteferrika Ltd. Şti)	

I hereby declare that all information in this document has been obtained and presented in accordance with academic rules and ethical conduct. I also declare that, as required by these rules and conduct, I have fully cited and referenced all material and results that are not original to this work.

Name, Last name : Serhat Demirel

Signature :

ABSTRACT

ORIGIN AND SIGNIFICANCE OF A QUARTZ-TOURMALINE BRECCIA ZONE WITHIN THE CENTRAL ANATOLIAN CRYSTALLINE COMPLEX, TURKEY

DEMİREL, Serhat

M.Sc., Department of Geological Engineering

Supervisor: Prof.Dr. M. Cemal Göncüoğlu

September 2004, 111 pages

The aim of this study is to investigate the petrography, geochemistry and evolution of quartz-tourmaline-rich rocks occurring in a wide breccia zone within the Late Cretaceous Kerkenez Granitoid (Central Anatolian Crystalline Complex (CACC), Turkey). The approximately 40-m wide main breccia zone has a NE-SW trend and is characterized by intense cataclastic deformation. The breccia zone can be traced several kilometers towards the west and generally occurs as tourmaline-filled faults and 1mm-30cm-thick veins within the granitoid.

On the basis of mineralogical and textural features, rocks within this zone are defined as tourmaline veins, tourmaline-breccias and quartz-tourmaline rocks. These rocks are generally composed of quartz, tourmaline and granitic fragments. Petrographical investigations and electron-microprobe analyses indicate that, there are three optically and chemically different tourmaline generations. From oldest to youngest, the tourmalines are classified as blue pleochroic feruvites, blue-green pleochroic schorls and green-light green pleochroic schorls. The chemistry of the tourmalines suggests that these tourmalines crystallized from boron rich fluids derived from an evolving magma.

Consequently, the quartz tourmaline-breccia zone is considered to have formed by the injection of overpressured boron rich fluids into faults and fractures

present within the Kerkenez Granitoid. Fluid-filled faults and fractures were sealed by quartz-tourmaline crystallization. This led to further fractionation in the magma, new fluid pressure accumulations, reactivation of faults and crystallization of different tourmaline generations.

Tourmaline-breccia zones are scarce in the literature and the presence of such rocks within the CACC is first reported in this study.

Keywords: Tourmaline-breccia, petrography, Kerkenez Granitoid, mineral chemistry, Central Anatolian Crystalline Complex.

ÖZ

ORTA ANADOLU KRİSTALEN KOMPLEKSİNDEKİ
(TÜRKİYE) KUVARZ-TURMALİN BREŞ ZONUNUN KÖKEN VE ÖNEMİ

DEMİREL, Serhat

Yüksek Lisans, Jeoloji Mühendisliği Bölümü

Tez Yöneticisi: Prof.Dr. M.Cemal Göncüoğlu

Eylül 2004, 111 sayfa

Bu çalışmanın amacı, Üst-Kretase yaşlı Kerkenez Granitoyiti (Orta Anadolu Kristalen Kompleksi, (OAKK), Türkiye) içindeki geniş bir breş zonunda yer alan kuvars-turmalince zengin kayaçların petrografisini, jeokimyasını ve oluşumunu araştırmaktır. Yaklaşık 40m kalınlığındaki ana breş zonu KD-GB yönelimlidir ve yoğun kataklastik deformasyon ile karakterize edilir. Breşik zon süreksiz olarak batıya doğru kilometrelerce izlenir ve genel olarak granitoyit içinde turmalin dolgulu faylar ve 1mm ile 30cm arasında değişen kalınlıklarda damarlar halinde bulunur.

Mineralojik ve dokusal özelliklerine göre bu zon içindeki kayaçlar turmalin damarları, turmalin-breşleri ve kuvars-turmalin kayaçları olarak tanımlanmıştır. Kayaçlar genel olarak kuvars, turmalin ve granitik parçalardan oluşur. Petrografik incelemeler ve elektron mikroprob analizleri kayaçlarda optik ve kimyasal açıdan farklı üç turmalin türünün varlığı ortaya koymuştur. Yaşlıdan gence doğru turmalinler mavi pleokroyik feruvitler, mavi-yeşil pleokroyik şörller ve yeşil-açık yeşil pleokroyik şörller olarak sınıflandırılmıştır. Turmalinlerin kimyası bu minerallerin evrimleşen bir magmadan gelen borca zengin sıvılardan kristallendiğini göstermiştir.

Sonuç olarak, kuvars-turmalin breş zonunun yüksek basınçlı borca zengin sıvıların Kerkenez Granitoyiti içineki mevcut fay ve çatlaklara dolmasıyla oluştuğu düşünülmektedir. Sıvılarca dolan fay ve çatlaklar turmalin ve kuvars kristallenmesi sonucu dolarak kapanmış ve bu olay magmanın daha fazla fraksiyonlaşmasına, yeni sıvı basıncı birikimine, fayların tekrar aktive olmasına ve değişik turmalin türlerinin kristallenmesine yol açmıştır.

Turmalin-breş zonları literatürde oldukça enderdir ve OAKK'deki varlıkları ilk kez bu çalışmayla ortaya konulmuştur.

Anahtar Kelimeler: Turmalin-breşi, petrografi, Kerkenez Granitoyiti, mineral kimyası, Orta Anadolu Kristalen Kompleksi.

ACKNOWLEDGMENTS

I am greatly indebted to my supervisor Prof. Dr. M Cemal Göncüoğlu for his guidance, constructive discussions, supervision throughout every stage of this study, and for critically reviewing and editing the manuscript.

I am grateful to Dr. Fatma Toksoy Köksal for her guidance in every stage of my research, and to Dr. Veysel Işık for his help during the field and structural-geology studies. I am highly indebted to Dr. Gültekin Topuz for the microprobe analyses and his constructive suggestions.

I am grateful to my friend Çağrı Buğdaycıoğlu for his valuable help, encouragement and suggestions during the preparation of this thesis. I would also like to thank to my friends, Çağıl Kolat, Gence Genç, Başak Şener and Yavuz Özdemir who were with me during the long work days and nights. I would also like to thank Orhan Karaman for his help in thin section preperation.

Last, but not least, I offer grateful thanks to my parents and my fiancé, Gülbike Kolcu, for their unlimited patience, unwavering support and encouragement in this study and all through my life. Without them this thesis would never have been completed.

This research was funded by TÜBİTAK-YDABAG 102Y123.

TABLE OF CONTENTS

LIST OF TABLES

TABLE

LIST OF FIGURES

FIGURE

CHAPTER 1

INTRODUCTION

1.1. Purpose and Scope

The main objective of the study is to investigate the petrography, geochemistry, origin and evolution of quartz-tourmaline rocks found in a wide brecciated zone within the Kerkenez Granitoid (Yozgat-Sorgun) in the northern part of the Central Anatolian Crystalline Complex (CACC; Göncüoğlu et al, 1991). The presence of such tourmaline cemented breccias has been previously reported from a few areas in the world (e.g. Roche, SW England, London and Manning, 1995; Williamson et al., 2000), but it is the first finding within the CACC in Turkey.

Tourmaline is a chemically resistant mineral which has a large P-T stability field and a complex chemical formula which monitors the fluid composition and reflects the chemical environment in which it is generated (Henry and Dutrow, 1996). Therefore the study of tourmaline may give important information about the source, chemical composition of the associated fluids and, hence, the evolution of the associated rocks.

This study includes detailed field, petrography, mineral geochemical and whole rock geochemical studies of quartz-tourmaline and associated rocks with the aim of verifying their formation mechanisms. A further aim is to investigate the chemical variations among tourmalines for a better understanding of the evolution of boron-rich fluids that generated these tourmaline-breccias.

The main objectives of the study can be summarized as follows:

1) To study the field occurrence and petrography of the tourmaline-rich rocks and associated brecciated granites.

2) To establish the relationship between deformation events and various tourmaline generations.
3) To determine the nature and elucidate the evolution of the hydrothermal fluids responsible for tourmaline formation.
4) To ascertain the geological mechanisms involved in the development of the various tourmaline generations.

1.2. Geographic Setting

The study area is located within the northeastern part of the Yozgat Batholith in Central Anatolia, along the southern margin of the Kerkenez granitoid. The study area lies to the southwest of Sorgun in Yozgat Province and is bounded by the Sorgun-Gelingülü road to the east, Köçeklioğlu to the west, Koyunculu to the south, and Sarıhacılı to the north. The study area covers an area of approximately 125 km^2 which is included in quadrangles i34-d1, i34-a4, i33-c2 and i33-b3 of the 1:25.000 topographic map of Turkey (Figure 1.1).

1.3. Methods of Study

The present study can be subdivided into two groups: field and laboratory studies.

1.3.1. Field Studies

Field studies were done during the summer of 2003 and include revision of the geological map prepared by Göncüoğlu et al. (1991, 1992, 1993, 1994) and detailed sampling. 102 oriented and non-oriented samples were collected from different locations and lithologies, including granitoids, tourmaline-breccias and sedimentary cover units. In so far as the granitoids were not the main targets of the study, they were studied for descriptive purposes and mainly to ascertain their relation to quartz-tourmaline rocks. Field studies show that sedimentary units were unrelated with tourmaline formation, so samples were collected mainly from the sandstones and conglomerates in order to check for the presence of tourmaline fragments within these sedimentary units.

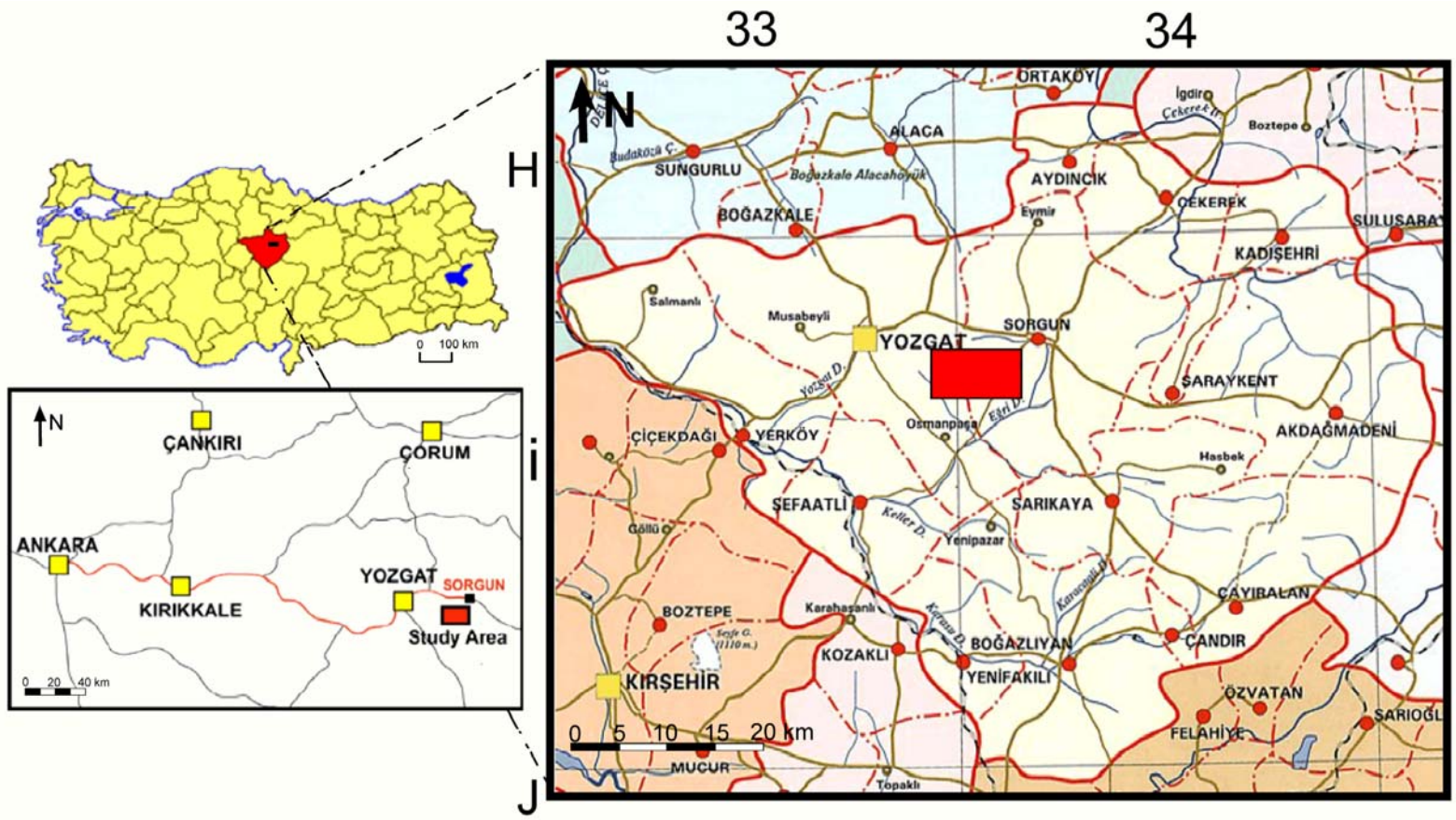

Figure 1.1: Location map of the study area.

Dip, strike and rake angles of various tourmaline-bearing structures (faults, veins, brecciated zones) were measured for kinematic analysis, and oriented samples were collected for further microtectonic studies. Thicknesses and trends of tourmaline veins were also measured in order to determine the general trends and kinematics of the vein systems.

1.3.2. Laboratory Studies

Laboratory work mainly consisted of detailed mineralogical and petrographical, investigations, microprobe and whole-rock analyses.

For mineralogical and petrographical analyses, 98 oriented and non-oriented thin sections were prepared at the thin-section preparation laboratory of Department of Geological Engineering (METU). Microscope studies were carried out using a Nikon Labophot polarizing microscope in order to elucidate processes involved in brecciation and tourmaline formation. Textural relationships and mineralogical contents of the samples were studied carefully. In that the studied rocks are generally composed only of quartz and tourmaline, the point counting method was not used.

Microprobe analyses were done in Heidelberg University (Germany). Tourmaline crystals in polished thin sections were analyzed by Dr. Gültekin Topuz. The electron microprobe at Heidelberg University is a CAMECA SX-51 equipped with five wavelength-dispersive spectrometers and an additional Si–Li detector (Oxford Instruments). Operating conditions were 15 kV accelerating voltage and 20 μA beam current. Counting times were usually 10 s except for Mg, Ca, Al (20 s) and Ti and Zn (30 s). Beam diameter was usually 1μm, except for analyses of feldspars that used a defocused beam (5–10 μm). Synthetic and natural oxide and silicate standards were used for calibration. PAP correction (Pouchou and Pichoir, 1984, 1985) was applied to the raw data. Detection limits were generally on the order of 0.1 wt. %.

The CLASTOUR software of Yavuz et al. (2002) was used in tourmaline formula calculations. CLASTOUR is a program package for IBM-compatible personal

computers. The program classifies most of the currently valid tourmaline end-members together with other hypothetical end-members and was developed to allow editing, storage and calculation of tourmaline analyses obtained both from electron-microprobe and wet-chemical studies. It was also designed to calculate entered tourmaline analyses into cation and molecular percentages, to share cation site-allocations at the different structural positions and to give mole percentages of the end-members of alkali-, calcic-, and X-site vacant-group tourmalines. As is mentioned in Chapter 4, among the different normalization schemes, 6-silica normalization was selected and tourmaline formulae were calculated according to this normalization. Formula calculations were also checked many times by using Excel formula sheets. Graphics and diagrams were plotted by using Microsoft Excel and the Golden Software Grapher.

Whole-rock analyses of 12 selected samples were done at ACME Laboratories (Canada). Major-oxide and minor element analyses were done by $LiBO_2$ fusion, diluted nitric digestion and ICP-ES (Inductively Coupled Plasma - Atomic Emission Spectrometry) which is capable of determining concentrations of 40 to 70+ elements simultaneously by measuring the intensity of light given off by samples aspirated into an argon gas plasma heated to > 10,000°K. Rare-earth and refractory-element analyses were done by $LiBO_2$ fusion and ICP-MS (Inductively Coupled Plasma- Mass Spectrometry) which is capable of determining the concentrations of 70+ elements simultaneously by measuring the mass of ions generated by an argon gas plasma heated to 10,000°K and passing through a magnetic quadropole to a detector capable of ultra low detection limits (ppb to ppt) with very wide linear ranges (up to 7 orders of magnitude). B concentrations were found by leaching of samples in hot (95 °C) aqua regia, which is a strong acid digestion (mixture of hydrochloric acid (HCl), nitric acid (HNO_3) and demineralised water (2:2:2) capable of decomposing metal salts, carbonates, sulphides, most sulphates and some oxides and silicates, and by ICP-ES. Results of the analyses were evaluated by using Minpet v2.02.

1.4. Previous Studies of Quartz-Tourmaline Rocks and Breccias

Tourmaline is the most important boron mineral in granitic rocks (London et al., 1996) and tourmaline-rich rocks are often associated with various types of magmatic-hydrothermal ore deposits including granitoid-related vein-type, greisen replacement, skarn, breccia-pipe and porphyry deposits which are economic sources for many base metal deposits (Slack 1996, Raith et al., 2004). During the last twenty years, studies on tourmaline from a wide variety of geologic settings have shown that important information may be gained from the careful study of tourmaline (Henry and Dutrow, 1996). Although there are several studies on tourmalines and tourmalinites, studies on tourmaline-breccias are exceptionally rare and most of the studies lack explanations of formation mechanisms.

1.4.1. Tourmalinites

Slack et al. (1984) defined tourmalinites as stratabound rocks containing 15% or more tourmaline by volume and tourmalinite formation has been generally related to submarine-hydrothermal or evaporitic processes and are unrelated to granitic rocks. On the other hand the studied rocks are associated with the Kerkenez Granitoid and, as will be discussed in the following chapters, the models concerning the formation of typical ‘‘tourmalinites’’ does not correspond to the geology of the study area. Thus, care must be taken when using the ‘‘tourmalinite‘‘ term. Accordingly, the studied rocks are termed simply quartz-tourmaline rocks, tourmaline-breccias (tourmaline-cemented breccias) and tourmaline veins on the basis of their field appearances and textural and mineralogical constraints.

Models concerning the tourmalinite formation include:

1. Metasomatic alteration of clastic metasediments by B-rich hydrothermal fluids of magmatic derivation (Appleby and Williams, 1988; Slack, 1996; Torres et al., 1996). According to Pesquera and Velasco (1997) subsolidus metasomatic replacement of preexisting silicates suggests that granitic magma attained saturation in aqueous vapor during the last stages of consolidation so that

boron-bearing fluids were expelled and interacted with metasediments leading to the formation of tourmalines. In the case of pegmatitic-granite induced tourmalinization, it is possible that boron formed part of the vapor phase by infiltration of surrounding rock-derived fluids into the granite and pegmatite-forming magma during its evolution. Later, during the last magmatic stages, most of this boron was expelled into metasediments yielding the observed tourmaline-rich marginal zones.

2. Syngenetic precipitation from boron-rich submarine- exhalative fluids (Ethier and Campbell, 1977; Slack et al., 1984; Plimer, 1986; Appel, 1985, 1995). Slack et al. (1984) suggested that on the basis of the stratiform geometry of many tourmalinites, their preserved sedimentary structures and their local association with Pb-Zn-Ag lodes and garnet quartzites tourmalinites are thought to have formed mainly by chemical precipitation from exhalative hydrothermal fluids. However, Slack (1993) proposed that the pure exhalative model has major difficulties. For instance, in order to provide lateral continuity, aqueous fluids should transport Al for large distances and fluids would be undersaturated with respect to tourmaline away from the submarine vent. Ethier and Campbell (1977) proposed that colloids and gels are able to transport significant amounts of Al and Si in submarine hydrothermal environments, and thus provide the direct precipitation of tourmaline from a hydrothermal fluid or brine. An alternative model is the exhalative transport of boron by Al-poor hydrothermal fluids and adsorption onto detritial clays, but this model is also problematic because of the limited content of boron in natural clays which would only provide a few volume percent of tourmaline during metamorphism or diagenesis (Slack, 1993).

3. Regional metamorphism of boron-rich sediments or diagenesis and metamorphism of boron-rich muds associated with evaporitic environments (Abraham et al., 1972).

4. Selective hydrothermal replacement of permeable clastic sediments induced by B-rich fluids of evaporitic provenance (Slack et al., 1993; Peng and Palmer, 1995), or replacement caused by diagenetic and metamorphic B-rich fluids

(Steven and Moore, 1995). According to this model formation of tourmalinites is believed to have taken place through the replacement of clay minerals in sediments. Fluids supposedly migrated along permeable sand rich beds and selectively replaced aluminous clay-rich beds; the composition of the tourmaline is mainly controlled by the bulk composition of the precursor sedimentary rocks because of a low fluid/rock ratio. Slack and Coad (1989) indicated that in case of high fluid/rock conditions, tourmaline composition is mainly controlled by the chemistry of the hydrothermal fluid, as is the case in many massive sulfide deposits.

1.4.2. Quartz-Tourmaline Rocks

None of the before mentioned models correspond to the geology of the study area, and there is no evidence for evaporitic sequences that might contain abundant boron. Although boron is gradually released during regional metamorphism, it is also unlikely that tourmaline-rich rocks were produced from sedimentary rocks under metamorphic conditions in the study area. As a result, care must be taken when using the term ‘tourmalinite’. Thus, as suggested above, the studied rocks are termed as quartz-tourmaline rocks, tourmaline-breccias and veins on the basis of textural and mineralogical constraints.

Badham (1980) studied quartz-tourmaline rocks of Cornwall (England) and emphasized lack of replacement textures. He also suggested that massive quartz-tourmaline rocks crystallize from a quartz tourmaline enriched magma which rose above the roof of a main granitic body. Charoy (1982) interpreted that these quartz-tourmaline rocks are undoubtedly of magmatic origin but, according to London and Manning (1995) the mechanism which can produce quartz- tourmaline rocks is not evident and definitive explanations remain enigmatic.

Slack (1993) proposed that some discordant quartz tourmaline veins in Rocky Mountains formed by remobilization of stratiform tourmalinites by released fluids during deformation and metamorphic processes and other quartz-tourmaline rocks form locally from magmatic or granite-related hydrothermal processes.

Deer et al. (1996) implied that tourmalinization may occur by the introduction of boron in the pneumatolytic stage of alteration. Boron attacks the granitic minerals and first biotites than the feldspars are replaced by tourmalines. Quartz is not replaced and if tourmalinization goes to completion, a quartz-tourmaline rock forms at the end.

Smith and Yardley (1996), on the basis of isotope studies, suggested that massive quartz-tourmaline rocks in southwestern England formed by crystallization of volatiles produced by degassing of granite-silicate liquids.

1.4.3. Tourmaline-Breccias

Tourmaline-cemented breccias are generally attributed to magmatic-hydrothermal systems related to magma emplacement.

Sillitoe and Sawkins (1971) interpreted tourmaline-breccias in their study area (Chile) as hydrothermal collapse breccias which formed by the collapse of the overlying rocks due to dissolution action of hydrothermal fluids.

Warnaars et al. (1984) proposed an explosive hydrothermal origin for tourmaline-bearing breccias in Los Bronces–Rio Blanco, Chile. Super-heated magmatic-hydrothermal solutions rose to near the surface and, with decreasing pressure, turned into jets of steam that fractured and possibly blew out of the overlying rocks.

London and Manning (1995) proposed that hydrothermal tourmaline-rich rocks formed by mixing of two fluids or reservoirs. One reservoir (granites) provides boron and the other reservoir (metapelites, amphibolites, biotite granite hosts) provide Fe and Mg. According to this model, tourmaline-cemented breccias form as a result of explosive loss of volatiles, but a general model for quartz-tourmaline rocks cannot be established. They also suggested that hydrothermal veins and breccias represent open chemical systems that derived fluid components from outside of the granites, which represent the magmatic source of the boron.

London et al. (1996) suggested that tourmaline-cemented breccias in SW England occur in pegmatites and most commonly in peraluminous leucogranites which are associated with polymetallic ore deposits (Sn-W-Cu). Tourmaline forms a fine-grained, massive-monomineralic matrix enclosing crystal and rock fragments, and the textural evidence for replacement of granite by quartz-tourmaline is usually equivocal or missing entirely. According to those authors tourmaline in breccias and veins represent much localized, late-stage concentrations of boron that may not have been manifested throughout the main stages of magma consolidation.

Skewes et al. (2003) suggested that rapid uplift and erosional unroofing coupled with decreasing magma supply at the base of magmatic systems trigger cooling and crystallization of melts in magma chambers and result in exsolution of magmatic fluids which can generate multiple hydrothermal breccias.

1.4.4. Tourmalinites and Other Tourmaline-Rich Rocks of Turkey

Mittwede et al. (1992) suggested that the schorl-dravite tourmaline series is abundant in the Menderes Massif, with various modes of occurrence. These include tourmalinites, tourmaline crystals within schists, gneisses and pegmatites, nodules and eye shaped concentrations within felsic gneiss units and joint fracture fillings with quartz in veins or layers, and as country-rock replacements accompanying sulfide mineralization near the margin of a unmetamorphosed post-kinematic granite. Joint and fracture-filling tourmalines are related to B-enriched late or post-magmatic/residual or hydrothermal fluids associated with emplacement of a granitic magma. Other tourmaline occurrences either represent presence of B in the depositional environment or B concentration via metamorphic to metasomatic processes. At one locality; tourmaline occurs in narrow (0-3cm) veins, joint and fracture fillings which occur at the margins of the biotite granodiorite body and associated sills and dikes. Andalusite hornfels reportedly occurs in the contact aureole of this granitic body.

CHAPTER 2

GEOLOGY OF THE STUDY AREA

2.1. Regional Geology

Turkey constitutes an important part of Alpine-Himalayan collision system and comprises several oceanic and continental terranes with different geological features (Göncüoğlu et al., 1996). It is widely accepted that Neotethys opened in this region during the Triassic and closed in the Late Cretaceous (Şengör and Yılmaz, 1981). During the closure of the northern branch of Neotethys, represented by the İzmir-Ankara-Erzincan Suture Belt, huge allochtonous nappes of almost complete ophiolitic sequences and tectonic mélanges were generated and thrusted southward onto the passive margin of the Tauride-Anatolide Platform (Göncüoğlu et al., 2000). This closure and emplacement of ophiolitic mélanges led to intense metamorphism and magmatism in central Anatolia.

The assemblages of magmatic, metamorphic and ophiolitic rocks in central Anatolia are defined as the Central Anatolian Massif (Ketin, 1966), Kırşehir Massif by Seymen (1981), the Kırşehir Complex by Lünel (1985) and finally the Central Anatolian Crystalline Complex by Göncüoğlu et al. (1991). Göncüoğlu et al. (1991) named the whole complex; including the Kırşehir, Akdağ and Niğde massifs, the Central Anatolian Crystalline Complex (CACC). Ophiolitic rocks were named the Central Anatolian Ophiolites (CAO), granitoids the Central Anatolian Granitoids (CAG) and metamorphic units the Central Anatolian Metamorphics (CAM) which are intruded by post-collisional granitoids.

The CACC lies in a triangular area bounded by the Tuzgölü Fault to the west, the Ecemiş Fault to the east and the İzmir-Ankara-Erzincan suture to the north, and represents the metamorphosed passive continental margin of the Anatolide-

Tauride platform, which has been separated from the main trunk of the Anatolides by the Tertiary Tuzgölü Basin to the south (Göncüoğlu et al., 1991, 1992, 1993) (Figure 2.1).

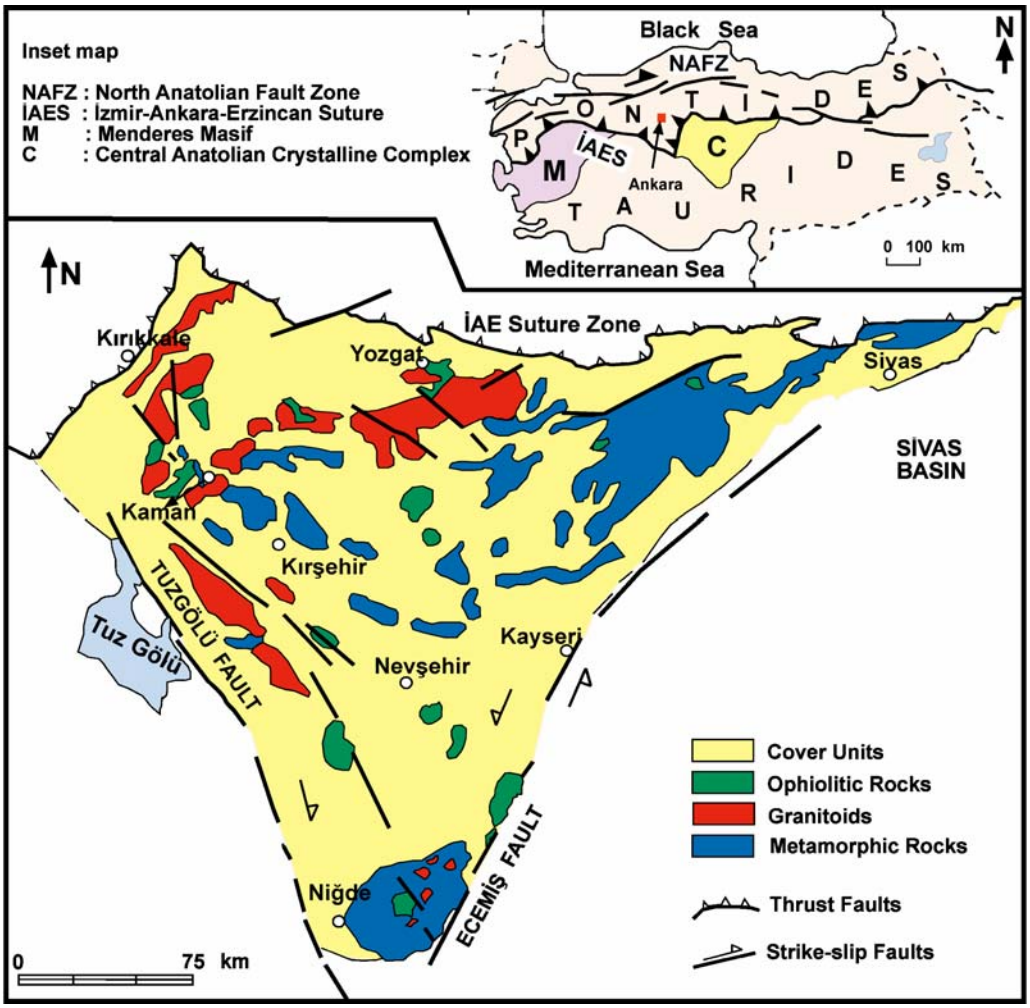

Figure 2.1: Simplified map of the Central Anatolian Crystalline Complex showing geological setting and main lithological units (After Yalınız and Göncüoğlu, 1998, from Toksoy, 1998).

The rocks that crop out within the Central Anatolian Crystalline Complex include metamorphic rocks, mélange slices and felsic to intermediate plutonic rocks, including granitoids and syenitoids. These rocks are generally overlain by latest

Maastrichtian-Paleocene and Eocene volcanic, clastic and carbonate rocks, Oligocene-Miocene evaporates and clastics and Miocene-Pliocene continental clastic rocks (Göncüoğlu et al., 1991, 1992, 1993). A generalized columnar section for the CACC is shown in Figure 2.2.

If cover units are not considered, the Central Anatolian Crystalline Complex can be divided into three principal lithologic units. These are the Central Anatolian Metamorphics, Central Anatolian Ophiolites and the Central Anatolian Granitoids.

1) **The Central Anatolian Metamorphics** (CAM) comprises amphibolite-facies metamorphic basement dominated by marble with subordinate pelitic to psamitic schists, gneisses and metabasites.

2) **The Central Anatolian Ophiolites** (CAO) comprise fragmented ophiolitic remnants of pillow lavas, dikes and gabbros with minor ultramafic rocks and plagiogranites.

3) **The syn-post collisional granitoids**, termed the Central Anatolian granitoids (CAG), and a later group of cross-cutting syenitoids (Göncuoğlu, 1986; Yalınız et al.,1997; Floyd et al., 2000)

Among these units, granitoids dominate the geology of the CACC and intrude the ophiolites and metamorphic rocks of the complex (Göncüoğlu et al., 1991, 1992, 1993; Aydın et al., 1998). The Central Anatolian Metamorphics are tectonically overlain by the Central Anatolian Ophiolites and intruded by the Central Anatolian Granitoids. Uppermost Maastrichtian, Lower Paleocene and Eocene carbonate, volcanic and clastic rocks, Oligocene-Miocene evaporates and clastic rocks and Miocene-Pliocene continental clastic rocks disconformably overlie these units (Göncüoğlu et al., 1991, 1992, 1993).

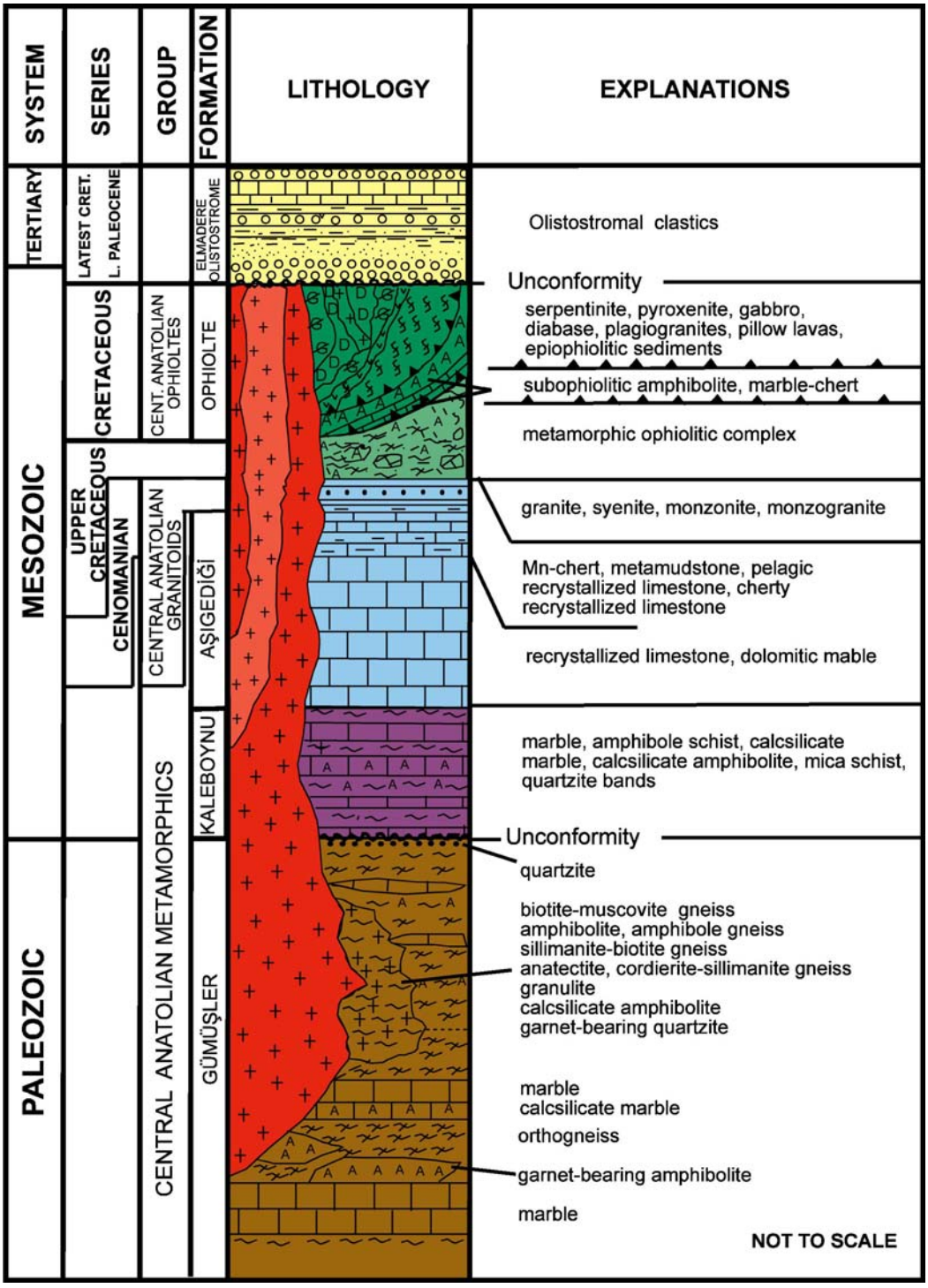

Figure 2.2: Generalized columnar section of Central Anatolian Crystalline Complex (Göncüoğlu et al., 1991, from Toksoy, 1998).

2.1.1. Central Anatolian Metamorphics (CAM)

The Central Anatolian Metamorphics (CAM) are mainly exposed in the southern, central and eastern-northeastern parts of the CACC and have been divided into three formations by Göncüoğlu et al. (1991). From bottom to top these include, the Palaeozoic Gümüşler Formation, and the Mesozoic Kaleboynu and Aşıgediği Formations.

The lowermost unit of CACC is represented by the Gümüşler Formation, generally composed of well-foliated sillimanite-cordierite bearing gneisses, pyroxene gneisses, mica schists, amphibolites, bands and lenses of marbles, calc-silicate marbles and migmatites. This sequence passes upward into the Kaleboynu formation above an unconformity, and the Kaleboynu formation comprises of a thick quartzitic band (which represents a pre-metamorphic transgression) followed by an alternation of marbles, sillimanite gneisses, amphibolites, calc-silicate amphibolites and quartzites. The upper unit of the CAM consists of a thick sequence of calcitic and dolomitic marbles passing upward into pelagic cherty marbles and is defined as the Aşıgediği Formation (Göncüoğlu, 1977, 1981, 1986, Göncüoğlu et al., 1991, 1992, 1993, 1996). The abundance of marbles with a carbonate platform affinity in the basement suggests that it is the metamorphosed equivalent of Tauride-Anatolide Platform (Göncüoğlu, 1977). Finally, this carbonate sequence has been overthrusted by the Central Anatolian Ophiolites, the event is responsible for the metamorphism in CACC basement.

The southward emplacement of ophiolitic nappes and related crustal thickening during the closure of İzmir-Ankara-Erzincan branch of Neotethys caused high-grade metamorphism in the Central Anatolian Units. The regional metamorphism is accepted to have occurred in the pre-mid Cretaceous (Göncüoğlu, 1982). Metamorphism consisted of an early medium pressure/ medium-high temperature event characterized by kyanite–biotite–garnet and cataclastic deformation (Göncüoğlu et al., 1993) and a later event characterized by medium-low pressure/high-temperature formation of andalusite–sillimanite–cordierite (Göncüoğlu et al., 1994).

2.1.2. Central Anatolian Ophiolites

Isolated outcrops of ophiolitic rocks in the CACC have been named the Central Anatolian Ophiolites (CAO) (Göncüoğlu et al., 1991, 1992, 1993, 1994). The CAO are found as allochtonous bodies in CACC and developed in a supra-subduction zone setting (Göncüoğlu and Türeli, 1994; Yalınız et al., 1997).

The CAO is comprised of dismembered and partially preserved ophiolitic rocks, and represented by ultramafic tectonites, cumulates composed of layered ultramafics and gabbros, isotropic gabbros, plagiogranites, dolerite dike complex, basaltic volcanics and pelagic and epi-ophiolitic sedimentary cover units, just as an ideal ophiolitic sequence (Yalınız and Göncüoğlu, 1998).

Ultramafic rocks mainly consist of peridotites, comprising mainly an alternation of dunites and harzburgites, and pyroxenites; serpentinization is common in these rocks. Gabbros are the most common rock unit within the Central Anatolian Ophiolites. The gabbros are mainly isotropic but some microgabbros and pegmatitic gabbros are also present. Basaltic units of the CAO are mainly composed of pillow lavas interbedded with pillow breccias. The epi-ophiolitic cover forms the uppermost part of the CAO and comprises volcanogenic olistrostromal units interbedded with pelagic sediments that are mainly made up of bedded pinkish cherty limestones, radiolarian cherts and micrites. Plagiogranites intrude the ophiolitic units of the CAO and are closely associated with the gabbroic parts of the CAO, but never intrude the Central Anatolian Metamorphics (Floyd et al., 1998, 2000; Yalınız and Göncüoğlu, 1998). The Central Anatolian Ophiolites were emplaced southward onto the passive margin of the Tauride-Anatolide Platform during closure of the İzmir-Ankara-Erzincan Ocean (Yalınız and Göncüoğlu, 1998).

2.1.3. Central Anatolian Granitoids

Rocks of granitoid composition in the CACC were termed the Central Anatolian Granitoids by Göncüoğlu et al. (1991, 1992). Although granitoids, that dominate the geology of CACC closely resemble one another with respect to their spatial

and temporal associations, they are physically and chemically different from each other and have been studied by various authors (Erkan and Ataman 1981; Lünel and Akıman 1984; Göncüoğlu, 1985; Göncüoğlu, 1986; Bayhan, 1986 1989; Göncüoğlu et al., 1991; Erler et al., 1991; Akıman et al., 1993; Göncüoğlu and Türeli, 1994; Güleç, 1994; Kadıoğlu and Güleç, 1996, 1999; Aydın and Önen, 1998; Yalınız and Göncüoğlu, 1999; Whitney and Dilek, 2001; Gençalioğlu-Kuşcu and Floyd, 2001; Gençalioğlu-Kuşcu and Floyd, 2002; İlbeyli et al., 2004).

On the basis of physical characteristics, the Central Anatolian Granitoids were divided into six groups by Erler and Göncüoğlu (1996). These include 1) two-mica leucogranites, 2) biotite-hornblende granites, 3) alkali feldspar granites, 4) granodiorites, 5) tonalites and 6) aplitic dikes.

On the basis of chemistry, the Central Anatolian Granitoids may be subdivided into three groups. The first group is located at the western edge of the CACC including a wide belt with large outcrops, extending from Sulakyurt in the north to Aksaray in the south. These granitoids are generally of monzogranitic, quartz-monzonitic, granodioritic in composition on a calc-alkaline trend. NE-SW trending the second group lies at the eastern edge of CACC and is represented by a narrow belt with small outcrops in metamorphic rocks, extending from Sivas in the north to Ulukışla in the south, and displays characteristics of both I- and S-type granites (and possibly classified as H-type). The last group is found at the northern edge between Yerköy, Yozgat, Sorgun, Sarıkaya, Osmanpaşa, and Şefaatli and these granitoids plot as island arc granitoids, within plate granitoids and collisional granitoids on trace element discrimination diagrams. These granitoid outcrops can reach batholitic proportions (Erler and Bayhan, 1995).

The CAM and CAO are intruded by granitoids and syenite emplacements postdate these granitic intrusions. The youngest igneous activity in the CACC is represented by the aplitic dikes that cut not only the granitoids but also the syenitoids. All of these units are unconformably overlain by Latest Cretaceous to

Eocene clastics, volcanics and carbonates. Therefore, the age of magmatism in the CACC should be in a time interval between Early and Late Cretaceous.

As suggested earlier, the CAG have been studied by various authors. According to these studies, granitoids of the CACC include: metaluminous or peraluminous syn-collisional to late/post-collisional S and I-type monzonitic to granitic-granodioritic rocks of western CACC (Akıman et al., 1993), the calc-alkaline Çelebi Granitoid (Bayhan, 1986), I-type Kaman intrusions (Erler et al., 1991), post-collisional calc-alkaline Ekecikdağ Granitoid (Göncüoğlu and Türeli, 1994), post-collisional H-type Terlemez quartz monzonite (Yalınız and Göncüoğlu, 1999), H-type and metaluminous and post-collisional Baranadağ quartz monzonites (Aydın and Önen, 1998), Agacoren Granitoid including monzonites, granites, and alkali feldspar granite (Kadıoğlu and Güleç, 1996), metaluminous-peraluminous Keskin Pluton including quartz monzonite, quartz monzodiorite, adamellite, granite, granodiorite (Bayhan, 1989) and S and I-type Yozgat Granitoid including peraluminous leucogranitoids and metaluminious monzogranites of subalkaline-calcalkaline character (Erler et al.,1991; Erler and Göncüoğlu, 1996).

Among these the Yozgat Batholith, within which the study area is located, represents one of the largest granitoids in the CACC. It has been studied mainly by Erler and Göncüoğlu (1996) Tatar and Boztuğ (1998) and Boztuğ (1995, 2000).

Erler and Göncüoğlu (1996) divided the Yozgat batholith into eight units on the basis of structural, textural and mineralogical features. The Yozgat subunit is a peraluminous leucogranitoid, and most of the other subunits are principally metaluminous monzogranites of subalkaline-calcalkaline character. S-type granitoids were derived by thickening of the continental crust due to the emplacement of ophiolitic nappes during collisional events, and the post-collisional I-type monzogranites formed by the melting of lower crust which was triggered by the heat resulted from the ponding of magmas at the crust mantle boundary (Erler and Göncüoğlu, 1996).

Tatar and Boztuğ (1998) suggested that the Yozgat granitoid is a composite batholith that comprises syncollisional S-type, two-mica granites, post-collisional I-types, a calcalkaline monzonitic association, and a post-collisional, M-type, tholeiitic gabbroic/dioritic association. They found that a hybrid magma source for the monzonitic association was derived by the mixing of coexisting felsic and mafic magmas, and that during the solidification of this hybrid magma, fractional crystallization process was effective.

Aydın et al. (1998) proposed a framework upon which a petrogenetic model for the diverse magmatism of the CACC can be based. In their study, the Yozgat, Agaçören, Ekecikdag and Cefalıkdag intrusions were reviewed to characterize the granitoid magmatism of the CACC, whereas the Idisdağı and Atdere intrusions were interpreted to represent the syenitoid magmatism of the complex. According to authors two main granitoid types are present in the complex. The first comprises the C-type peraluminous leucogranites, considered to be products of syncollisional magmatism which can be attributed to crustal thickening with or without any direct contribution from mantle-derived mafic magma. The second comprises the H-type, hornblende ± Kfeldspar megacryst ± mafic microgranular enclave-bearing metaluminous granites. These features require a mantle-derived mafic magma contribution for the genesis of these rocks, which can be explained in terms of mafic magma underplating of lower crust as a result of lithospheric delamination following crustal thickening. As a result, the H-type granitoids can be considered products of post-collisional magmatism of the CACC. According to these authors, the emplacement of granitoid magmas was followed by post-collisonal alkaline syenitoid magmatism where the quartz syenitoids predate the feldspathoid bearing syenitoids. The type of magmatism varies overtime from peraluminous, and metaluminous to alkaline- peralkaline through time.

Boztuğ (2000) summarized the intrusive associations of central Anatolia as syn-collisional S-type peraluminous leucogranites, post-collisional I-type metaluminous monzonites, and A-type post-collisional and within plate alkaline associations. Collision of Anatolide-Pontide microplates in the Late Cretaceous

produced metamorphism and various episodes of magmatism in central Anatolia, which are summarized as a syn-collisional peraluminous episode, a post-collisional calc-alkaline hybrid, and a post-collisional within plate alkaline episode. Boztuğ suggested that the Yozgat batholith can be divided into five distinct units which were solidified from a single magma derived by mixing-mingling between underplating mafic and crustal felsic magmas. Fractional crystallization and assimilation processes occurred during solidification and produced reverse zoning within the Yozgat granitoid. Geochemical data show that the Yozgat Batholith formed by partial melting in a post-collisional, crustal-thickening environment.

2.2. Geology of the Study Area

The study area lies in the central northern part of the CACC, just to the south of Sorgun, and in the NE part of Yozgat Batholith. Major units that crop out in the study area include the Kerkenez Granitoid, Eocene sedimentary-volcanic units, Miocene-Pliocene sediments, and Quaternary alluvium deposits. A geological map of the study area is presented in Figure 2.3.

2.2.1. Kerkenez Granitoid

The Yozgat Granitoid constitutes the largest intrusive complex of the overall post-collisional Central Anatolian magmatism (Erler et al., 1991). According to structural features, boundary relationships and mineralogical and petrographical characteristics, the Yozgat Batholith can be divided into eight distinct units. From west to east these include: 1) Yerköy-Şefaatli, 2) Yozgat, 3) Kerkenez, 4) Gelingüllü, 5) Karlıtepe, 6) Sivritepe, 7) Ocaklı, 8) Mugallı plutonic units (Erler and Göncüoğlu, 1996). The Yozgat batholith is suggested to be a composite batholith (Tatar and Boztuğ, 1997). Granitoids of the study area belong to the Kerkenez group of the composite Yozgat Batholith.

The SE-NW and SW boundaries of the Kerkenez Granitoid are faulted and the W and SW margins are bounded by Upper Cretaceous pink pelagic limestones, radiolarite, basalt and diabase assemblage of the Central Anatolian Ophiolites.

Eocene andesites and sandstones lie to the S and Eocene sandstone-marl alternation is present at the northern margins of the Kerkenez Granitoid (Erler and Göncüoğlu, 1996). On the basis of field observations and stratigraphic relationships Ketin (1963) suggested a post-Late Cretaceous-Pre-Lutetian age for the granitoid.

Different episodes of magmatic activity have been observed in the study area. Briefly, the first one is the Kerkenez Granitoid which cuts the Central Anatolian Metamorphics (CAM) and Ophiolites (CAO) the others are the mafic and aplitic dikes. Mafic dikes are present but scarce. The youngest igneous activity is represented by aplitic dikes that cut not only the granitoids but also the mafic dikes. Enclaves have also been observed within the aplitic dikes.

Boztuğ (1995) defined the Kerkenez granitoid as monzonite, quartz monzonite and adamellite, whereas Yardımcılar (1995) defined the Kerkenez Granitoid as granite and quartz monzonite. Erler and Göncüoğlu (1996) suggested that these rocks are monzogranites according to Streckeisen (1979) and subdivided, the Kerkenez Granitoids thus; hornblende-biotite granitoids and alkali-feldspar megacrystic granitoids.

As suggested by Erler and Göncüoğlu (1996), two types of granitoids have been observed in the study area. The first is the hornblende-biotite (HB Granites) granites and the other is the alkali feldspar megacrystic (AFM Granites) granites. The HB Granites are present in the eastern and northeastern parts of the study area and especially in the vicinity of Şahmuratlı village (Figure 2.3). They are coarse grained and generally composed of quartz, plagioclase, orthoclase, hornblende and biotite. Biotite is scarce compared to hornblende. The AFM Granitoids occur in the western and southwestern parts of the study area. They include K-feldspar megacrysts which can reach up to 3 cm in maximum dimensions and show flow textures and distinct magmatic lineation.

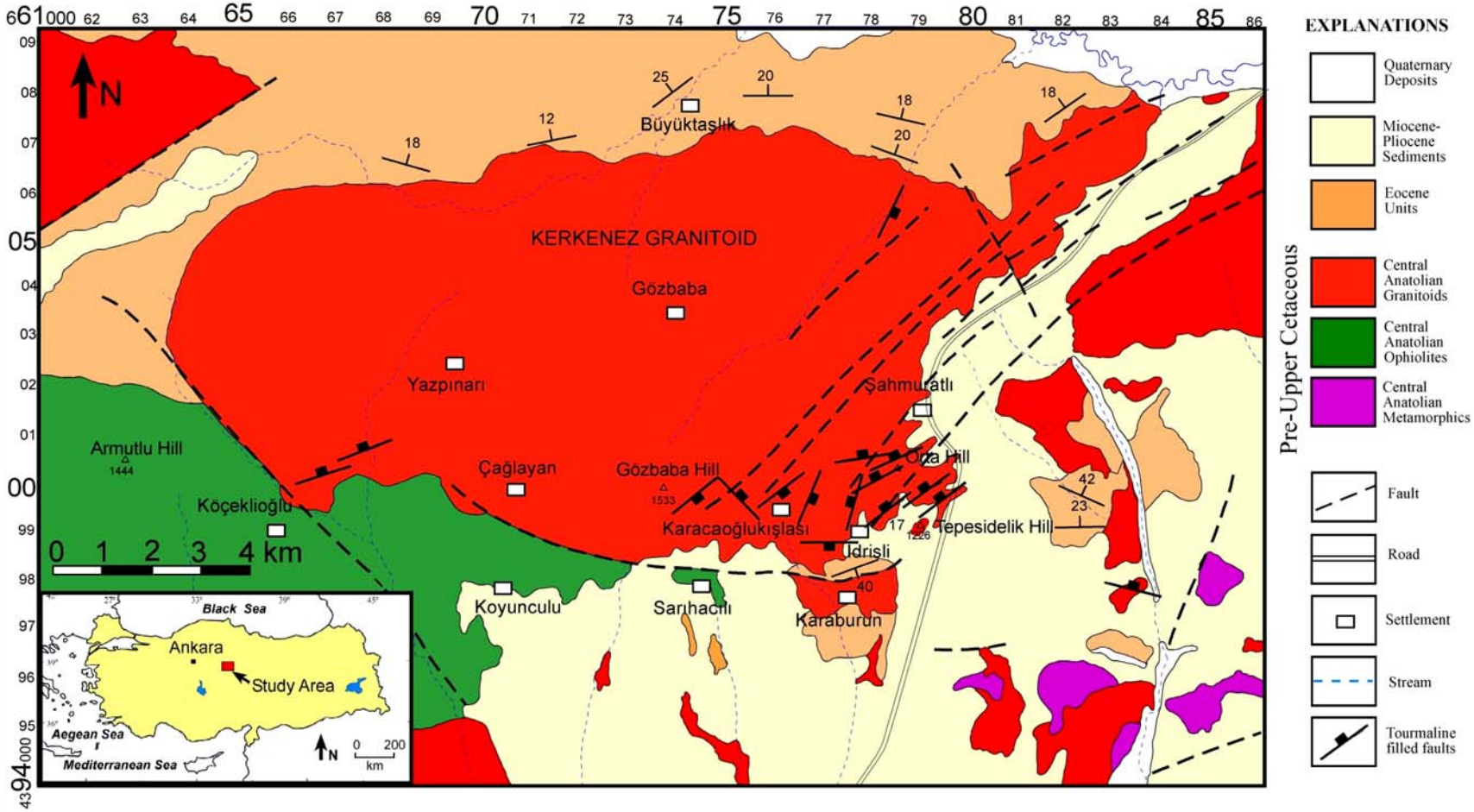

Figure 2.3: Geological map of the study area (after Göncüoğlu et al., 1994).

The studied granites are generally weathered and locally in lower areas are covered by granitic soil. Higher elevated areas most commonly have rounded topography because of erosion (Figure 2.4). Deformation, fracturing and brecciation due to closely spaced faulting is common among HB Granitoids especially at the northeastern part of the Kerkenez Granitoid (Figure 2.3). Breccias are composed of angular granitic rock and mineral fragments that are cemented by a black tourmaline matrix.

Figure 2.4: General view to west of the Kerkenez Granitoid.

2.2.2. Breccia Zone

A wide breccia zone has been observed within these highly fractured and deformed granites. Brecciated rocks abundantly crop out in the vicinity of Orta Hill (1 km SW of Şahmuratlı Village ($^{6}78^{625}$E -$^{44}00^{250}$N)). Contacts with host rock can not be clearly observed because of soil cover. Fields which lie above the main breccia zone are scattered with enormous amounts of quartz-tourmaline rock and fragments of breccia (Figure 2.5.a). Brittle deformation is clearly observed within granitoids. The studied rocks have a characteristic black color

which makes them easy to identify in the field. They are composed of a black microcrystalline matrix, which looks very similar to glass in hand specimen and make up the 15%-75% of the total rock volume. The other constituents are angular to subrounded granitic fragments, quartz porphyroclasts and recrystallized milky quartz which is thought to have formed coevally with the microcrystalline matrix. Although the black matrix has a similar appearance to glass, petrographical studies indicate that it is mainly composed of microcrystalline quartz and tourmaline.

The main structural features of the study area are the NE-SW striking faults. These are generally normal faults with minor strike-slip components. Just like the faults, the tourmaline-breccia zone continues several kilometers away from the Şahmuratlı Village with a NE-SW trend and can be traced along the western and southwestern margins of the granitoid in the form of thin tourmaline-filled veins and networks within the AFM Granites. Along the main zone, brecciation, tourmalinization and later erosion were very intensive and the rocks are generally found in the field as fragmented blocks that range up to 1 meter across (Figure 2.5.b). Therefore it is difficult to observe large outcrops (Figure 2.5.c). The width of the main breccia zone is thought to be more than 40 meters in the vicinity Orta Hill.

Tourmaline-rich rocks found in this zone can be divided into three groups on the basis of their mineralogical and textural features.

1) quartz-tourmaline rocks
2) tourmaline-breccias (tourmaline-cemented breccias)
3) tourmaline veins

It should be noted that this subdivision (quartz-tourmaline rock, tourmaline-breccia and tourmaline veins) is only for descriptive purposes, genetically and temporally, these rock groups are closely related to each other and must be considered as a single unit. All of these rock types are quite fresh compared to the host rock granitoid; this situation is most probably due to their mineral contents. As quartz and tourmaline are resistant minerals to alteration and weathering, these rocks are little affected by weathering.

2.2.2.1. Quartz-Tourmaline Rocks

The first group of tourmaline-rich rocks comprises massive quartz-tourmaline rocks that contain few or no granitic fragments (Figure 2.5.d). Tourmaline is the dominant mineral and makes up 50-80% of the rock by volume. The quartz-tourmaline rocks have a characteristic black color; minor light colored parts are made up of quartz. The quartz has a milky white color and typically shows no signs of deformation (Figure 2.5.e). Most of these quartz-tourmaline rocks were brecciated by later faulting. This deformation is marked by the presence of fault planes and slickensides on quartz-tourmaline outcrops and fragments (Figure 2.6.d). In the field, the quartz-tourmaline rocks generally occur as large blocks (Figure 2.5.f).

2.2.2.2. Tourmaline-Breccias

As the name implies, the tourmaline-breccias show brecciated texture and characteristics of brittle deformation. These rocks consist of angular-subangular granitic fragments, the matrix (tourmaline cement) is limited compared to the massive quartz-tourmaline rocks and jigsaw-puzzle texture, elongated, oriented and dislocated granitic fragments are common. Some breccias have higher matrix-clast ratios relative to others, and include subangular-subrounded granitic fragments. Figure 2.6 shows the general occurrences of the tourmaline-breccias.

2.2.2.3. Tourmaline Veins

Granitoids which lie closer to the main zone include abundant cross-cutting veins. Veins are made up of tourmaline and, locally quartz. Away from the main zone, tourmalines are found in thin veins or networks of veinlets (Figure 2.7.a-b). These cross-cutting tourmaline-rich vein fillings are termed tourmaline veins in this study. Various tourmaline veins have been found in the study area with variable widths ranging from several mm's to ≤30 cm's. Figures 2.7.c-e show mm-to cm-scale tourmaline veins. Veins are wider in the vicinity of main zone and get narrower away from the faults.

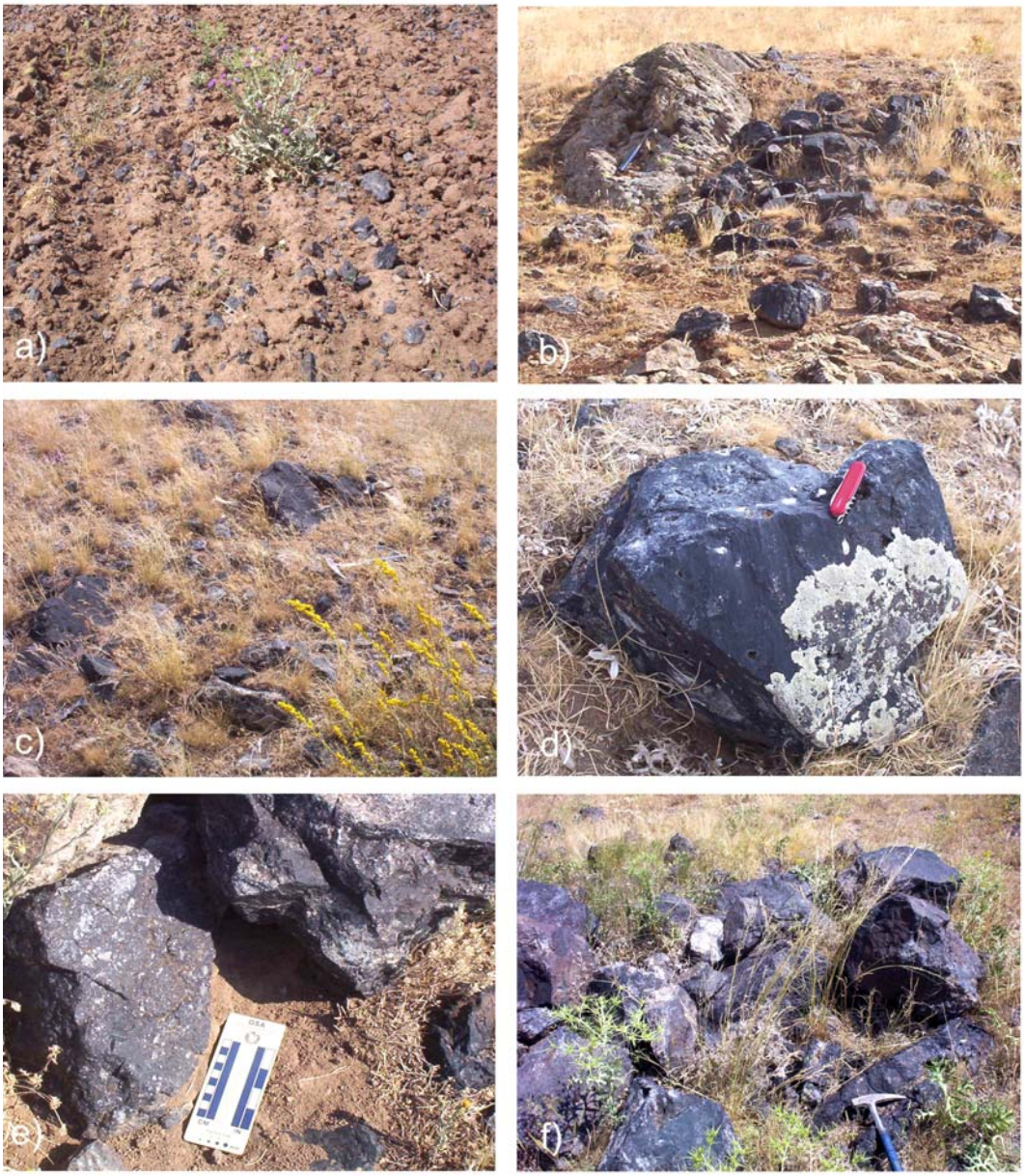

Figure 2.5: a) Field photographs of q-t rock and tourmaline-breccia fragments above the main breccia zone; b) fragmented q-t rocks in contact with granite; c) q-t rock and breccia outcrops; d-e) general view of the massive quartz-tourmaline rocks; f) large fragmented blocks of quartz-tourmaline rock.

Figure 2.6: a) Highly brecciated granitoid fragment with abundant cross-cutting tourmaline veins; b-c) general view of the tourmaline-breccias including elongated and deformed granitic fragments; d) massive quartz-tourmaline rock with slickensides (center) and two tourmaline-breccia fragments at left and right sides; e) close-up view of the tourmaline-breccia of Figure 2.6.d with subrounded granitic fragments; f) close-up view of the angular tourmaline-breccia of Figure 2.6.d showing jigsaw-puzzle texture.

Some wide tourmaline veins have appearances similar to the cross cutting mafic dikes (Figure 2.7.f). The AFM granites also host cross-cutting tourmaline veins.

Generally, angular clasts within the tourmaline-breccias are found close to the wall rock or within the wall rock (in the vicinity of intense deformation), in contrast subrounded fragments that are found in thick tourmaline veins and rest in a more tourmaline-rich matrix and show more or less flow textures. This may be an indicator of boron-rich fluid activity during the brecciation event and/or tourmaline-vein formation. Angular clasts indicate brittle deformation (which took place in the shallower levels of the continental crust) and little transportation of the clasts. On the other hand, the presence of sub-rounded clasts and the high amount of tourmaline matrix in some parts of the zone is most probably due to more turbulent conditions and a greater amount of clast transportation by fluid activity. No banding, folding, lineation, foliation or any effects of ductile deformation have been observed either in the tourmaline-breccias or in the other quartz-tourmaline rocks. The quartz-tourmaline rocks contain milky white, more or less rounded and irregularly shaped quartz fragments but this is due to the embayment by the tourmaline matrix. All rock units show clear evidence of brittle and cataclastic deformation.

Fault surfaces are generally covered with black tourmaline (Figure 2.8.a). Intrusions of variably sized tourmaline injection veins into host granitic rock are common in most of the faults (Figure 2.8.b). These features indicate that hydrothermal fluids circulated along faults within the granitoid and led to tourmaline crystallization in open spaces and fractures.

Sometimes the boundaries between the tourmaline coating and the granite are sharp and reach up to 5 cm in thickness (Figure 2.8.c). Various parallel to irregular tourmaline-filled veins are abundant in the vicinity of fault surfaces. Veins connect with each other and form networks, and thicker veins locally branch into several tiny veins. In addition to tourmaline, epidote mineralization is common in the study area (Figure 2.8.d). The epidote has the characteristic apple green color, has been observed only on fault surfaces, and locally occurs together with tourmalines.

Figure 2.7: a) Highly brecciated granitoid with abundant cross cutting tourmaline veins; b) tourmaline veins within the highly altered and deformed granite, thickness of the veins varies between 0.5-4 cm; c-d) close-up view of tiny cross cutting tourmaline veins within granite; Veins include various granitic fragments; e) tiny tourmaline veins within undeformed alkali feldspar megacrystic granite; f) a thick tourmaline vein (~25cm) cutting across the granite.

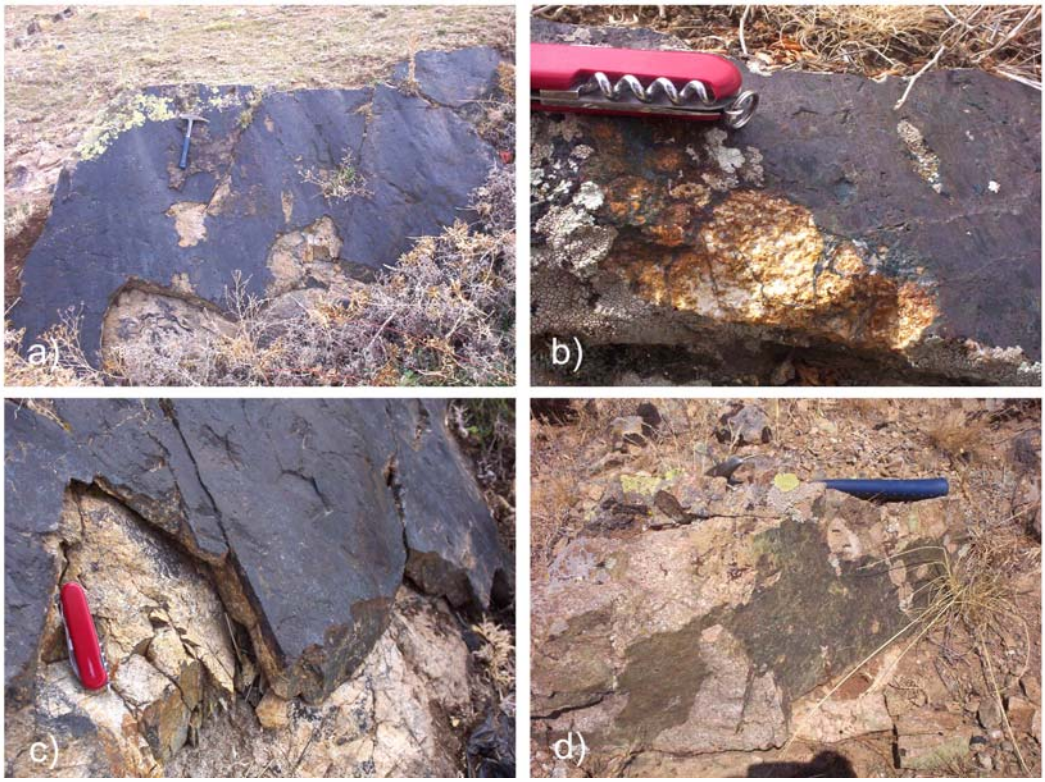

Figure 2.8: a) General view of a tourmalinized fault surface indicating reactivation of faults after tourmaline formation; b) close-up view of a fault surface with slickensides covered with tourmaline and showing tiny tourmaline injection veins; c) close-up view of a tourmaline-coated fault surface; d) general view of epidote-coated fault surfaces.

Slickensides have been observed in massive quartz-tourmaline rocks and tourmaline-breccias (Figure 2.6.d, Figure 2.8.a-b), indicating that the faults reactivated after the arrival of the boron-rich hydrothermal fluids. This idea is also supported by petrographical studies which discovered the presence of tourmaline porphyroclasts within a finer tourmaline-rich matrix. Insofar no tourmaline is present within the unaltered granites; these tourmalines must have been derived from hydrothermal fluids. Rakes indicate normal faulting in the study area, but as these faults are thought to have been reactivated after formation of the tourmaline-breccias, they may have overprinted the previous fault patterns.

Megacrystic alkali-feldspar granitoids with flow textures (Figure 2.9.a) are less affected by deformation than the Şahmuratlı HB Granitoids. Within these

granitoids, tourmaline veins occur mostly along fault surfaces and as minute fracture fillings. Tourmaline filled faults within the megacrystic alkali-feldspar granitoids display minor displacements relative to the HB granites, and no tourmaline-breccia formation has been observed within the AFM granites. Injection of tourmalines from fault surfaces into the host rock is quite limited, probably due to the relatively less deformed and fractured character of the alkali feldspar megacrystic granites. Vein thickness does not reach cm scale in most of the AFM granites, and varies from 1mm to 6mm. Epidote occurs together with tourmaline in some veins; host rock is found to be more altered in these cases. The AFM granites are transitional with the HB granites and are crossed by several aplitic dikes (Figure 2.9.b).

2.2.3. Sedimentary Units

Eocene sedimentary units unconformably overlie the Kerkenez Granitoids in the study area and are represented by two different formations in the Sorgun area. The Yozgat Granitoid constitutes the basement of these units, indicating a pre-Eocene age for the intrusion of the Yozgat Batholith. The lower Eocene unit starts with basal conglomerates - conglomeratic sandstones at the bottom, and towards the top it includes thick sandstone beds, bituminous shales, coal seams and mudstone-sandstone alternations. This unit is unconformably overlain by fossil-bearing Middle-Upper Eocene units which includes Nummulites bearing green marl at the bottom and marl-sandstone-conglomerate alternation at the top. The Eocene succession ends with andesitic-basaltic lava flows, and tuffs. Coal seams are developed in the lower part of the Eocene unit and indicate a fluvial-lacustrine environment (Karayiğit et al. 1997). Palynological investigations of the coal seam indicate a Early Eocene age (Karayiğit et al., 1996). To the south of the study area Göncüoğlu et al. (1994) also reported the following fossils, indicative of an Early Eocene age: Orbitoides, Alveolina (elongated), Nummulites, Textularidae, Miliolidae.

Lower Eocene sandstones and conglomerates are grayish-yellowish, medium-to thick-bedded, and mainly composed of granitic mineral and rock fragments (Figure 2.9.c). In addition to these constituents, tourmaline-breccia clasts have

also been observed within the sandstones. Consequently it can be concluded that the quartz-tourmaline rocks developed and were deformed between the Late Cretaceous and Early Eocene. A general view of the Eocene sedimentary succession is given in Figure 2.9.d

The Miocene-Pliocene units (Göncüoğlu et al., 1993) are represented mainly by conglomerates, sandstones and limestones. Tourmaline-breccia fragments have also been observed within the Miocene-Pliocene units.

Figure 2.9: a) Megacrystic alkali-feldspar granitoids with flow textures; b) granitic enclaves within aplitic dikes that cross cut alkali feldspar megacryst granites; c) general view of Lower Eocene sandstones in the study area; d) general view of the Eocene sedimentary succession in the study area.

2.3. Structural Geology

Field observations and statistical analysis of field measurements have been used to understand the structural geology of the study area. Stereograms and rose diagrams of the fault planes and fractures associated with quartz-tourmaline rocks of the study area were prepared from field measurements and plotted on the Schmidt net lower hemisphere projection.

The Kerkenez Granitoid is intensely faulted and is characterized by numerous fractures and veins. Deformation is localized especially in the eastern part of the granitoid. In general faults strike NE-SW but some NW-SE striking faults are also present. Most of the fault surfaces are covered with tourmaline, epidote or both. Cataclastic deformation and brecciation is more intensive along tourmaline-filled faults. There are also faults which do not contain any tourmaline. These faults have NW-SE and NE-SW trends and are thought to represent younger faulting activity which was not related to tourmaline-breccia formation in the study area.

Faults younger than the tourmaline-breccia formation belong to the Yozgat-Akdağmadeni-Boğazlıyan fault system. This system is suggested to have been inherited from the final phase of collisional tectonic regime and reactivated in the Late Miocene. This fault system also indicates NNE-SSW directed compression during the first stage of paleotectonic regime (Dirik and Göncüoğlu, 1996).

A majority of the faults that are related to the tourmaline-breccias are normal faults with minor strike-slip components. There are also reverse and strike-slip faults in the study area. Thicker tourmaline filled veins lie almost parallel to fault surfaces and form mm-to cm-scale irregular vein networks. Thin tourmaline veins lie in several different orientations. Therefore, only the main tourmaline veins are plotted on the rose diagrams. As seen from the figures below, the distribution of the tourmaline fractures in granitoids has a general NE-SW trend over the entire area (Figure 2.10). The distribution of fractures and veins indicate a NNW-SSE oriented extensional regime and WSW-ENE oriented compressional regime within the Kerkenez Granitoid, which operated during fracturing and boron-rich fluid emplacement.

The poles of fault planes are distributed in the NW and SE quadrants of the diagram, indicating a NE-SW trend and dips toward the SE and NW. The majority of the poles lie in the NW quadrant (Figure 2.11). Figure 2.12 shows the movement of fault planes. The majority of hanging walls moved toward the NW, and some toward the SE and SW. The general characteristics of the fault planes indicate NW-SE-directed extension in the study area.

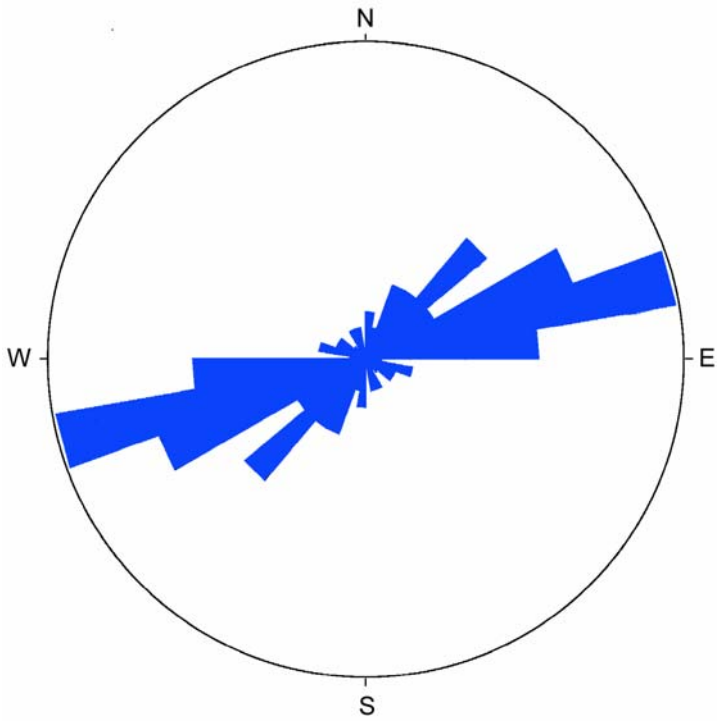

Figure 2.10: Rose diagram of the fractures and tourmaline veins in the study area.

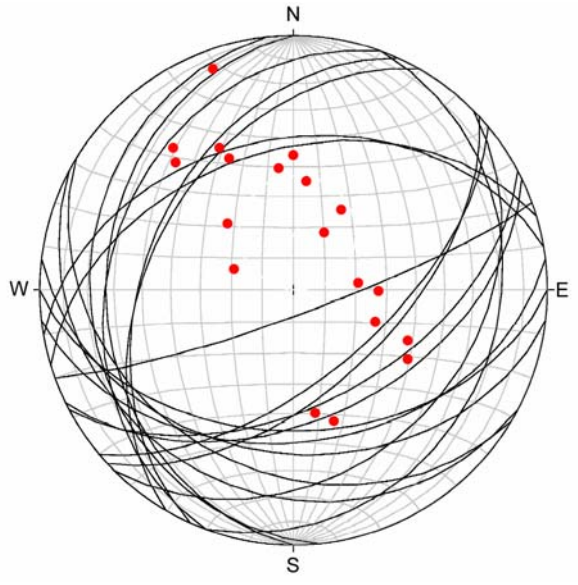

Figure 2.11: Lower hemisphere stereonet projections of tourmaline filled fault planes and poles.

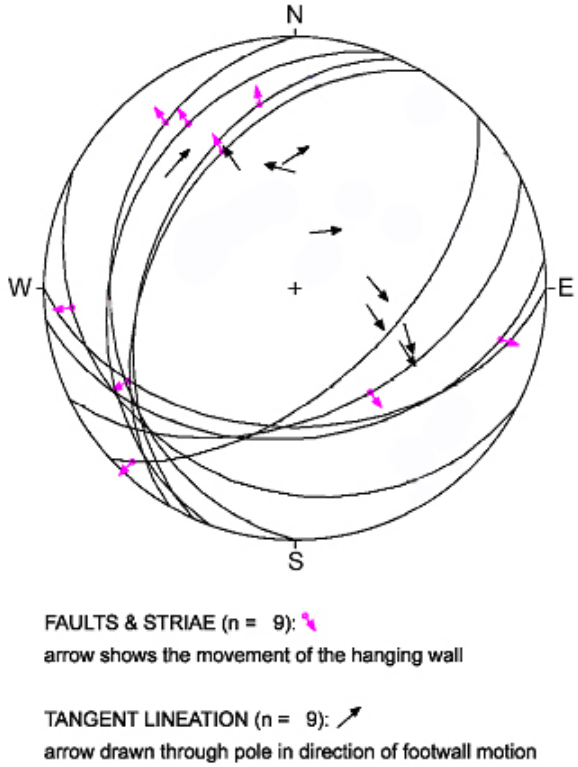

Figure 2.12: Lower hemisphere stereonet projections of tourmaline-filled faults showing the movement directions of hanging and footwall blocks.

CHAPTER 3

PETROGRAPHY

3.1. Introduction

98 thin sections were prepared for petrographical investigation of the studied rocks. Eight thin sections were from sedimentary units including Eocene sandstones and limestones, 66 thin sections were from tourmaline-breccias and quartz-tourmaline rocks, and 24 thin sections were from granitoid host rocks. The thin sections were examined under a microscope in order to elucidate textural characteristics, mineralogical content and cross-cutting relationships. The granitoid rocks are accepted as the host rocks and were generally examined with the aim of determining their relationship to the tourmaline-breccias. As they are not the primary target of this study, the granitoid rocks were examined only for descriptive purposes. The Eocene units were studied mainly to determine their clast contents in order to find clues for the relative age of breccia formation. Tourmaline-rich rocks were subdivided into three groups, as suggested in the field study, and investigated in order to understand the deformation types and histories, textural relationships, mineralogical properties and relationships of different tourmaline generations.

3.2. Host Rocks

The studied rocks were found within the Kerkenez Granitoid, either in the form of tourmaline-breccias wherein tourmaline makes up the matrix and granitic rock and mineral fragments dominate the clasts; or as tourmaline veins which cross-cut the granitoids as tiny veins, veinlets or networks of fracture fillings. Thus, the Kerkenez Granitoid is established as the host rock of the quartz-tourmaline rocks.

3.2.1. Hornblende-Biotite Granitoids

Hornblende-biotite granitoids mainly crop out in the eastern parts of the Kerkenez Granitoid. Petrographically, the HB granitoids can be defined as granites, quartz monzonites and monzonites which are phaneritic, holocrystalline and weakly porphyritic to equigranular. The main mineral constituents are plagioclase, orthoclase, hornblende and quartz (Figure 3.1.a). Biotite and pyroxene are also present but less abundant relative to other constituents. Plagioclase is the dominant mineral and quartz content is variable. Accessory minerals are apatite, titanite, zircon, allanite and fluorite. Quartz is generally anhedral, fresh and coarse-grained. K-feldspar is typically coarser grained than any of the other minerals. Poikilitic texture, Carlsbard twinning and perthitic texture are widespread features. Moreover, intensive kaolinization and sericitization can be observed in some samples. Plagioclases are generally subhedral-prismatic and generally have polysynthetic twinning, compositional zoning is less frequently observed in plagioclases. Hornblendes are characterized by their dark-light green pleochroism (Figure 3.1.b). They are generally subhedral-euhedral crystals and associated with titanite and opaque minerals. Some of the hornblendes have simple twinning and chloritization is common. Biotites are generally flake shaped and have brown pleochroism (Figure 3.1.c). Typically they are partly or completely altered to pale green pleochroic chlorite. Pyroxenes typically occur as subhedral-euhedral crystals and have colorless-pale green pleochroic varieties (Figure 3.1.d). Zircon commonly occurs as small and subhedral-euhedral crystals. Titanite is found as subhedral-euhedral diamond-shaped crystals and has very high relief. Typically they are brown and display simple twinning. Perthitic, granophyric, graphic (Figure 3.1.c) and poikilitic textures can be found in almost all samples and the main alteration types are kaolinization, sericitization and chloritization.

3.2.2. Alkali K-feldspar Megacrystic Granitoids

The AFM granitoids are phaneritic, holocrystalline, porphyritic rocks. Porphyritic texture can be observed in hand specimens. The AFM granitoids generally consist of prismatic and aligned K-feldspar megacrysts which can reach up to 3

cm in maximum dimension (Figure 3.1.e). Other constituents are plagioclase and quartz. Accesory minerals are zircon, titanite and opaque minerals. Mafic phases are represented mainly by hornblende and less by biotite and pyroxene (Figure 3.1.f). Magmatic lineation marked by alignment of prismatic feldspars is common among AFM granitoids. Some samples are intensely altered. The most common type of alteration is kaolinization of the K-feldspars. Other alterations are sericitization and chloritization. Kelyphitic rims, uralitization and replacement by hornblende are the most common features of pyroxenes (Figure 3.1.f). Effects of later hydrothermal alteration and epidote formation are observed in some samples.

3.3. Quartz-Tourmaline Rocks

The studied quartz-tourmaline rocks are dominated by tourmalines which show five modes of occurrence. These include:

1) Very fine-to fine-grained tourmalines in tourmaline-breccia matrix (Figure 3.2.a).
2) Tourmaline-breccias with tourmaline porphyroclasts (Figure 3.2.b).
3) Fine-to medium-grained tourmalines disseminated throughout different parts of the quartz-tourmaline rocks (Figure 3.2.c, Figure 3.2.d).
4) Acicular and radiating tourmalines concentrated along fractures (Figure 3.2.e).
5) Acicular-prismatic fine-grained tourmalines overgrown on and/or enclosed in quartz (Figure 3.2.f).

Tourmalines also show different optical properties such as variable colors and pleochroism. On the basis of their optical properties, the tourmalines can be divided into three groups and the most discriminating factor is pleochroism. The first group consists of tourmalines with bright dark blue-blue-green pleochroism and that are generally anhedral-subhedral and prismatic. The second group is represented by tourmalines having light blue-green-brown pleochroism and that occur generally as anhedral-subhedral grains. These two types are the most common ones among the studied samples.

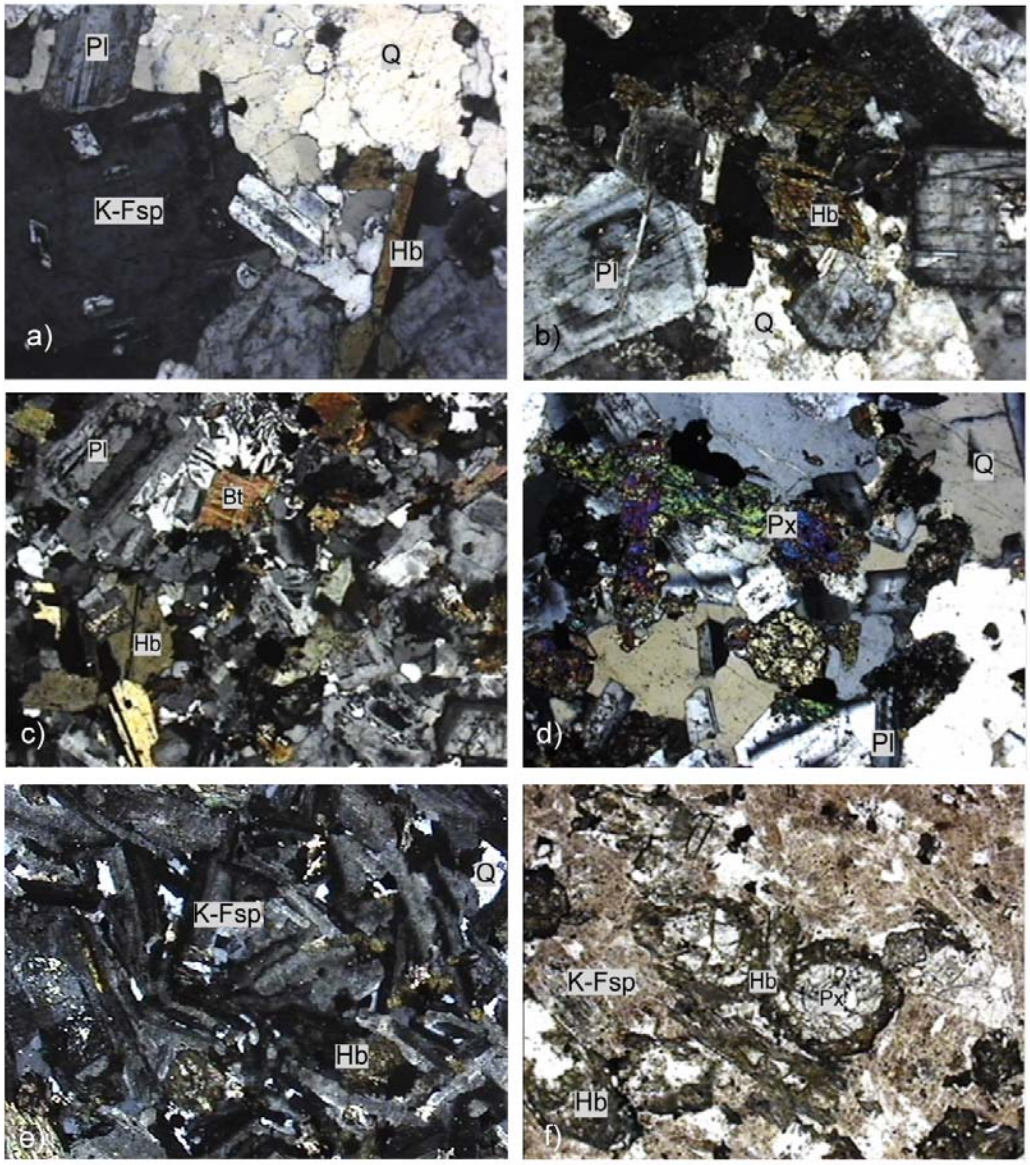

Figure 3.1: Photomicrographs showing general characteristics of the studied granitoid rocks; a) XPL, x4; b) XPL, x4; c) XPL, x4; d) XPL, x4; e) PPL, x4; f) XPL, x4 (Bt: Biotite, K-Fsp: K-Feldspar, Hb: Hornblende, Pl: Plagioclase, Px: Pyroxene, Q: Quartz).

The last group of tourmalines is characterized by pale green pleochroism, high birefringence and locally acicular and of radiating habit. The former two types are generally found together and generally consist of coarser crystals. The pale-green tourmalines cross-cut and sometimes replace the others and represent the youngest generation of tourmalines.

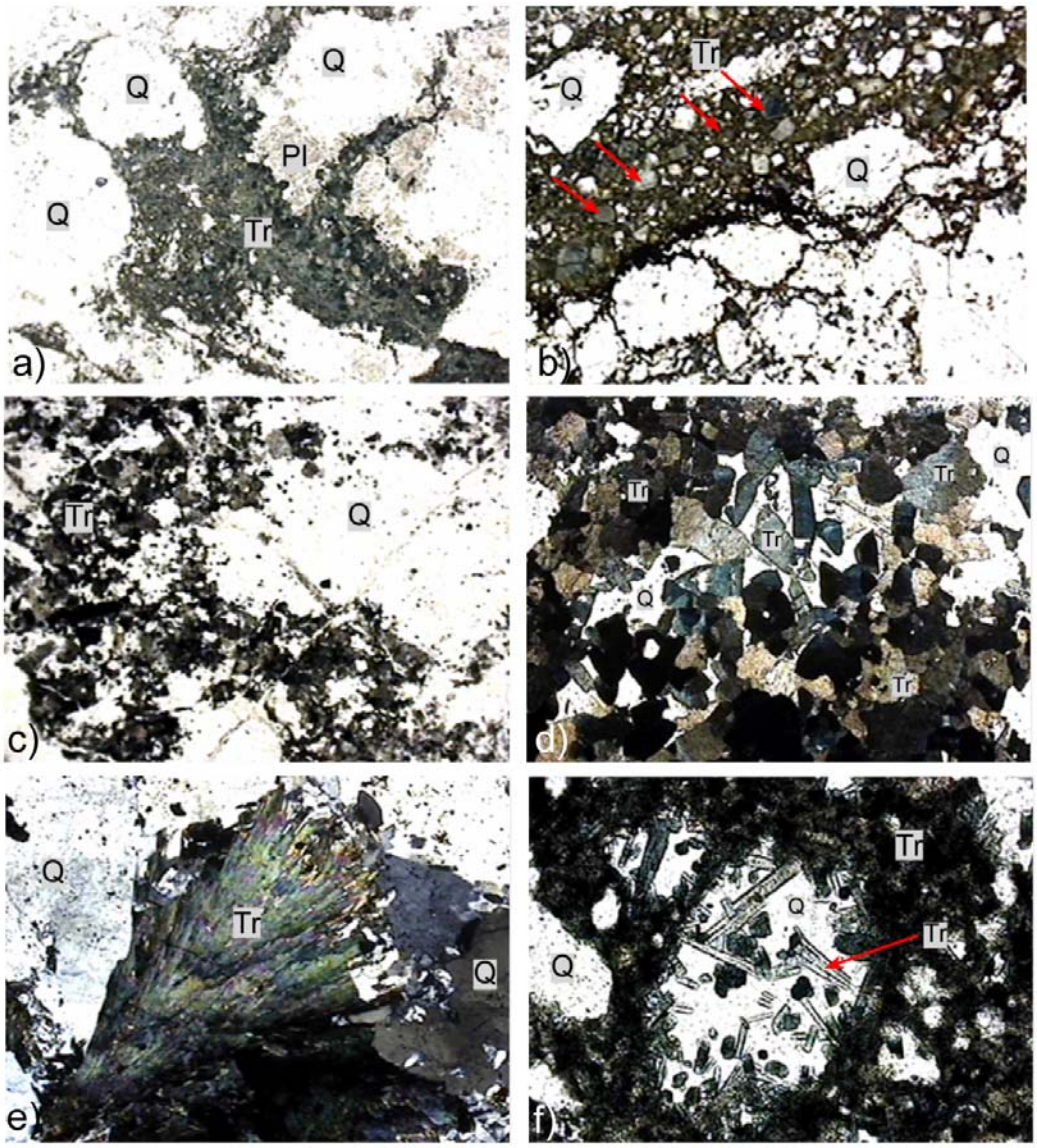

Figure 3.2: Photomicrographs showing different tourmaline occurrences in the studied samples; a) PPL, x4; b) PPL, x4; c) PPL, x4; d) PPL, x4; e) XPL, x4; f) PPL, x10 (Pl: Plagioclase, Q: Quartz, Tr: Tourmaline).

Many of the tourmalines do not show distinct zonation. However backscattered images that were taken during microprobe studies indicate some zonation and cellular morphologies (Figure 4.1) within the tourmalines. Taylor and Slack (1984) suggested that formation of multiple growth zones in tourmaline is indicative of a high fluid–rock interaction. The cellular textures, patchy zoning, and pale discordant reaction rims are interpreted as metasomatic features and relatively homogeneous tourmalines are considered as magmatic tourmalines

(Ruiz et al., 2003). Some tourmaline crystals show color zoning which is characterized by a sharp boundary between dark blue cores and blue-green rims (Figure 3.3). However, most of the tourmalines show irregular color zoning and lack a distinct zonation. Thus the studied tourmalines appear to be hydrothermal-magmatic tourmalines that have not been greatly modified since their formation. On the basis of their optical properties, all of the tourmalines can be defined as schorl. Zoned tourmalines have dark blue cores and light green rims; this indicates that the dark blue pleochroic tourmalines are older than the light colored and green pleochroic tourmalines.

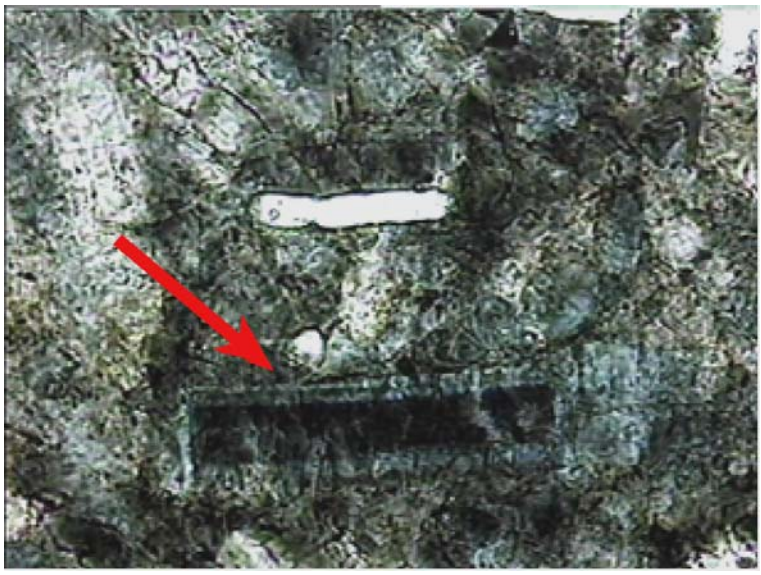

Figure 3.3: Photomicrograph showing zoning in a prismatic tourmaline crystal, PPL, x40.

In some samples, dark tourmalines are replaced by these younger tourmalines. Change in tourmaline composition indicates a change in the boron rich fluid composition. Therefore tourmaline crystallization and fluid infiltration was polyepisodic, and marked by distinct tourmaline generations as revealed in mineral-chemistry studies presented in the following chapter.

3.3.1. Tourmaline-Breccias

The tourmaline-breccias are mainly composed of angular granitic rock and mineral fragments and very fine-to fine-grained matrix. Microscopic textures are quite similar to macroscopic textures, and effects of brittle deformation and cataclasis are very clear in most of the samples (Figure 3.4.a). Ductile deformation has not been observed in any of the samples and no foliation or preferred orientation is present in any of tourmaline-breccias. However cataclastic flow is observed locally. Quartz is the dominant mineral compared to the other granitic minerals; less frequently plagioclase and rarely orthoclase occur in the tourmaline-breccias. Fracturing and grain size reduction are present and are observed in all of the granitic fragments. Plagioclases have generally not survived cataclastic deformation, so most of the plagioclases are fractured and have glided along twinning planes. Small dislocations have occurred where thin tourmaline veins cut across plagioclase crystals. Plagioclase and orthoclase generally occur in quite less deformed host rock or within coarse granitic rock fragments, and are quite limited as mineral fragments. Angular fragments of variable, sized quartz are present both in the matrix and the host rock giving the rock a poorly sorted appearance (Figure 3.4.b). Quartz generally has angular outlines with numerous internal fractures; recrystallization and subgrain formations are visible, and undulose extinction is widespread.

Angular rock and mineral fragments are separated from each other by a tourmaline-rich fine grained matrix, which fills the spaces between the fragments. The matrix consists of tourmaline crystals of various sizes, escaping into fractures and giving way to embayments. Crystal sizes of the matrix tourmalines are variable in different parts of the rocks. This is most probably due to different nucleation and cooling rates. In most cases, the matrix is fine-grained and composed of the light green tourmalines of the latest generation. In cases where the matrix is cryptocrystalline, it is very dark-colored and nearly isotropic. Only at high magnifications can the presence of green and very fine grained tourmalines be observed within the matrix. The coarser-grained matrix is generally composed of all three tourmaline groups and includes variably sized crystals. Green-brown pleochroic tourmalines predominate in the matrix and

dark blue tourmalines generally are the coarsest crystals. Light green tourmalines locally fill the spaces between the other tourmaline groups and in some places replace them.

In addition to quartz fragments, some angular to sub-rounded tourmaline porphyroclasts are found within the microcrystalline matrix. This indicates that deformation continued after the formation of the earlier tourmalines and that there were various periods of deformation and tourmaline crystallization. Most of the breccias are fresh and there are no effects of any alteration. Interestingly, there are no mafic minerals, such as hornblende or biotite within the quartz-tourmaline-breccias or their hosts. This situation may reflect replacement of mafic phases by tourmalines, but no evidence of such replacement has been found during petrographical studies. Fuchs and Lagache (1994) suggested that, circulation of boron-rich fluids can induce transformation of chlorite into tourmaline. As most of the hornblendes and biotites were replaced by chlorite in the host rock, this may be the case in the study area. Another possibility is that the mafic phases were ground and swept away by the frictional forces during cataclastic deformation, prior to introduction of boron-rich fluids.

The tourmaline-breccias display very similar textures in the field and under the microscope. Dislocations of quartz and granitic fragments produce jigsaw-puzzle textures which can also be observed macroscopically in most of the tourmaline-breccias. Mortar texture is observed in the coarser recrystallized quartz fragments. Dislocation of quartz by matrix embayments is another widespread texture. Although tourmalines are microcrystalline within the matrix, medium grained tourmalines are present in less deformed parts of the tourmaline-breccias. Cataclastic deformation is found to take place before the emplacement of tourmaline precipitating hydrothermal fluids. Arrival of fluids into the already deformed and brecciated granitoid changed some textures and filled the open spaces via tourmaline crystallization. Fluid introduction and volume increase by crystallization produced further deformation. These features are reflected by jigsaw-puzzle textures, penetration of matrix into deformed host rock by dislocating minerals and minor flow textures (Figure 3.4.c, Figure 3.4.d).

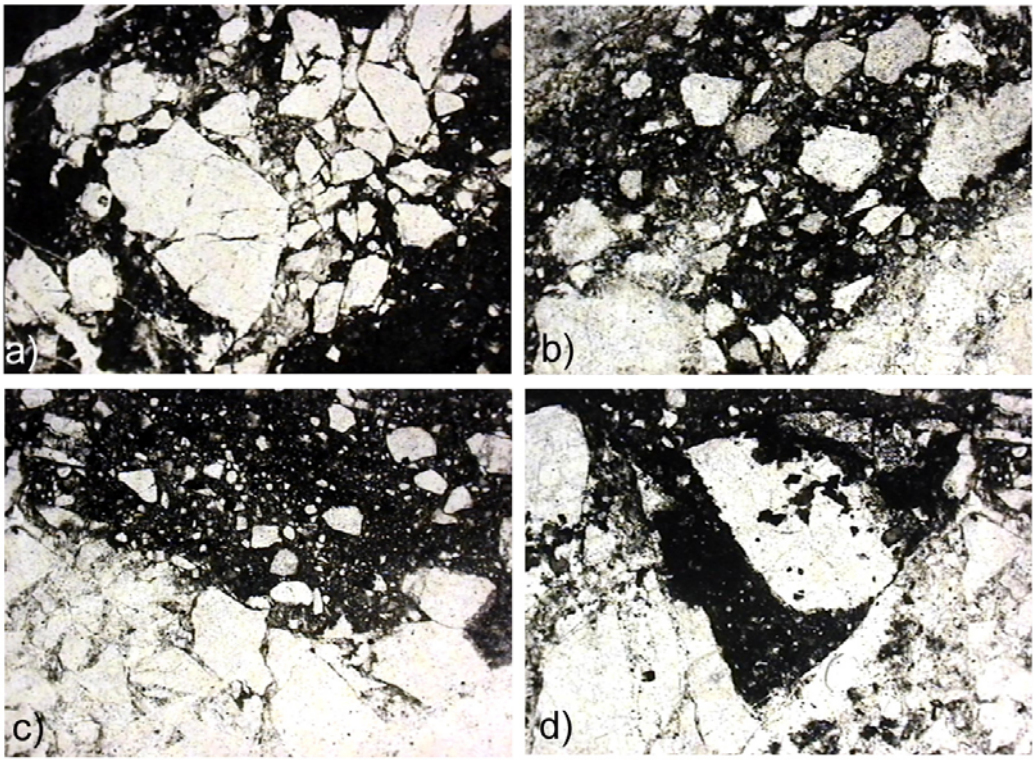

Figure 3.4: Photomicrographs showing the jig-saw puzzle textures in tourmaline-breccias a) PPL, x4 b) PPL, x4 c) PPL, x4 d) PPL, x4.

3.3.2. Tourmaline Veins

In field studies, tourmaline-rich vein fillings that cross-cut granitoids have been defined as tourmaline veins. These veins are also common at the microscopic scale. The tourmalines in veins are very fine-grained and locally cryptocrystalline; crystal size increases within wider veins together with the increase in number of plagioclase- and K-feldspar-bearing granite clasts (Figure 3.5.a). Elongated, locally sub-rounded but generally angular clasts of wall rocks occur locally in the veins. The clasts are generally composed recrystallized quartz. Other minerals occur in very minor amounts. Tourmaline makes up much of the matrix, follows closely spaced fractures, and also occurs as very finely disseminated crystals throughout veins. Veins range from less than one millimeter to several millimeters in width and they are composed of anhedral-subhedral, and locally fibrous to stubby prismatic tourmaline crystals which show sharp to diffuse vein-host rock contacts. Most of the tiny veins are

somehow connected to larger main veins, indicating the propagation of fractures (Figure 3.5.b). Away from the main veins, branching veins get narrower and terminate in the less deformed inner parts of the host rock and produce jigsaw-puzzle textures as well as minor dislocations of granitic minerals (Figure 3.5.c-d).

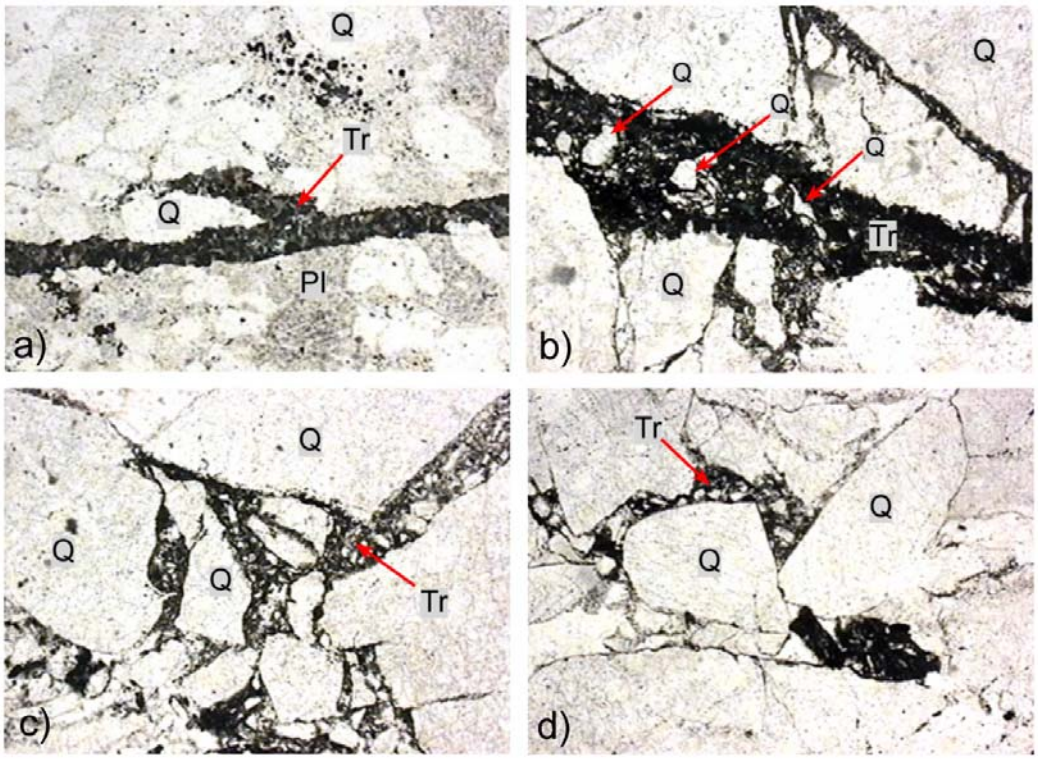

Figure 3.5: Photomicrographs showing tourmaline veins in tourmaline-breccias; a) PPL, x4; b) PPL, x4; c) PPL, x4; d) PPL, x4 (Q: Quartz, Tr: Tourmaline).

3.3.3. Quartz-Tourmaline Rocks

Quartz-tourmaline rocks are texturally different from the tourmaline-breccias. As the name implies, these rocks are almost completely composed of quartz and tourmaline. Neither granitic polymineralic fragments nor plagioclase nor orthoclase clasts occur within the quartz-tourmaline rocks. Quartz and tourmaline make up nearly 95% of the rock volume; other minerals are albite, muscovite, chlorite and K-feldspar. These minerals can only be observed with

high magnifications, or may be recognized in microprobe studies. Effects of cataclasis, cataclastic flow and brecciation cannot be observed in most of the quartz-tourmaline rocks and, as a whole, the quartz-tourmaline rocks have granoblastic texture which is made up of coarse grained quartz and tourmalines (Figure 3.6.a).

The tourmalines are of variable size; fine-to medium-and coarse-grained minerals occur together and have distinct optical properties. Brown-blue-green pleochroic tourmalines are most common, and the other tourmalines have dark blue-blue pleochroism with lower interference colors (Figure 3.6.b). Although the tourmalines can be differentiated from one another in terms of optical properties, they are closely related to each other. Zoned tourmalines are abundant relative to the other groups, but most of tourmalines lack distinct zonation. As mentioned earlier, complex zoning is not present and zoned crystals have dark-colored cores and lighter-colored rims.

Quartz is typically coarser-grained than tourmaline, and is generally recrystallized, fractured and shows undulatory extinction. They are similar to tourmaline-breccia clasts. Some quartz crystals lack undulatory extinction and are undeformed; they are believed to crystallize from the same fluids as the tourmalines and seem to have escaped from later deformations.

Fluid inclusions in quartz crystals have been observed in the tourmaline-breccias and tourmaline veins, but quartz crystals in the quartz-tourmaline rocks contain more fluid inclusions. These properties indicate higher fluid/host rock ratios during formation of the quartz-tourmaline rocks. Tourmaline overgrowths on quartz are abundant and almost every quartz clast has tourmaline overgrowths. Generally tiny prismatic and locally anhedral tourmaline overgrowths cover the margins of quartz clasts, giving them an irregular shape (Figure 3.6.c). Fine prismatic, light green tourmaline overgrowths are another widespread property of this group. They radiate into the quartz clasts from the surrounding tourmaline-rich zone and locally cross-cut each other. Opaque minerals are more abundant than in the tourmaline-breccias. Opaque phases are generally represented by reddish black minerals. Another opaque phase is a

blood red mineral which locally overgrows tourmalines and represents the youngest mineral generation, except for later hydrothermal minerals, such as epidote and calcite (Figure 3.6.d).

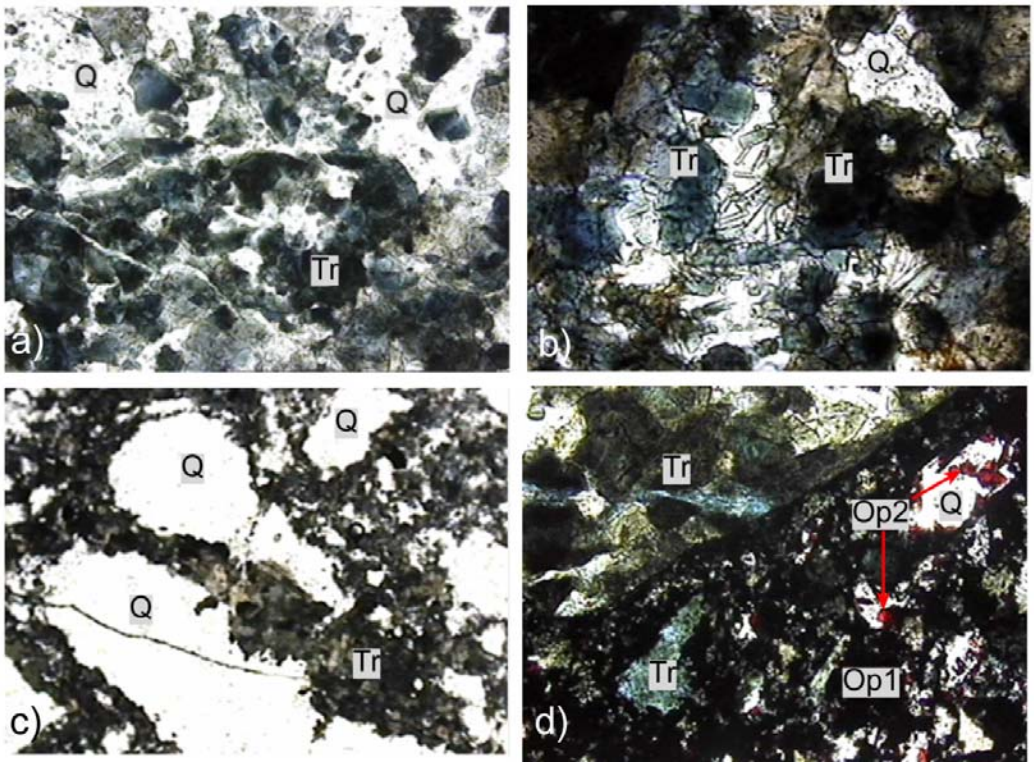

Figure 3.6: Photomicrographs showing quartz-tourmaline rocks; a) PPL, x4; b) PPL, x4; c) PPL, x10; d) PPL, x10 (Op: Opaque, Q: Quartz, Tr: Tourmaline).

The presence of deformed quartz clasts and overprinted breccia textures indicate that quartz-tourmaline rocks and tourmaline-breccias are genetically closely related to each other. The major difference appears to have been fluid/rock ratio.

3.4. Deformational Patterns

As mentioned in the previous chapter, different periods of host-rock and tourmaline deformation have been observed during the course of these petrographical studies. In general, the first deformation event (D1) began with

cataclastic deformation and brecciation within the Kerkenez Granitoid. The presence of jigsaw-puzzle textures together with oriented grains with minor dislocations, indicate the presence of fluid activity during or soon after initial brecciation. Cataclastic deformation is represented by fracturing, grain-size reduction, comminution, recrystallization, mortar texture and undulose extinction in quartz and granitic fragments of the hosts. In most of the samples, tourmalines are unaffected by brecciation; they are medium-to coarse-grained in quartz-tourmaline rocks and finer-grained in tourmaline-breccias. Within narrower veins, grain size decreases and tourmalines become finer-grained and even cryptocrystalline. Most of the quartz clasts are found as porphyroclasts, but some fine-grained unfractured fresh quartz is also present within the tourmaline matrix. Various prismatic tourmaline overgrowths on quartz indicate that tourmaline and quartz crystallized together following deformation. No mafic minerals, such as hornblende or biotite, are present within quartz-tourmaline rocks or tourmaline-breccias. Presence of other granitic minerals, such as orthoclase and plagioclase are quite limited within the tourmaline matrix, they were observed in only a few of the studied samples.

The first phase of cataclastic deformation (D1) and tourmaline formation was followed by other deformation phases, which are reflected in comminution of both quartz and tourmaline (Figure 3.7.a). Tourmaline porphyroclasts found in very-fine grained, light green tourmaline cement indicate the reactivation of faults and secondary deformation (D2) (Figure 3.7.c). Tourmaline porphyroclasts are generally represented by single, sub-angular tourmaline crystals, however some porphyroclasts are made up of aggregates of several tourmalines. The last phase of deformation (D3) is characterized by grain-size reduction and comminution of quartz. No tourmaline formation has been observed associated with D3 deformation; consequently D3 is assumed to have been associated with younger faulting activity in the study area (Figure 3.7.b) that postdated tourmaline formation. Most probably there were several other deformation phases in the study area which have affected the tourmaline rocks and overprinted the main deformational fabrics. However, these deformations cannot be systematically identified via thin-section studies only.

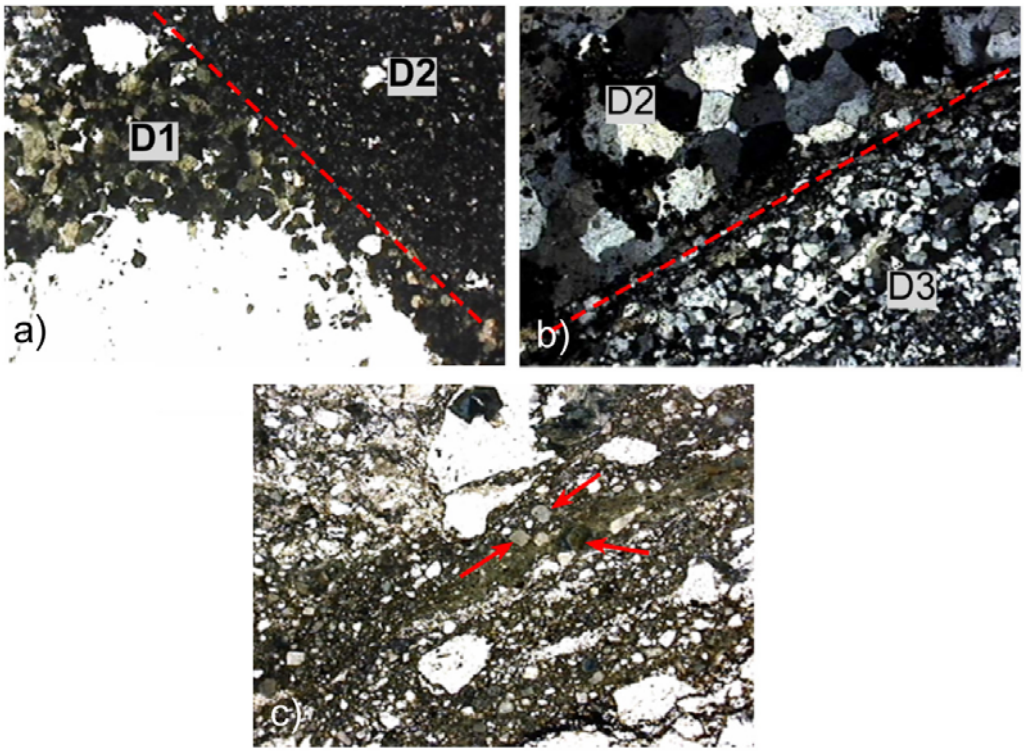

Figure 3.7: Photomicrographs showing different deformations; a) PPL, x4; b) PPL, x10; c) PPL, x10; d) PPL, x4.

Late hydrothermal activity postdating the D3 event is represented by various minerals, veins and alteration products. These include tourmaline, epidote, calcite and quartz. These tourmalines represent the youngest tourmaline generation, as mentioned above. They are light green in color and pleochroism, and generally concentrate along fractures within tourmaline-breccias (Figure 3.8.a).

These tourmalines generally have acicular habit; they locally concentrate along fractures and crystallize into granitic fragments in the form of radial growth patterns and tourmaline suns (Figure 3.8.b, Figure 3.8.c). Intense alteration can be observed together with these youngest tourmalines. Alteration includes kaolinization, and typically sericitization in feldspars. Iron oxides and blackish-reddish opaque minerals occur together with light green tourmalines. In addition to opaque minerals, epidotes are sometimes found to be in equilibrium with tourmalines, and locally younger epidote veins cross-cut tourmalines (Figure

3.8.d). Epidotes can easily be identified by their colorless or yellowish color, moderate-high relief, patchy birefringence, and high-order interference colors. In the field, the epidotes occur as olive-green coatings on fault surfaces. In addition to epidote veins, some microcrystalline-cryptocrystalline quartz veins cut across the studied rocks. They are mostly composed of quartz, but some very-fine grained muscovites can be identified within the quartz veins (Figure 3.8.e). Some of the studied samples, especially the hydrothermally altered ones, are characterized by abundant cross-cutting calcite veins (Figure 3.8.f). Alkali-feldspar megacrystic granites contains more calcite than to the HB granites. Calcite locally occurs as mm-to cm-scale cross-cutting veins or, in places, disperses into the rock.

3.5. Eocene Sandstones and Conglomerates

Sandstones and conglomerates are generally poorly sorted and grain-supported, and are mainly composed of granitic-rock and mineral fragments (Figure 3.8.g). The most common constituent is angular-subrounded quartz. Next to the quartz clasts; well-rounded, quartz-tourmaline rock fragments are found within the sandstones/conglomerates (Figure 3.8.h). The cement is predominantly composed of calcite, clay, and the matrix includes fine-grained sub-angular quartz fragments. The presence of quartz-tourmaline rock fragments within these rocks indicates that cataclastic deformation, brecciation and associated tourmaline formation were older than the Early Eocene.

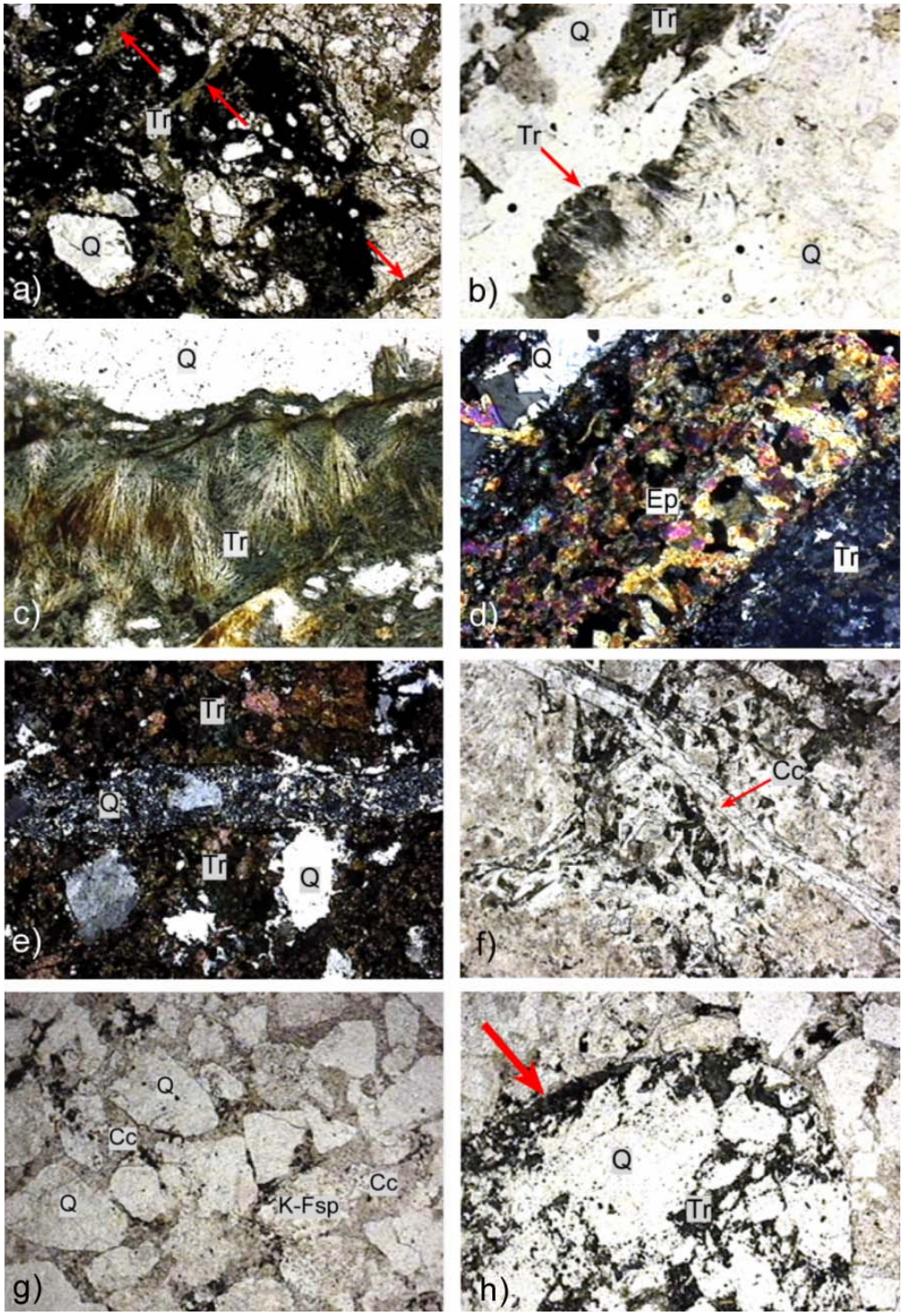

Figure 3.8: Photomicrographs showing late hydrothermal tourmaline occurrences (a,b,c) and veins cross-cutting tourmaline-breccias (d,e,f). For explanations see text; a) PPL, x4; b) PPL, x4; c) PPL, x10; d) XPL, x10; e) PPL, x10; f) PPL, x10; g) general view of Eocene sandstones, PPL, x4; h) tourmaline-breccia pebble within Eocene sandstone, arrow shows the pebble, PPL, x4 (Cc: Calcite, Ep: Epidote, K-Fsp: K-Feldspar, Q: Quartz, Tr: Tourmaline).

CHAPTER 4

MINERALOGY AND CHEMISTRY OF TOURMALINES

4.1. Introduction

Tourmaline is a common accessory mineral phase in many igneous and metamorphic rocks (London et al. 1996). In the last decade it has been the subject of a large number of studies. This is due to the fact that tourmaline is stable over a wide range of pressures and temperatures, is resistant to weathering and alteration, has variable composition and is able to exchange components and volatile species with coexisting minerals and fluids as external conditions change. As a result of these properties, tourmaline can preserve a chemical record of changing conditions during its growth. (Manning, 1982; Farmer and Halls, 1993; London and Manning, 1995; Henry and Dutrow, 1996; Henry and Guidotti, 1985; Slack, 1996; Trumbull and Chaussidonr, 1999; Keller et al., 1999; Dutrow and Henry, 2000; Jiang et al., 2002). Thus, it is an important mineral for tracking the compositional evolution of igneous and metamorphic rocks, and can, in many cases, serve as a monitor of fluid infiltration (Dutrow and Henry, 2000).

The general formula for tourmaline can be expressed as:

$$\mathbf{XY_3Z_6(T_6O_{18})(BO_3)_3V_3W}$$ (Hawthorne and Henry, 1999)

X= Na, Ca or Vacant
Y= Li, Fe^{+2}, Mg, Mn, Al, Cr^{+3}, Fe^{+3}, V^{+3}, Ti^{+3}
Z= Mg, Al, Fe^{+3}, V^{+3}, Cr^{+3}
T= Si, Al, B
B= B, Vacant
V= OH, O
W= OH, F, O

The relatively large X site contains Na, Ca, K, and vacancies; the two distinct octahedral sites, Y and Z, are occupied by a variety of divalent, trivalent and tetravalent cations, and Si with lesser Al dominates the tetrahedrally coordinated T site. The triangular B site is occupied exclusively by B, whereas the two anionic sites, V and W, contain OH, F and O_2. Of particular importance to the proper classification of tourmaline is the fact that F exclusively enters the W site, and O_2 tends to partition into this site (Hawthorne, 1996; Dutrow and Henry, 2000).

The structure of tourmaline allows many possible substitutions. For that reason, several different types of normalization schemes have been proposed to calculate the unit-cell contents of tourmaline analyses. Moreover, the crystal chemistry of tourmaline is difficult to characterize fully via microprobe studies insofar as some significant components, such as Li, Fe^{3+} and H_2O, cannot be directly determined. However, it is possible to calculate the complete tourmaline chemical analysis using several types of normalization schemes and assuming stoichiometric values.

4.2. Normalization Procedures

Normalization schemes used in tourmaline geochemistry studies have been based on 31 oxygens (Rosenberg et al., 1986), 24.5 oxygens (Manning, 1982), 19 total cations, 15 cations excluding those on the X-site and boron (Hawthorne et al., 1993), and 6 silica (Gallagher, 1988). Among these normalizations most frequently used ones are 31 oxygens, 15 cations and 6 silica.

The 31 anion normalization (27O + 4OH, O, F) assumes that OH + F = 4 (Henry and Dutrow 1996, Burns et al., 1994). If OH + F is less than 4 in the V and W anionic sites, the calculation of cations will be underestimated; because it is likely that OH + F < 4, this normalization procedure is not recommended (Henry and Dutrow, 1996). Insofar as OH and F are not measured in microprobe analyses, the 31 oxygen normalization was not chosen in this study.

The 15 cation normalization procedure assumes that the Y, Z, and T sites are full with no vacancies, and that all cations in these sites have been measured for thorough analysis (Henry and Dutrow 1996). Henry and Dutrow (1996) have recommended this normalization scheme for tourmalines with little or no Li in the Y site, and for which all other important cations have been measured. This normalization is generally recommended for tourmalines from metasedimentary rocks as they typically contain no Li.

The 6 silica normalization assumes that the tetrahedral site is exclusively filled with the stoichiometrically ideal 6 Si. Normalizing on the basis of 6 Si provides accurate results as long as the measured SiO_2 contents are accurate and no substantial amount of Al substitutes for Si in the tetrahedral site. This normalization procedure is advantageous for microprobe data because it is not dependent on H values, and is the best option for granitic and pegmatitic tourmalines where significant Li might be present (Hawthorne and Henry, 1999). As a result, most reasonable results have been obtained by the structural formula calculation based on the 6 silica normalization scheme of Gallagher (1988), and is used for all tourmaline analyses in the study.

4.2.1. Estimation of Light Elements

While the electron microprobe is accurate for many major and minor elements, the ability to analyze Li, H and B (significant light elements in tourmaline) is beyond its capabilities. Consequently, electron-microprobe analysis of tourmaline must be supplemented by assumptions or calculations based on tourmaline stoichiometry.

BO_3 necessary to produce three B cations in the structural formula was calculated from the stoichiometry constraints of Hawthorne (1996) and Bloodaxe et al. (1999) as B=3 apfu.

Li presents a more complicated problem, however, as Li can occur in tourmaline in variable amounts in the Y site. Fortunately, Li can be calculated stoichiometrically based on microprobe data if all other cations have been

analyzed and a proper cation basis of normalization established (Burns et al., 1994, Dutrow and Henry, 2000).

Li can be calculated by the equation (Li (apfu) = 15 - (Y site cations + Z site cations + tetrahedral site cations (apfu)). As Z and T sites are fully occupied, Li was estimated by subtracting the sum of the Y-site cations from 3 (Li=3-ΣY), assuming no vacancies in the octahedral sites (Henry and Dutrow, 1996).

The amount of ferric iron in the Y-site was calculated as the total amount of Fe in the Y-site in excess of number of Ca atoms at X-site (Lynch and Ortega, 1997). Fe was reported as Fe_{total} in the study and calculations were made with the CLASTOUR Program (Yavuz et al., 2002).

The chemical diversity and structural requirements of tourmaline produce a large number of possible end-member species. There are currently 14 tourmaline end members that have been accepted by the International Mineralogical Association (IMA) (Hawthorne and Henry, 1999). These end-members are presented in Table 4.1.

4.3. Microprobe Analyses

The studied tourmaline samples have been selected from the most representative massive tourmaline-breccia bodies that occur in the vicinity of Şahmuratlı Village.

In total 57 tourmaline and 36 other mineral (3 quartz, 4 muscovite, 6 albite, 6 epidote, 4 chlorite, 2 phengite, 8 K-feldspar, 3 opaque [rutile]) microprobe analyses were done from three polished thin sections. Results of microprobe analyses of tourmalines are presented in Table 4.2. The silica equals 6 atoms per formula unit (apfu) normalization scheme was applied in formula calculations on the basis of the structural formula $XY_3Z_6(T_6O_{18})(BO_3)_3V_3W$, which was proposed by Hawthorne and Henry (1999) (Table 4.3). Analyzed points are represented as backscattered images in Figures 4.1 and 4.2.

Table 4.1: Tourmaline end-members that have been accepted by the IMA (Hawthorne and Henry 1999).

Species	**(X)**	**(Y_3)**	**(Z_6)**	**T_6O_{18}**	**$(BO_3)_3$**	**V_3**	**W**
Alkali Tourmaline							
Elbaite	Na	$Li_{1.5}\ Al_{1.5}$	Al_6	Si_6O_{18}	$(BO_3)_3$	$(OH)_3$	(OH)
Schorl	Na	$Fe^{2+}{}_3$	Al_6	Si_6O_{18}	$(BO_3)_3$	$(OH)_3$	(OH)
Dravite	Na	Mg_3	Al_6	Si_6O_{18}	$(BO_3)_3$	$(OH)_3$	(OH)
Olenite	Na	Al_3	Al_6	Si_6O_{18}	$(BO_3)_3$	$(O)_3$	(OH)
Chromdravite	Na	Mg_3	Cr_6	Si_6O_{18}	$(BO_3)_3$	$(OH)_3$	(OH)
Buergerite	Na	$Fe^{3+}{}_3$	Al_6	Si_6O_{18}	$(BO_3)_3$	$(O)_3$	F
Povondraite	Na	$Fe^{3+}{}_3$	$Fe^{3+}{}_4Mg_2$	Si_6O_{18}	$(BO_3)_3$	$(OH)_3$	O
Vanadiumdravite	Na	Mg_3	V_6	Si_6O_{18}	$(BO_3)_3$	$(OH)_3$	(OH)
Calcic Tourmaline							
Liddicoatite	Ca	Li_2Al	Al_6	Si_6O_{18}	$(BO_3)_3$	$(OH)_3$	F
Uvite	Ca	Mg_3	$MgAl_5$	Si_6O_{18}	$(BO_3)_3$	$(OH)_3$	F
Hydroxy-feruvite	Ca	$Fe^{2+}{}_3$	$MgAl_5$	Si_6O_{18}	$(BO_3)_3$	$(OH)_3$	(OH)
X-site Vacant Tourmaline							
Rossmanite	□	$LiAl_2$	Al_6	Si_6O_{18}	$(BO_3)_3$	$(OH)_3$	(OH)
Foitite	□	$Fe^{2+}{}_2Al$	Al_6	Si_6O_{18}	$(BO_3)_3$	$(OH)_3$	(OH)
Magnesiofoitite	□	Mg_2Al	Al_6	Si_6O_{18}	$(BO_3)_3$	$(OH)_3$	(OH)

In microprobe analyses, it is found that there are large variations in TiO_2 (0.01-1.270 wt. %), CaO (0.03-3.050 wt. %), MgO (1.240-6.760 wt. %), Na_2O (1.180-5.640 wt. %), and smaller variations are observed for SiO_2 (32.250-37.630 wt. %), MnO (0.01-0.17 wt. %), Cr_2O_3 (0.01-0.05 wt. %), K_2O (0.01-0.13 wt. %) and Li_2O (0.066-1.012 wt. %).

Chemically and petrographically, three different tourmaline groups have been identified and are named Group A, Group B and Group C. Petrographical investigations and cross-cutting relationships suggest that Group A represents the oldest and Group C the youngest tourmaline generation. Group C tourmalines are characterized by their light color, and generally occur in the rims of weakly zoned tourmalines.

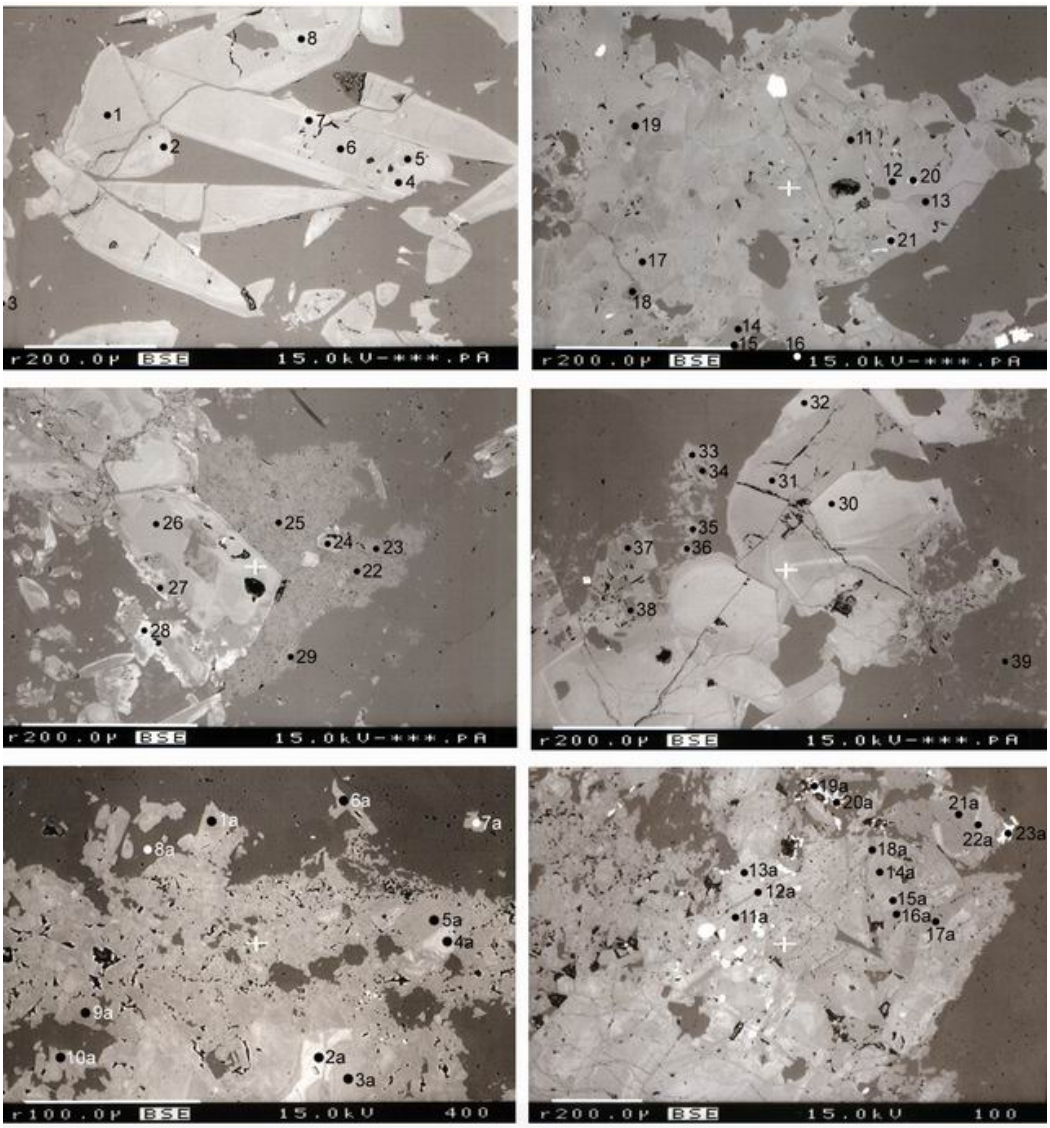

Figure 4.1: Photomicrographs showing tourmalines and microprobe-analyze points.

Backscattered photomicrographs were digitally enhanced in order to reveal the optical differences between tourmaline groups (Figure 4.3). Group C tourmalines cross-cut earlier generations and sometimes form acicular crystals. They can easily be differentiated from Group A and Group B tourmalines by their lighter color.

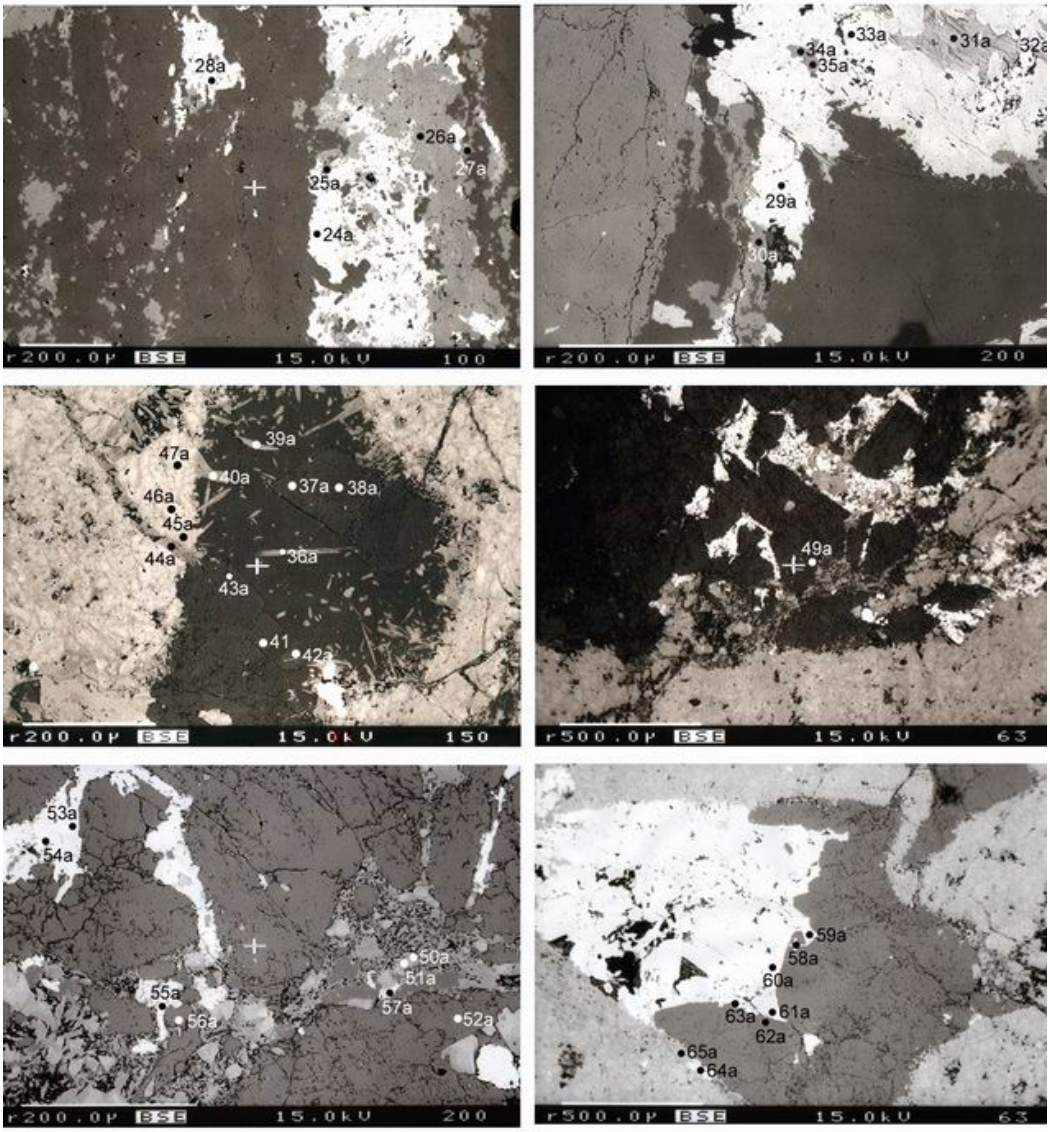

Figure 4.2: Photomicrographs showing tourmalines and microprobe-analyze points.

Representation of the microprobe data on the Ca -X_{vac}-Na+(K) ternary diagram (Figure 4.4.a) of Hawthorne and Henry (1999) supports the recognition of these three, distinct tourmaline groups. Most of the samples plot in the alkali-tourmaline group field, and a few samples plot in the calcic tourmaline group. Alkali tourmalines can be subdivided into two groups, according to their Na and Ca contents. The first alkali-tourmaline group is characterized by an increasing linear trend towards the Ca corner and small X-site vacancies.

Table 4.2: Microprobe analyses of tourmalines from the Kerkenez Granitoid.

Sample	1	2	3	4	6	8	9	11	12	13	14	15	16	17	18
SiO_2	36.090	34.990	34.780	34.950	36.300	35.270	35.730	35.950	35.080	35.640	36.720	36.960	32.250	35.080	37.630
TiO_2	0.050	0.410	0.550	0.420	0.010	0.370	0.060	0.260	0.800	0.280	0.040	0.030	0.030	0.630	0.000
Al_2O_3	29.320	25.690	22.790	23.040	30.250	25.210	28.960	26.570	21.930	26.410	32.480	32.150	21.980	21.910	32.040
Cr_2O_3	0.010	0.020	0.000	0.000	0.000	0.020	0.000	0.010	0.010	0.010	0.000	0.010	0.000	0.000	0.000
FeO	15.960	17.600	19.630	17.510	15.420	17.930	15.770	14.120	17.740	14.990	13.400	12.040	23.160	17.350	9.950
MnO	0.020	0.070	0.110	0.130	0.020	0.020	0.020	0.050	0.050	0.060	0.080	0.100	0.020	0.050	0.050
MgO	3.040	3.880	4.540	5.680	2.660	4.300	3.300	5.780	6.070	5.530	2.900	3.200	3.280	6.760	4.010
CaO	0.380	1.400	2.500	2.300	0.300	1.460	0.430	1.640	2.730	1.590	0.040	0.090	0.090	3.050	0.160
Na_2O	2.350	2.000	1.540	1.580	2.360	2.050	2.460	1.890	1.340	1.940	1.780	1.670	2.730	1.180	1.700
K_2O	0.020	0.070	0.040	0.070	0.030	0.060	0.030	0.010	0.040	0.050	0.000	0.020	0.070	0.040	0.030
Total	87.639	86.462	86.889	86.116	87.813	87.058	87.078	86.754	86.352	86.817	87.721	86.886	83.610	86.474	86.582
Sample	19	21	24	26	27	28	30	31	32	37	38	1a	2a	3a	4a
SiO_2	35.570	33.600	35.960	35.890	36.750	33.150	34.810	35.610	34.490	35.700	36.640	35.970	33.690	34.870	34.280
TiO_2	0.310	0.230	0.050	0.080	0.030	0.070	0.650	0.080	0.620	0.050	0.010	0.070	0.720	1.270	0.900
Al_2O_3	25.830	15.570	29.080	28.750	32.520	20.850	22.190	28.910	23.700	31.810	32.510	29.890	24.200	25.960	24.450
Cr_2O_3	0.030	0.020	0.010	0.000	0.000	0.000	0.010	0.000	0.010	0.000	0.000	0.000	0.000	0.000	0.000
FeO	15.480	29.260	15.360	16.440	13.460	24.890	19.110	16.450	19.850	12.000	11.900	12.800	21.650	16.340	20.310
MnO	0.050	0.150	0.090	0.010	0.050	0.000	0.080	0.070	0.050	0.170	0.060	0.010	0.100	0.070	0.030
MgO	5.630	3.730	3.270	3.090	2.370	3.510	5.090	2.820	3.660	3.310	3.120	4.230	1.770	3.950	2.790
CaO	1.680	0.040	0.310	0.410	0.040	0.050	2.750	0.370	1.420	0.140	0.030	0.440	1.990	1.020	1.710
Na_2O	1.950	2.950	2.200	2.400	1.630	2.880	1.340	2.470	2.100	1.800	1.600	2.340	1.740	2.150	1.840
K_2O	0.040	0.070	0.070	0.030	0.010	0.080	0.060	0.040	0.060	0.050	0.020	0.030	0.040	0.060	0.030
Total	86.885	86.070	86.846	87.474	87.324	85.480	86.579	87.132	86.276	85.254	86.365	86.184	85.900	85.978	86.535
Sample	5a	6a	7a	9a	10a	11a	12a	13a	14a	15a	16a	17a	18a	21a	22a
SiO_2	35.220	35.650	35.120	35.660	34.950	34.390	35.800	34.440	34.930	34.370	35.710	35.790	35.630	35.500	34.170
TiO_2	0.110	0.230	0.830	0.330	0.820	0.810	0.500	1.030	0.220	0.700	0.230	0.160	0.550	0.200	0.680
Al_2O_3	28.600	28.200	26.190	30.120	27.160	24.740	29.540	23.900	27.640	24.700	30.180	31.020	29.560	28.910	24.330
Cr_2O_3	0.000	0.050	0.020	0.020	0.000	0.000	0.010	0.010	0.030	0.000	0.000	0.050	0.020	0.000	0.000
FeO	16.100	15.630	15.610	14.400	15.220	17.740	15.030	19.720	16.670	18.010	14.270	14.570	13.920	14.510	20.330
MnO	0.000	0.000	0.020	0.000	0.070	0.030	0.080	0.070	0.030	0.050	0.050	0.010	0.000	0.080	0.070
MgO	2.860	3.430	4.660	3.130	4.080	3.850	3.640	3.490	3.190	4.400	3.360	2.660	4.010	3.660	2.380
CaO	0.390	0.530	1.120	0.200	0.870	2.210	0.230	1.900	0.870	2.070	0.150	0.160	0.220	0.680	1.810
Na_2O	2.490	2.380	2.100	2.060	2.260	1.630	2.350	1.680	2.250	1.710	2.260	2.060	2.320	2.280	1.760
K_2O	0.030	0.030	0.040	0.010	0.040	0.040	0.000	0.060	0.040	0.050	0.000	0.010	0.020	0.040	0.040
Total	86.127	86.584	85.999	86.181	85.704	85.751	87.288	86.546	86.099	86.126	86.417	86.689	86.388	86.199	85.836
Sample	36a	39a	40a	43a	44a	45a	46a	47a	50a	51a	54a	66a			
SiO_2	35.810	36.330	36.830	36.300	36.120	35.190	34.620	34.940	36.130	35.080	36.180	34.770			
TiO_2	0.020	0.010	0.030	0.020	0.030	0.570	0.740	0.700	0.030	0.550	0.070	0.680			
Al_2O_3	28.060	29.580	30.050	29.010	30.200	23.660	22.250	22.240	13.320	23.310	27.600	22.440			
Cr_2O_3	0.000	0.010	0.000	0.000	0.000	0.050	0.010	0.040	0.050	0.000	0.000	0.000			
FeO	14.010	13.190	11.560	13.950	12.780	15.670	16.730	17.380	4.160	18.040	13.170	17.830			
MnO	0.080	0.030	0.080	0.160	0.080	0.050	0.090	0.070	0.010	0.130	0.100	0.070			
MgO	3.660	4.130	4.480	3.800	4.020	6.730	6.530	6.370	1.240	5.380	4.370	6.340			
CaO	0.360	0.050	0.310	0.200	0.240	2.640	2.850	2.720	0.840	2.920	1.110	2.850			
Na_2O	2.080	2.030	2.190	2.250	2.160	1.380	1.240	1.310	5.640	1.200	2.010	1.290			
K_2O	0.050	0.040	0.000	0.020	0.020	0.020	0.020	0.040	0.130	0.050	0.030	0.040			
Total	84.960	85.981	86.338	86.381	86.092	86.273	85.420	86.200	65.079	87.040	85.628	86.507			

Table 4.3: Atomic proportions of tourmalines on basis of 6 silica normalization scheme. (* Calculated by stoichiometry)

Sample	1	2	3	4	6	8	9	11	12	13	14	15	16	17	18
Si	6.000	6.000	6.000	6.000	6.000	6.000	6.000	6.000	6.000	6.000	6.000	6.000	6.000	6.000	6.000
B	3.000	3.000	3.000	3.000	3.000	3.000	3.000	3.000	3.000	3.000	3.000	3.000	3.000	3.000	3.000
Ti	0.006	0.053	0.071	0.054	0.001	0.047	0.008	0.033	0.103	0.035	0.005	0.004	0.004	0.081	0.000
Al	5.745	5.192	4.633	4.661	5.893	5.054	5.731	5.226	4.420	5.240	6.255	6.151	4.819	4.416	6.021
Cr	0.001	0.003	0.000	0.000	0.000	0.003	0.000	0.001	0.001	0.001	0.000	0.001	0.000	0.000	0.000
Fe(tot)	2.219	2.524	2.832	2.514	2.131	2.551	2.214	1.971	2.537	2.110	1.831	1.634	3.603	2.481	1.327
Mn	0.003	0.010	0.016	0.019	0.003	0.003	0.003	0.007	0.007	0.009	0.011	0.014	0.003	0.007	0.007
Mg	0.753	0.992	1.167	1.453	0.655	1.090	0.826	1.438	1.547	1.388	0.706	0.774	0.910	1.723	0.953
Ca	0.068	0.257	0.462	0.423	0.053	0.266	0.077	0.293	0.500	0.287	0.007	0.016	0.018	0.559	0.027
Na	0.757	0.665	0.515	0.526	0.756	0.676	0.801	0.612	0.444	0.633	0.564	0.526	0.985	0.391	0.526
K	0.004	0.015	0.009	0.015	0.006	0.013	0.006	0.002	0.009	0.011	0.000	0.004	0.017	0.009	0.006
Li*	0.273	0.227	0.280	0.299	0.317	0.252	0.218	0.325	0.385	0.217	0.192	0.422	0.000	0.291	0.693
Sample	**19**	**21**	**24**	**26**	**27**	**28**	**30**	**31**	**32**	**37**	**38**	**1a**	**2a**	**3a**	**4a**
Si	6.000	6.000	6.000	6.000	6.000	6.000	6.000	6.000	6.000	6.000	6.000	6.000	6.000	6.000	6.000
B	3.000	3.000	3.000	3.000	3.000	3.000	3.000	3.000	3.000	3.000	3.000	3.000	3.000	3.000	3.000
Ti	0.039	0.031	0.006	0.010	0.004	0.010	0.084	0.010	0.081	0.006	0.001	0.009	0.096	0.164	0.118
Al	5.135	3.277	5.718	5.664	6.257	4.447	4.507	5.741	4.859	6.301	6.274	5.876	5.079	5.264	5.043
Cr	0.004	0.003	0.001	0.000	0.000	0.000	0.001	0.000	0.001	0.000	0.000	0.000	0.000	0.000	0.000
Fe(tot)	2.183	4.369	2.143	2.298	1.838	3.767	2.754	2.318	2.887	1.686	1.629	1.785	3.224	2.351	2.973
Mn	0.007	0.023	0.013	0.001	0.007	0.000	0.012	0.010	0.007	0.024	0.008	0.001	0.015	0.010	0.004
Mg	1.415	0.993	0.813	0.770	0.577	0.947	1.308	0.708	0.949	0.829	0.761	1.052	0.470	1.013	0.728
Ca	0.304	0.008	0.055	0.073	0.007	0.010	0.508	0.067	0.265	0.025	0.005	0.079	0.380	0.188	0.321
Na	0.638	1.021	0.712	0.778	0.516	1.011	0.448	0.807	0.708	0.586	0.508	0.757	0.601	0.717	0.624
K	0.009	0.016	0.015	0.006	0.002	0.018	0.013	0.009	0.013	0.011	0.004	0.006	0.009	0.013	0.007
Li*	0.216	0.308	0.305	0.256	0.318	0.000	0.335	0.213	0.216	0.153	0.326	0.277	0.000	0.197	0.133
Sample	**5a**	**6a**	**7a**	**9a**	**10a**	**11a**	**12a**	**13a**	**14a**	**15a**	**16a**	**17a**	**18a**	**21a**	**22a**
Si	6.000	6.000	6.000	6.000	6.000	6.000	6.000	6.000	6.000	6.000	6.000	6.000	6.000	6.000	6.000
B	3.000	3.000	3.000	3.000	3.000	3.000	3.000	3.000	3.000	3.000	3.000	3.000	3.000	3.000	3.000
Ti	0.014	0.029	0.107	0.042	0.106	0.106	0.063	0.135	0.028	0.092	0.029	0.020	0.070	0.025	0.090
Al	5.742	5.593	5.273	5.972	5.495	5.087	5.835	4.907	5.595	5.082	5.976	6.129	5.866	5.758	5.035
Cr	0.000	0.007	0.003	0.003	0.000	0.000	0.001	0.001	0.004	0.000	0.000	0.007	0.003	0.000	0.000
Fe(tot)	2.293	2.200	2.230	2.026	2.185	2.588	2.106	2.873	2.394	2.629	2.005	2.042	1.960	2.051	2.985
Mn	0.000	0.000	0.003	0.000	0.010	0.004	0.011	0.010	0.004	0.007	0.007	0.001	0.000	0.011	0.010
Mg	0.726	0.860	1.187	0.785	1.044	1.001	0.909	0.906	0.817	1.145	0.841	0.665	1.006	0.922	0.623
Ca	0.071	0.096	0.205	0.036	0.160	0.413	0.041	0.355	0.160	0.387	0.027	0.029	0.040	0.123	0.340
Na	0.822	0.777	0.696	0.672	0.752	0.551	0.764	0.567	0.749	0.579	0.736	0.670	0.757	0.747	0.599
K	0.007	0.006	0.009	0.002	0.009	0.009	0.000	0.013	0.009	0.011	0.000	0.002	0.004	0.009	0.009
Li*	0.224	0.311	0.198	0.172	0.160	0.213	0.074	0.169	0.157	0.045	0.142	0.136	0.095	0.232	0.182
Sample	**36a**	**39a**	**40a**	**43a**	**44a**	**45a**	**46a**	**47a**	**50a**	**51a**	**54a**	**66a**			
Si	6.000	6.000	6.000	6.000	6.000	6.000	6.000	6.000	6.000	6.000	6.000	6.000			
B	3.000	3.000	3.000	3.000	3.000	3.000	3.000	3.000	3.000	3.000	3.000	3.000			
Ti	0.003	0.001	0.004	0.002	0.004	0.073	0.096	0.090	0.004	0.071	0.009	0.088			
Al	5.541	5.757	5.769	5.651	5.912	4.754	4.544	4.501	2.607	4.699	5.394	4.564			
Cr	0.000	0.001	0.000	0.000	0.000	0.007	0.001	0.005	0.007	0.000	0.000	0.000			
Fe(tot)	1.963	1.822	1.575	1.928	1.775	2.234	2.425	2.496	0.578	2.580	1.826	2.573			
Mn	0.011	0.004	0.011	0.022	0.011	0.007	0.013	0.010	0.001	0.019	0.014	0.010			
Mg	0.914	1.017	1.088	0.936	0.995	1.710	1.687	1.630	0.307	1.371	1.080	1.631			
Ca	0.065	0.009	0.054	0.035	0.043	0.482	0.529	0.500	0.149	0.535	0.197	0.527			
Na	0.676	0.650	0.692	0.721	0.696	0.456	0.417	0.436	1.816	0.398	0.646	0.432			
K	0.011	0.008	0.000	0.004	0.004	0.004	0.004	0.009	0.028	0.011	0.006	0.009			
Li*	0.569	0.398	0.553	0.460	0.302	0.214	0.233	0.267	2.417	0.260	0.677	0.135			

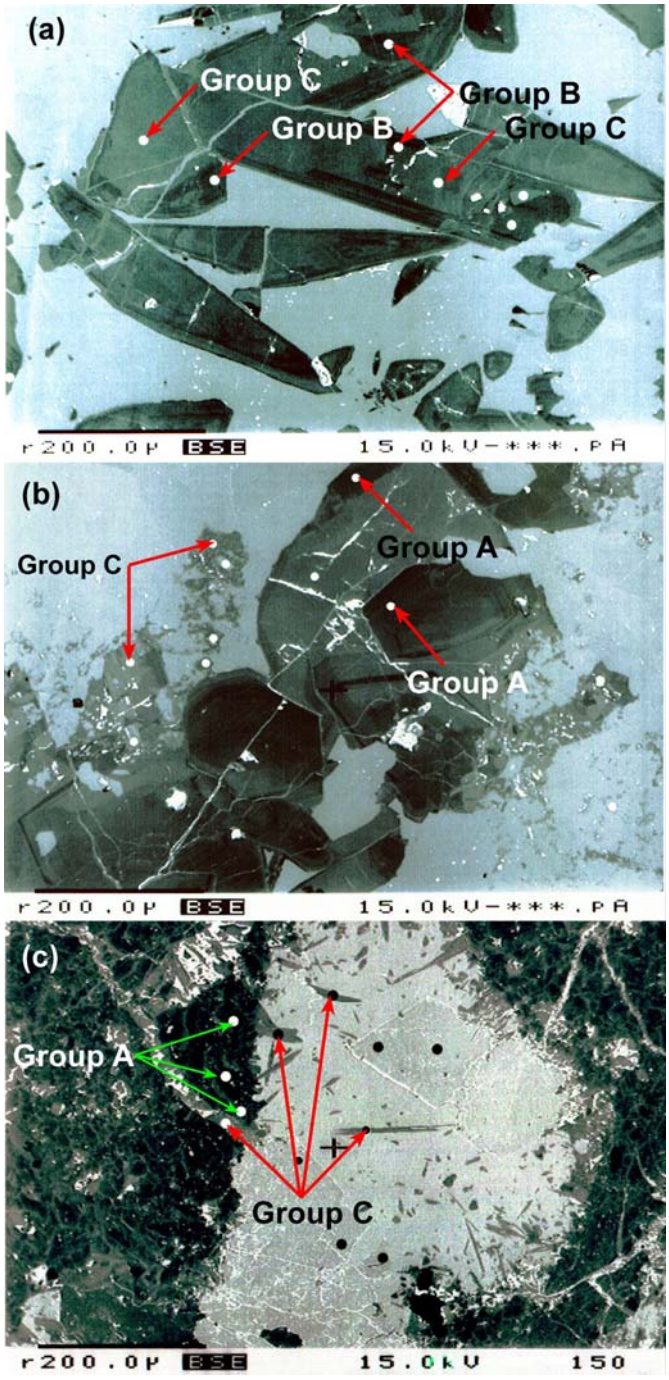

Figure 4.3: Digitally enhanced photomicrographs of tourmaline groups. White spots show the analyzed points. a) Group C tourmalines together with Group B tourmalines. Group B tourmalines can easily be identified by their darker color; b) Group A has the darkest color and occur at the rims of other tourmalines. c) Younger Group C tourmalines cross-cut dark colored Group A tourmalines and are intergrown with quartz as acicular crystals

On the other hand, the second group has lower Ca and higher X-site vacancies. Third group tourmalines lie in the calcic tourmaline field and have high Ca and low vacancies in their X sites.

Alkali group tourmalines plot in the schorl part of the $LiAl_2$-$MgAl_2$-$Fe^{+2}Al_2$ ternary diagram (Figure 4.4.b). Consequently alkali tourmalines belong to the schorl group, but some samples plot relatively closer to the dravite field because of their higher Mg contents. Calcic tourmalines plot in the feruvite field in the Li_2Al-Mg_3-$Fe^{+2}{}_3$ ternary diagram (Figure 4.4.c) Therefore, our microprobe studies show that there exist three compositionally different tourmaline generations in the studied samples; this was also suggested in the 'petrography' chapter. The Fe and Mg rich group has darker colored tourmalines and color gets lighter toward more Fe-, Ca-and Mg-poor groups (towards Group A to C).

According to Dutrow and Henry (2000) growth of markedly different compositions suggests that a compositionally distinct fluid was associated with each stage of tourmaline growth. Therefore, the presence of three compositionally different tourmaline groups (Group A, B, C) indicates that the composition of the boron- rich fluids had changed at least three times during the formation of the tourmalines.

The Na/(Na+Ca) vs Fe/(Fe+Mg) discrimination diagram of alkali-calcic tourmalines (Figure 4.5.a) also proves the existence of three distinct group of tourmalines. Groups B and C plot in the schorl field, and Group A tourmalines lie in the feruvite area. Feruvite was first found by Grice and Robinson (1989) in Cuvier Island, New Zealand. Grice and Robinson (1989) suggested that feruvite was formed by hydrothermal replacement of silicates in a pegmatitic rock. Group C is characterized by its high Na/(Na+Ca) ratio. Group B tourmalines have Na/(Na+Ca) ratios between 0.53-0.86. Group A has the lowest Na/(Na+Ca) ratio which is less than 0.5. As a result of the Ca abundance in their X-sites, Group A tourmalines are found to be a member of calcic tourmalines and are named as feruvite. Groups B and C lie close to the dravite boundary. Their Fe/(Fe+Mg) ratios, indicate the presence of schorl-dravite solid solution, but all analyzed tourmalines are schorl in composition.

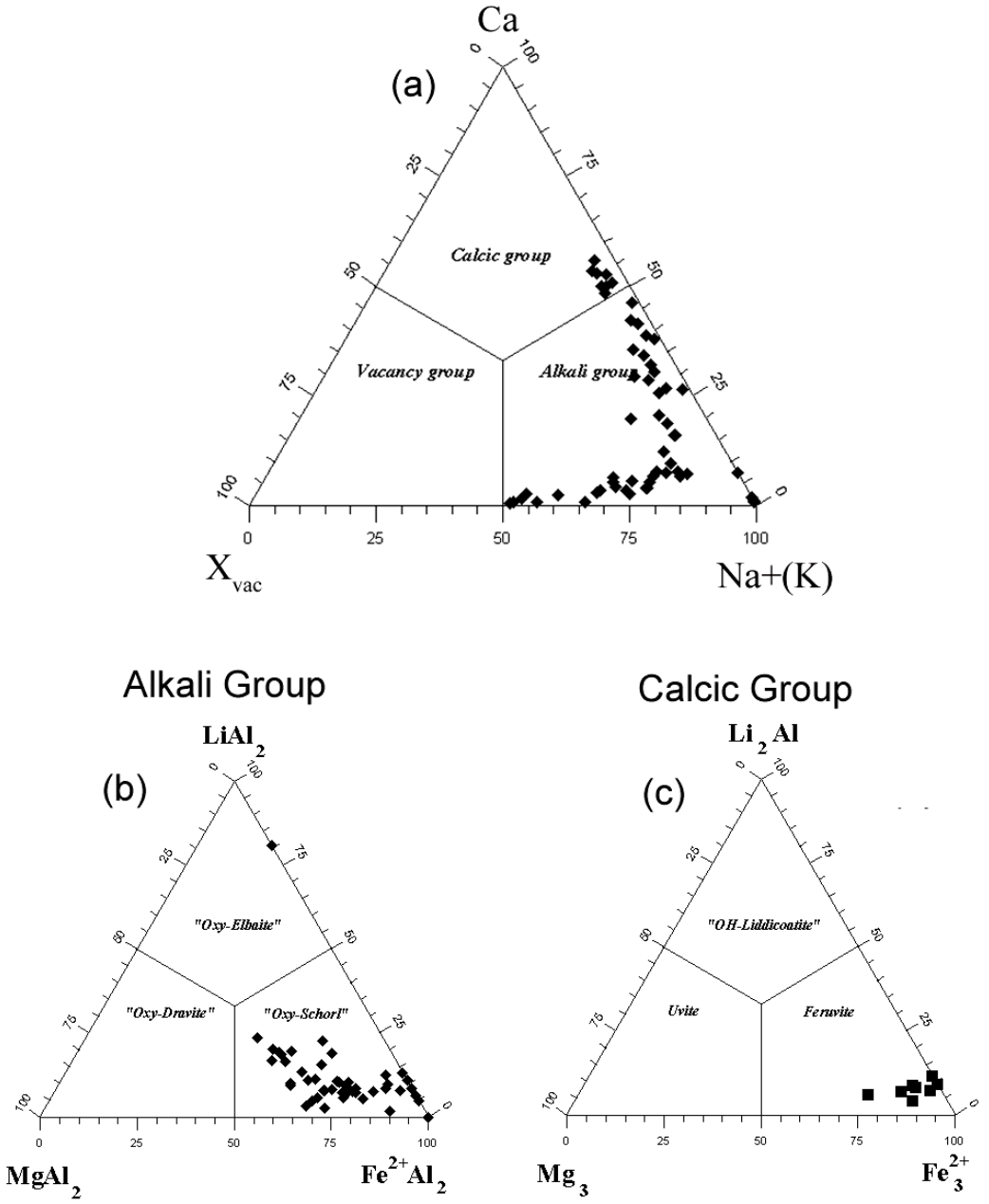

Figure 4.4: General chemical groups and subdivisions of the tourmalines. a) Classification of the principal groups of tourmaline based on X-site occupancy. b) Alkali tourmaline subgroups based on X and Y site occupancies. c) Calcic tourmaline subgroups based on X and Y site occupancies (from Hawthorne and Henry 1999).

The $X_{vac}/(Na+X_{vac})$ vs Mg/(Fe+Mg) discrimination diagram of alkali-X site vacant tourmalines (Figure 4.5.b) shows that all samples lie in the schorl field. Among the three groups, Group C tourmalines have the highest vacancies. As they have very low Ca contents, their X sites are dominated by Na and vacancy. Therefore, one of the main discrimination factors for the studied tourmalines are the Na-Ca amounts of their complex chemical formulae.

Figure 4.6 shows that changes from Group A to Group B are best described with the operation of the exchange vector $NaAlCa_{-1}Mg_{-1}$. Na increases at cost of Ca in Group B. Group C shows a reverse order, which is more consistent with the exchange vector $NaMg\square_{-1}Al_{-1}$. According to the exchange vector, vacancy and Al increase, and Na and Mg decrease within the group.

Dutrow and Henry (2000) explained this Na depletion in terms of albite crystallization and Keller et al. (1999) suggested that significant X-site vacancies and loss of Na indicate either partitioning of Na into coexisting albite or crystallization of alkali-deficient tourmalines from fluids that became depleted in alkalis as a consequence of albite precipitation. The presence of newly formed albite together with tourmaline in the studied samples also supports this idea.

Among the three groups, Group A has the highest Ca and low X-site vacancy. Compositional heterogeneity within the last generation (Group C) is best described by the exchange vector $\square AlNa_{-1}Mg_{-1}$. Changes from Group B to Group A are more consistent with operation of the exchange vectors $CaMg_3OH\square_{-1}Al_{-1}O_{-1}$ and $CaMg_2\square_{-1}Al_{-2}$ (Figure 4.7) and differentiation within the groups can also be described by these exchange reactions.

This general trend implies that Group A represents the less-evolved former portion of Group B tourmalines. Group A has the lowest Na and X-site vacancy, and Group B has relatively higher Na content. Low X-site vacancy in Group B tourmalines is due to the presence of Ca. In contrast to other groups, Group C tourmalines have high Na contents with minor Ca in their X-site. X-site vacancy increases as Na content decreases, resembling the removal of Na from the X-site during the formation of the Group C tourmalines.

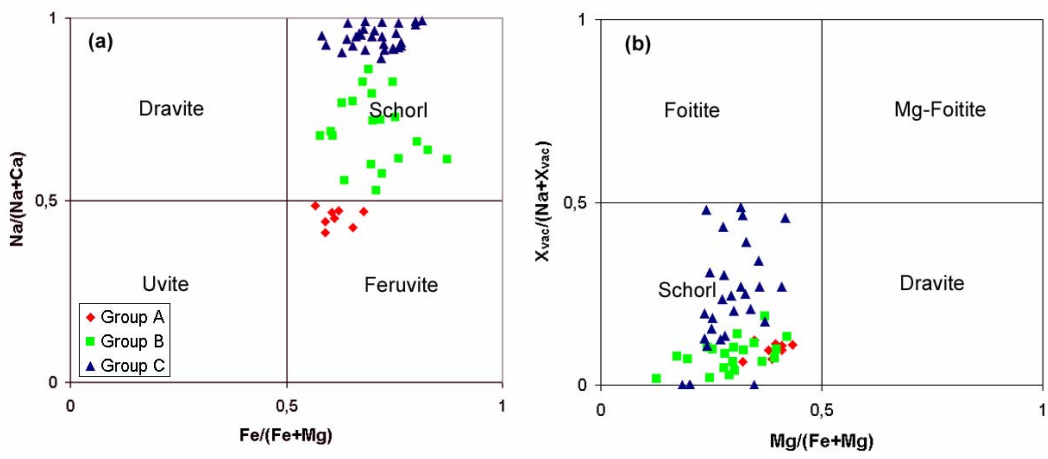

Figure 4.5: a) Plot of Na/(Na + Ca) vs. Fe/(Fe + Mg) ratios of tourmalines from the Kerkenez Granitoid. b) Plot of $X_{vac}/(Na+X_{vac})$ vs Mg/(Fe+Mg) ratios of tourmalines from the Kerkenez Granitoid.

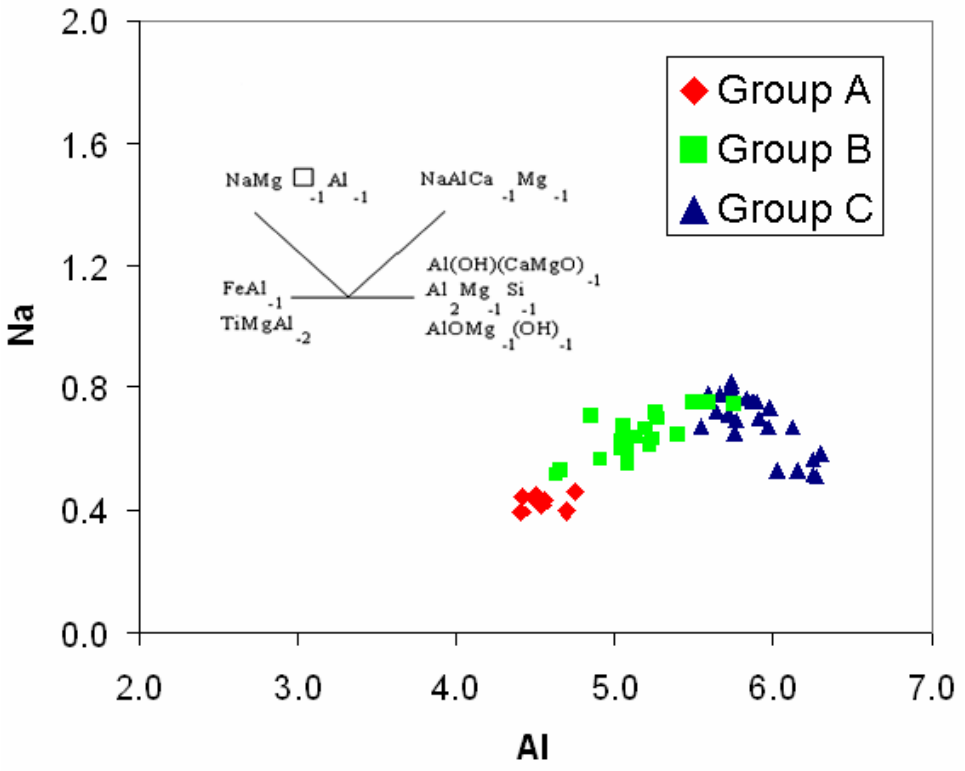

Figure 4.6: Plot of a Na vs. Al. The vectors represent the possible exchange operator that could have operated in these tourmalines

Plots of these tourmalines on the Mg vs Fe diagram clearly indicate that there is a gradual decrease in Fe and Mg contents from Group A to Group C (Figure 4.8.a). Group A tourmalines have the highest Mg amounts which can range up to 1.8. Group B tourmalines are rich in Fe but they have lower Mg contents compared to Group A. Group C has the lowest Mg and Fe contents. Fe contents decrease with increasing X-site vacancy in Group C tourmalines, which means that more evolved tourmalines have higher vacancies and less Na with respect to vacancy in their X-sites. This is also shown in Figure 4.8.b, Na content decreases as Fe+Mg content increases in Group C, and Group A and B shows a reverse order in which Na content gradually increases as Fe and Mg decrease. Group A has higher Fe+Mg contents than Group B, and enrichment in Fe in Group B can be explained by Fe-Mg exchange reaction or, in other words schorl-dravite solid solution.

Group A tourmalines have the lowest Al, and there is a gradual increase in Al and decrease in Fe toward the youngest group. Group B tourmalines have intermediate Al and high Fe contents; increase in Fe contents can be explained by the presence of schorl-dravite solid solution within Group B tourmalines (Figure 4.8.c). Figure 4.8.d shows that last generation of tourmalines (Group C) has the highest Li and the lowest Fe+Mg contents and represents a late stage of the magma body. The Ca-Fe(t)-Mg diagram of Henry and Guidotti (1985) (Figure 4.9) shows that all tourmaline generations plot in the Li-poor granitoids and associated pegmatites field. As a result, all three tourmaline generations have a similar magmatic source.

In the ternary plot of Al-$Al_{50}Fe(tot)_{50}$-$Al_{50}Mg_{50}$ (Henry and Guidotti, 1985) (Figure 4.10) Group A tourmalines plot in field 6 and close to field 3, which indicates that the first generation of tourmalines developed in an environment characterized by Fe-rich quartz–tourmaline rocks, calc-silicate rocks or metapelites. Group B tourmalines lie in fields 3 and 6, (Fe-rich quartz–tourmaline rocks, calc-silicate rocks, and metapelites Fe-rich quartz–tourmaline rocks hydrothermally altered granites), indicating the hydrothermal alteration within the granites. The final generation (Group C) plots in field 2, implying an environment of Li-poor granitic rocks and associated pegmatites and aplites.

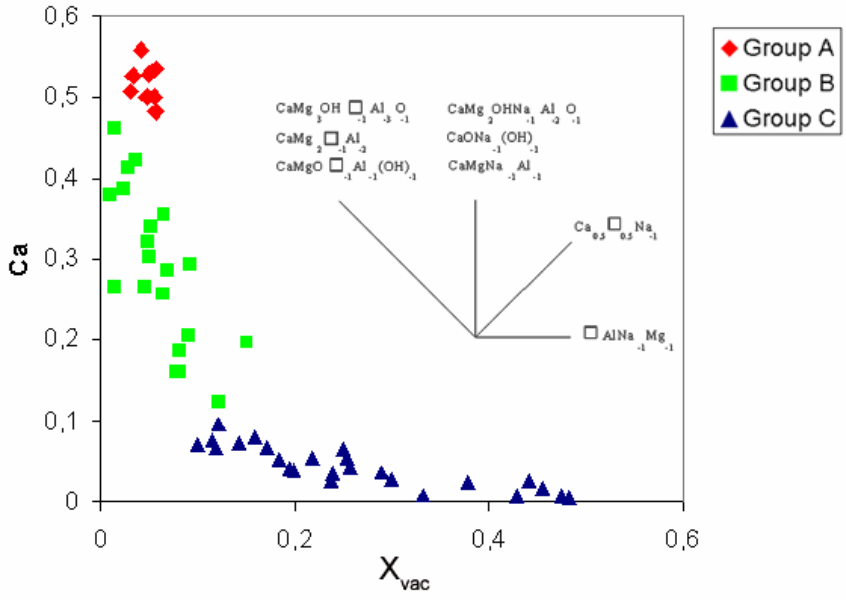

Figure 4.7: Plot of Ca vs. X_{vac}. The lines represent the possible exchange vectors that may have operated in these tourmalines.

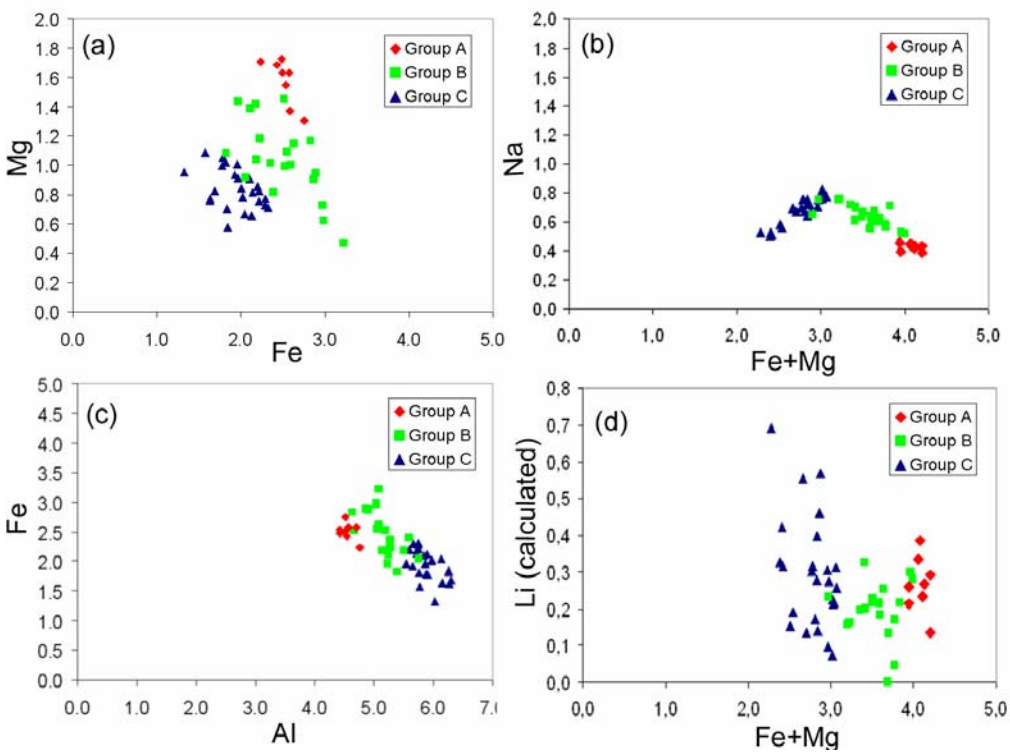

Figure 4.8: a) Plot of Mg vs. Fe; b) variation of Na against Fe+Mg; c) plot of Fe vs. Al; d) variation of Li against Fe+Mg. Li is calculated by stoichiometry.

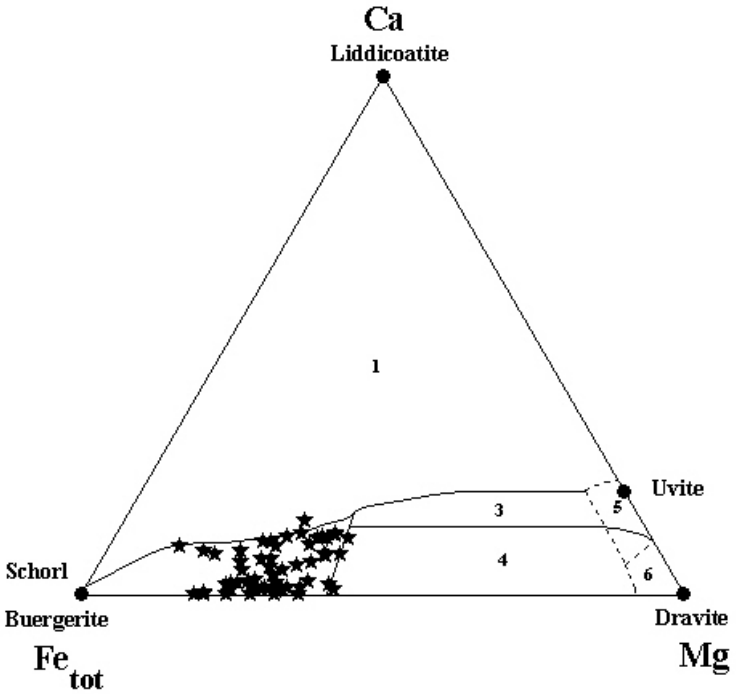

Figure 4.9: Microprobe compositions of tourmalines from the Kerkenez Granitoid plotted on Ca-Fe(t)-Mg diagram of Henry and Guidotti (1985). The fields are: 1) Li-rich granitoid pegmatites and aplites; 2) Li-poor granitoids and their associated pegmatites; 3) Ca-rich metapelites and metapsammites and calc-silicate rocks; 4) Ca-poor metapelites, metapsammites and quartz-tourmaline rocks; 5) metacarbonates; 6) metaultramafics.

The microprobe analyses show that there is a gradual change in the chemical compositions of the different three tourmaline generations. The general progression of the three generations implies that fluids giving way to their crystallization were generally undergoing fractionation and becoming successively enriched in Na, Al and Li, and depleted in Ca and Mg.

The first generation, Group A has Mg/(Mg+Fe) ratios between 0.35-0.44 and Na/(Na+Ca) ratios of 0.41-0.49. In contrast, later generations (Groups B and C) have nearly similar Mg/(Mg+Fe) ratios of 0.20-0.40 and 0.19-0.41, respectively. Group C tourmalines are characterized by their high X_{vac} and low Ca contents. They have very high Na/(Na+Ca) ratios (0.89-0.99). Group B tourmalines have lower Na/(Na+Ca) ratios (0.53-0.86) due to their lower $X_{vac,}$ and higher Ca contents with respect to Group C tourmalines.

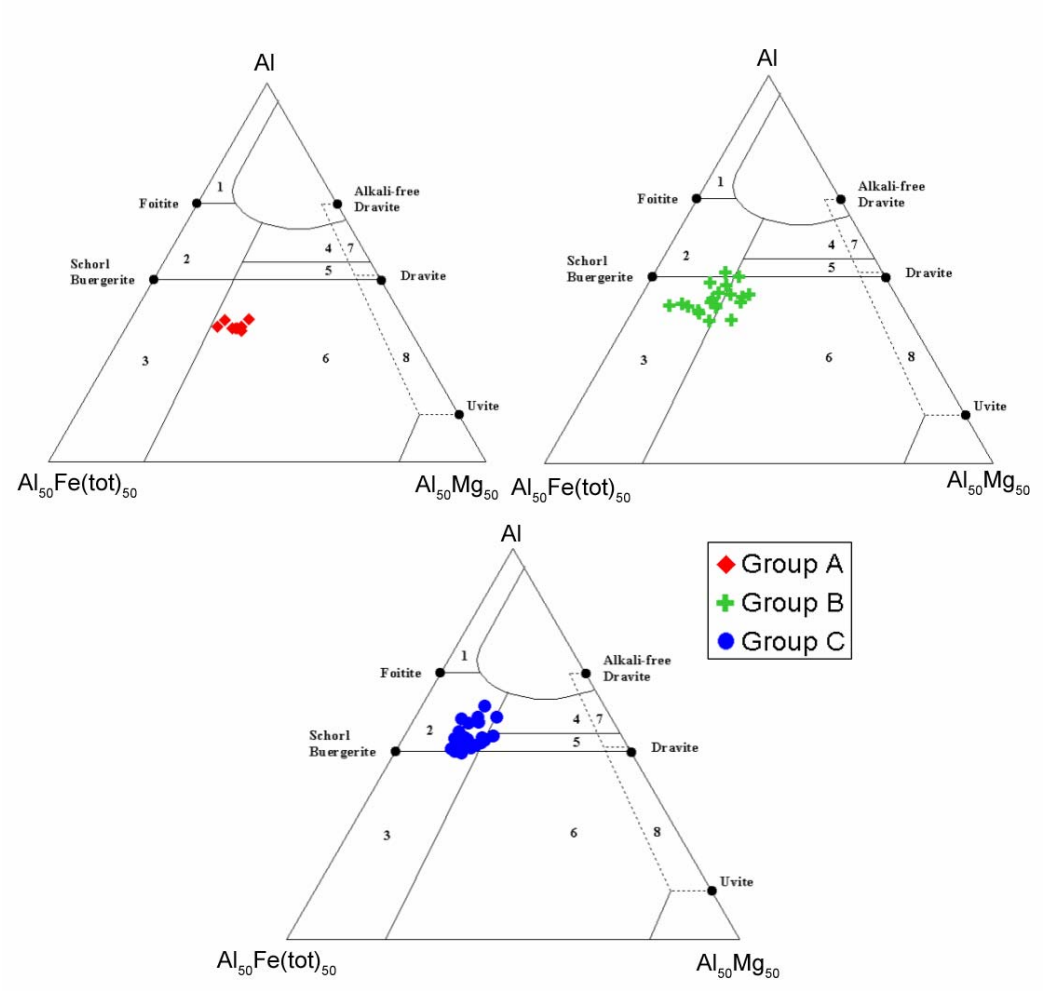

Figure 4.10: Al-$Al_{50}Fe(tot)_{50}$-$Al_{50}Mg_{50}$ diagram in molar proportions for tourmaline from the Kerkenez Granitoid (Henry and Guidotti 1985). 1) Li-rich granitic pegmatites and aplites; 2) Li-poor granitic rocks and associated pegmatites and aplites; 3) Fe-rich quartz–tourmaline rocks hydrothermally altered granites ; 4) metapelites and metapsammites coexisting with an Al-saturating phase; 5) metapelites and metapsammites not coexisting with an Al-saturating phase; 6) Fe-rich quartz–tourmaline rocks, calc-silicate rocks, and metapelites; 7) Low-Ca meta-ultramafic and Cr, V-rich metasedimentary rocks; 8) metacarbonates and meta-pyroxenites.

There is a successive enrichment in Na, Al and Li from Group A to Group C, indicating that later fluids are enriched in these components. Figure 4.11 shows that chemical variation in these tourmaline groups has been somehow controlled by elbaite substitution ($LiAlFe_{-2}$), an indicator of fractionation and internal evolution of pegmatites and of compositional evolution of tourmalines in pegmatites (Keller et al., 1999; Roda-Robles et al., 2004)

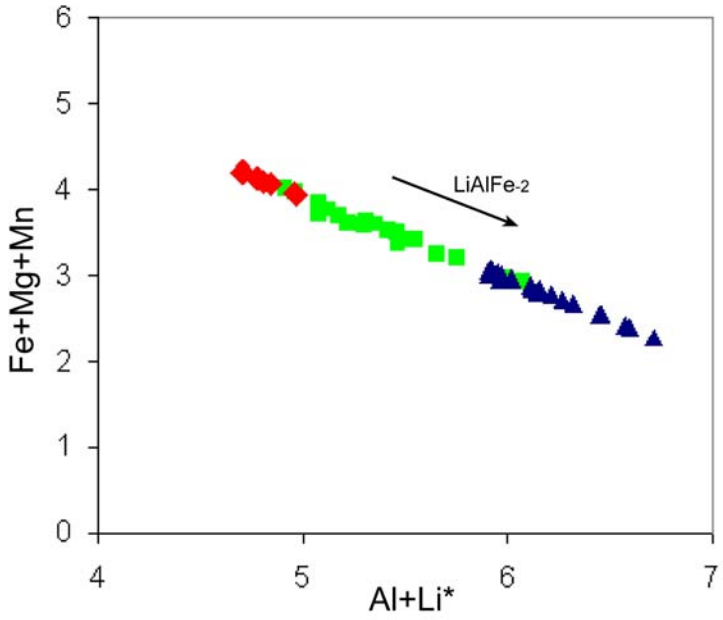

Figure 4.11: Plot of Fe+Mn+Mg vs. Al+Li. Arrow indicates elbaite substitution. Symbols are the same as in previous figures (* calculated by stoichiometry).

In conclusion, study of these tourmaline compositions indicates that they have a magmatic origin. The source of the tourmalines is thought to have been a deep seated, but as unproven relict magma chamber with preserved pegmatitic fluids. Detailed study of the compositional differences of the tourmaline groups and their hosts may help to elucidate the evolution of the late-stage pegmatitic fluids in the Yozgat Batholith.

CHAPTER 5

WHOLE ROCK GEOCHEMISTRY

5.1. Introduction

Twelve representative bulk samples were collected from the quartz-tourmaline-breccias, quartz-tourmaline rocks and quartz-tourmaline veins for major-and trace-element analyses. The results of the analyses are reported in Tables 5.1 and 5.2.

5.2. Major Oxides

The studied samples have variable SiO_2 wt% content (66.11-91.39wt %), but most of the samples have SiO_2 contents between 66-75%. Sample 15c contains abundant quartz and this is reflected by its bulk chemistry with its very high SiO_2 (91.39%wt) contents. The Al_2O_3 vs SiO_2 binary diagram (Figure 5.1.a) shows that most of the samples have nearly identical Al_2O_3 contents. On the other hand samples 15c and 75 have lower Al_2O_3 relative to the other samples. Sample 75 is characterized by its high Fe_2O_3 content, and samples 15c and 72e have the lowest Fe_2O_3 contents (Figure 5.1.b). These properties can be explained by the mineral contents of the samples. Sample 75 includes high amounts of opaque minerals, and enrichment in Fe_2O_3 indicates that the opaque minerals are rich in Fe. As suggested earlier, sample 15c has high quartz content and sample 72e is composed of thin tourmaline-rich veins and includes high amounts of granitic fragments. Sample 4 is different from the other samples in terms of CaO contents (Figure 5.1.c) this is due to the presence of calcite in the sample. Sample 72e has high Na_2O contents (Figure 5.1.d). As discussed earlier, this sample contains granitic fragments and its enrichment in Na_2O can be explained by the presence of plagioclase. On the basis of K_2O contents, Sample 1a is also different from the other samples (Figure 5.1.e), the presence of K-feldspar is reflected by the increase in K_2O. TiO_2, Cr_2O_3, MnO and P_2O5

contents are quite low in all samples, and are variable. MgO contents are variable, and samples 72e and 15c have the lowest MgO (Figure 5.1.f).

Table 5.1: Major element analyses (wt%) of quartz-tourmaline rocks and tourmaline-breccias.

Samples	1a	1d	1e	1g	4	5	15c	61	72	72a	72e	75
SiO_2	68.13	68.81	67.98	71.27	69.46	71.13	91.39	68.13	69.79	66.11	75.29	70.63
Al_2O_3	14.41	14.69	14.18	13.75	12	12.7	3.13	16	12.6	14.5	12.4	8.25
Fe_2O_3	8.68	10.7	11.3	10.1	10.2	9.24	2.89	10.9	10.9	12.4	4.72	17.03
MgO	1.47	2	2.21	1.39	2.81	2.44	0.55	0.98	2.72	3.22	0.5	1.59
CaO	0.69	0.5	0.63	0.45	2.16	0.91	0.21	0.29	0.56	0.58	0.47	0.26
Na_2O	0.88	1.22	1.22	1.02	0.89	0.74	0.26	1.06	1.23	1.16	5.67	0.66
K_2O	3.48	0.05	0.04	0.04	0.02	0.65	0.02	0.03	0.11	0.05	0.1	0.02
TiO_2	0.27	0.32	0.29	0.33	0.18	0.21	0.02	0.56	0.2	0.21	0.2	0.1
P_2O_5	0.05	0.08	0.09	0.08	0.07	0.03	0.03	0.11	0.02	<.01	0.03	0.01
MnO	0.03	0.03	0.04	0.03	0.05	0.03	0.03	0.04	0.03	0.04	0.02	0.02
Cr_2O_3	0.12	0.19	0.13	0.12	0.06	0.09	0.14	0.13	0.08	0.08	0.08	0.154
LOI	0.8	1.1	1.4	1.4	2	1.6	1	1.5	1.3	1.6	0.6	1.1
Total	99	99.7	99.5	100	99.9	99.8	99.7	99.7	99.6	99.9	100	99.83

Consequently it can be suggested that the rocks are especially rich in SiO_2, Al_2O_3 and Fe_2O_3, other constituents occur in minor amounts, and some variations can be explained by the presence of discrete mineral phases. This chemical behavior parallels with the tourmaline chemistry. In Chapter 4, tourmalines were suggested to be Fe-rich schorls and feruvites, they consist mainly of Fe_2O_3, Al_2O_3 and SiO_2.

The problem is the paucity of B, as tourmalines are borosilicate minerals which, on average, contain 10 wt% BO_3, thus, higher B contents should be expected. Trace-element analyses show that the B content of the samples varies between 37-377 ppm, which is not in accordance with the amount of tourmaline in the whole-rock samples. Most probably, the aqua regia used for decomposition of the whole rock samples in ACME Laboratories, did not totally dissolve BO_3, because BO_3 is quite resistant to acid leaching. Best results could be obtained by Na_2O_2 fusion; unfortunately this type of analysis could not be performed.

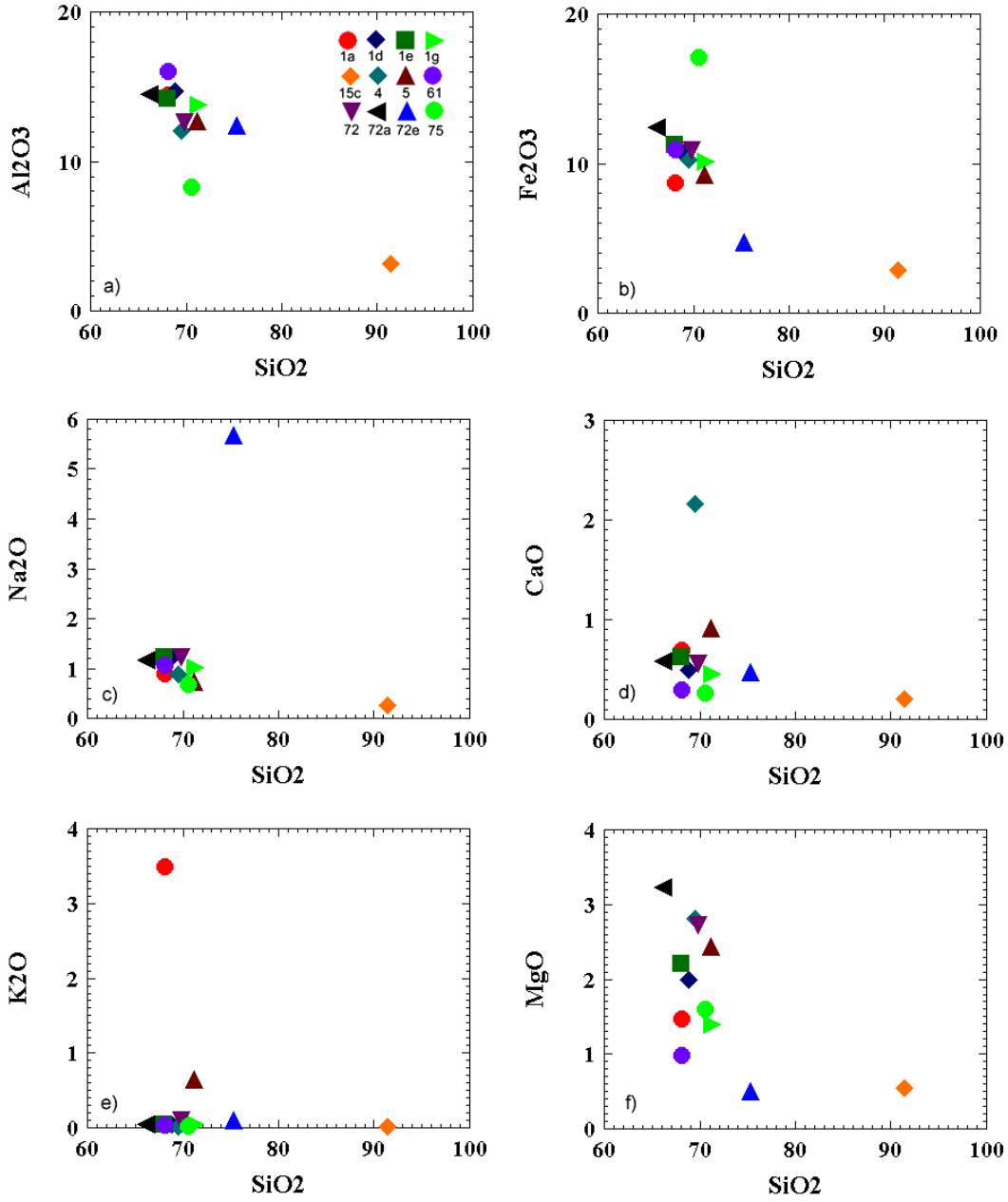

Figure 5.1: Harker diagrams of the studied samples (all values are in wt%).

5.3. Rare-Earth Elements

According to chondrite normalized REE diagrams, the samples display two different REE patterns. The first group of samples (Group 1) (1a, 1d, 1e, 1g, 4, 5, 15c, 61) is enriched in LREEs and has a flat, depleted chondrite normalized HREE pattern (Figure 5.2.a). The second group of samples (Group 2), (72, 72a, 72e, 75) is depleted in LREEs relative to HREEs and includes lower concentrations of REEs. The two groups display very different, nearly opposite chondrite-normalized REE patterns (Figure 5.2.a). Unfortunately, because of the very fine crystal size of the tourmalines, no tourmaline crystals were analyzed individually and tourmaline – tourmaline-rich rock REE characteristics can not be compared. However, it is important to note that, typically tourmaline separates exhibit REE patterns very similar to their corresponding whole-rock samples (Raith et al. 2004).

Petrographical studies of the samples revealed that these two chemically different groups are also different from each other in terms of textural features and mineralogy. Group 1 samples generally include coarser tourmaline crystals and cataclastic deformation effects are minor compared to group 2. The tourmalines do not show any signs of deformation. Group 2 samples were rebrecciated after the D1 deformation, and some of them include various tourmaline porphyroclasts. Group 2 samples were also affected more by later hydrothermal activity. Another important discrimination factor is the mineralogy of the samples. Apart from some small exceptions, all samples include significant amounts of quartz and tourmaline.

The presence of minerals containing small amounts of REEs, such as quartz or carbonates, has a diluting effect on REE concentrations (McLennan 1989). Therefore, some dilution of REEs is likely in the studied samples.

Although mineral contents are almost the same (tourmaline+quatz) in most of the samples, group 2 samples contain high amounts of opaque minerals, which appear to change the REE concentrations and the REE patterns of group 2 samples.

Table 5.2: Trace element analyses of quartz-tourmaline rocks and tourmaline-breccias.

Samples		1a	1d	1e	1g	4	5	15c	61	72	72a	72e	75
Be	ppm	2	3	5	3	1	2	2	23	2	2	1	2
Co	ppm	4.4	7.2	8.4	11.8	4.9	5.2	3.6	2.6	15	16.2	5.1	3.7
Cs	ppm	3.1	0.4	0.6	0.4	0.3	0.5	1	0.5	0.5	0.2	0.5	0.1
Ga	ppm	32.7	38.4	38.1	29.9	36.7	33.4	7.6	32.1	30.3	32.9	14.1	13.9
Hf	ppm	4.4	5.6	5.3	5.9	1.2	3	<0.5	9.5	3.5	4.2	3.7	1.8
Nb	ppm	4.7	5.8	6.6	11.7	<0.5	1.7	1.5	40.4	0.9	0.5	2.2	0.8
Rb	ppm	133.3	1.5	1.6	1	<0.5	19.7	1.6	1.2	7.3	2.8	3.3	0.6
Sn	ppm	7	14	30	9	22	16	4	37	43	51	12	123
Sr	ppm	579.7	384.6	507.2	310.1	655.2	548.1	137.3	317.5	213.3	222.7	149.6	110.2
Ta	ppm	0.3	0.5	0.6	0.8	<0.1	0.2	0.1	1.6	<0.1	<0.1	0.1	<0.1
Th	ppm	24.7	24.9	22.1	31	4.7	16.4	1.3	149.7	0.6	0.7	1.4	0.3
U	ppm	3.3	2.4	2.6	3.6	1.1	1.4	0.3	17.1	0.9	0.8	0.8	0.8
V	ppm	29	28	48	30	148	65	19	67	97	100	32	39
W	ppm	7.3	5.9	4.1	16.5	0.5	1.6	1.4	24.4	12.8	10.6	5.9	217.3
Zr	ppm	153.2	187.6	171.6	209.1	38.4	100	7.9	402.3	121.2	125	110.9	54.8
Y	ppm	6.7	3.6	3.8	7.8	2.9	5.2	4.1	24.4	8.4	8.3	14.8	20.5
La	ppm	36.4	12.5	13.7	32.6	2.2	24	26.9	98	1.3	1.6	1.7	0.7
Ce	ppm	59.3	11	20.8	20.3	3.5	57.8	8.3	64.7	2.4	1.7	3.1	1.5
Pr	ppm	5.55	1.89	2.32	5.38	0.4	3.89	3.72	11.61	0.3	0.33	0.35	0.13
Nd	ppm	17.9	6	7.4	16.1	1.5	11.7	11.2	33.7	1.1	1.1	1.3	0.6
Sm	ppm	2.5	0.9	1	2.4	0.3	1.7	1.5	4.6	0.3	0.3	0.6	0.4
Eu	ppm	0.46	0.21	0.28	0.48	0.22	0.34	0.35	0.8	0.16	0.17	0.24	0.15
Gd	ppm	1.6	0.65	0.74	1.57	0.45	1.09	1.03	3.01	0.57	0.66	1.09	1.59
Tb	ppm	0.25	0.11	0.11	0.25	0.07	0.18	0.19	0.6	0.15	0.15	0.25	0.37
Dy	ppm	1.17	0.5	0.65	1.26	0.44	0.9	0.71	3.46	1.04	1.06	1.93	2.7
Ho	ppm	0.2	0.12	0.13	0.26	0.09	0.17	0.13	0.72	0.29	0.31	0.5	0.68
Er	ppm	0.59	0.35	0.46	0.81	0.22	0.53	0.35	2.69	1.07	1.08	1.77	2.12
Tm	ppm	0.11	0.06	0.07	0.13	<0.05	0.07	0.06	0.45	0.15	0.2	0.3	0.34
Yb	ppm	0.66	0.41	0.57	0.94	0.25	0.6	0.29	2.73	1.49	1.66	2.1	2.34
Lu	ppm	0.12	0.1	0.13	0.17	0.05	0.11	0.06	0.46	0.3	0.33	0.4	0.48
Ba	ppm	814.8	18.2	33	13.5	19.4	105.1	21.9	7.8	34	17.5	30.6	6.4
Ni	ppm	37	90	60	42	21	41	72	29	51	40	31	84
Sc	ppm	3	2	4	3	3	7	2	3	21	22	14	7
Mo	ppm	24.1	39	26.4	22.2	10.6	16.2	25.8	24.8	16.2	13.7	17.5	33.2
Cu	ppm	31.4	57.1	36.8	48.9	16.1	20.2	36.8	34.8	26.3	19.2	21.2	37.5
Pb	ppm	11.1	7.7	14.1	50.9	58	15.3	82	16.2	25.5	20.3	42	16.2
Zn	ppm	7	8	6	7	3	4	6	6	7	5	9	5
Ag	ppm	0.1	0.1	0.1	0.5	0.1	0.1	0.3	<0.1	0.2	0.1	0.1	0.7
Mn	ppm	81	92	175	98	190	82	196	74	124	159	115	54
Fe	%	0.57	0.93	0.85	0.72	0.3	0.41	0.55	0.7	2.3	2.38	2.39	7.48
As	ppm	2.7	2.3	3.4	8.3	3.4	2.1	5.2	16.6	4.8	2.1	1.7	1.3
Au	ppb	1.7	3.7	5.1	3	1.4	25.7	1.3	24.2	26.7	0.6	97.5	3.7
Cd	ppm	<0.1	<0.1	<0.1	<0.1	<0.1	<0.1	0.1	0.1	0.1	0.1	0.1	<0.1
Sb	ppm	0.2	0.3	0.3	0.3	0.2	0.2	0.7	1.3	0.7	0.2	0.2	0.2
Bi	ppm	0.5	1.4	6.4	2.6	0.3	0.6	0.4	0.2	0.9	0.4	0.8	0.6
Cr	ppm	771.7	1230	836	741.3	350.3	499.8	733.3	778.7	473.9	419.1	518.4	875.4
B	ppm	219	377	292	249	137	165	70	276	156	159	37	215

Group 1

Group 1 samples are characterized by a descending chondrite normalized LREE and nearly flat HREE pattern (Figure 5.2.b). Samples 4 and 61 are different from the general progression of the group; 61 is enriched whereas 4 is depleted in REEs with respect to the rest of the group. Sample 61 is texturally quite different from the other samples; it contains coarse, acicular, radiating tourmaline crystals. This difference can also be ascertained from the REE concentrations of the sample; it is especially enriched in La, and other LREEs are not very different from the general progression of the group. Another distinction is the enrichment in HREEs with respect to the other samples. Sample 4 is characterized by its low REEs; this may be due to the diluting effect of calcite, or the presence of some opaque minerals. If these samples (4 and 61) are not considered, group 1 samples exhibit similar chondrite-normalized REE patterns and concentrations (Figure 5.2.b). Major variations occur in Ce; samples 1d, 1g, 15c and 61 are depleted in Ce. In addition to Ce, some variations occur in the Ho and Tm of the group. Only sample 4 has a positive Eu anomaly, the rest of the group have a flat pattern with no distinct enrichment or depletion.

Group 2

Group 2 samples are characterized by low concentrations of REEs and slightly decreasing LREE and increasing HREE patterns (Figure 5.2.c). Chondrite normalized REE patterns of samples 72, 72a and 72e are similar. The only difference is the negative Ce anomaly in sample 72e. Hydrothermal alteration, regional metamorphism and/or influence of accessory minerals can produce REE mobility in tourmalinites (Ruiz et al., 2003). Thus especially the LREEs of group 2 samples may have been mobilized during formation of opaque phases and/or later faulting and hydrothermal events. Sample 75 has a different pattern; it display strong LREE depletion (especially Pr and Nd) and HREE enrichment. As suggested earlier, sample 75 is rich in Fe_2O_3 and includes the highest percentage of opaque minerals among the group 2 samples. Therefore, the different REE concentrations of the group 2 samples are most probably related to the abundance of opaque minerals.

As discussed in chapter 1, tourmalinites can form via various mechanisms (metasomatic replacement of clastic metasediments by B-rich hydrothermal fluids of magmatic derivation; syngenetic precipitation from boron-rich submarine-exhalative fluids; regional metamorphism of boron-rich sediments or evaporites) and each mechanism is reflected through different REE signatures.

High-temperature acidic hydrothermal fluids discharged from active submarine vent sites are very low in ΣREEs but show a pronounced enrichment in LREEs, and especially in Eu (Michard 1989; Klinkhammer et al., 1994; Douville et al., 1999). Tourmalinites of exhalative origin preserve comparable patterns in the more proximal and distal parts of hydrothermal systems. With increasing distance from the source, the patterns become less LREE enriched and may develop negative Eu and positive Ce anomalies due to changes in physicochemical parameters (Lottermoser, 1989). Proximal exhalites have similar LREE enrichments but positive Eu anomalies; distal ones can have negative Eu anomalies (Lottermoser, 1989). For tourmalinites formed in a marine evaporitic environment, there should be a strong seawater signature (very low ΣREE, negative Ce and Eu anomalies) or flat REE patterns (Frimmel and Jiang, 2001). Tourmalinites formed in a non-marine evaporitic setting also have low ΣREEs and flat REE patterns (Slack, 1993).

REE patterns of the studied samples with enriched-depleted LREEs and nearly flat HREEs without significant negative Eu anomalies are very different from the before mentioned REE characteristics of classical tourmalinites.

Some samples (1a, 1d, 1g and 61) show some Ce depletions but according to Raith et al. (2004), Ce variations are unrelated to the tourmalinisation process and Ce anomalies in the tourmaline rocks are inherited from the precursor or host rock, possibly reflecting an oxidation stage prior to tourmalinization. None of the studied samples exhibit negative Eu anomalies; on the other hand, sample 4 has significant Eu enrichment. Lack of negative Eu anomalies may be due to the Eu enrichment of boron-rich fluids (Slack, 1993). Therefore, the

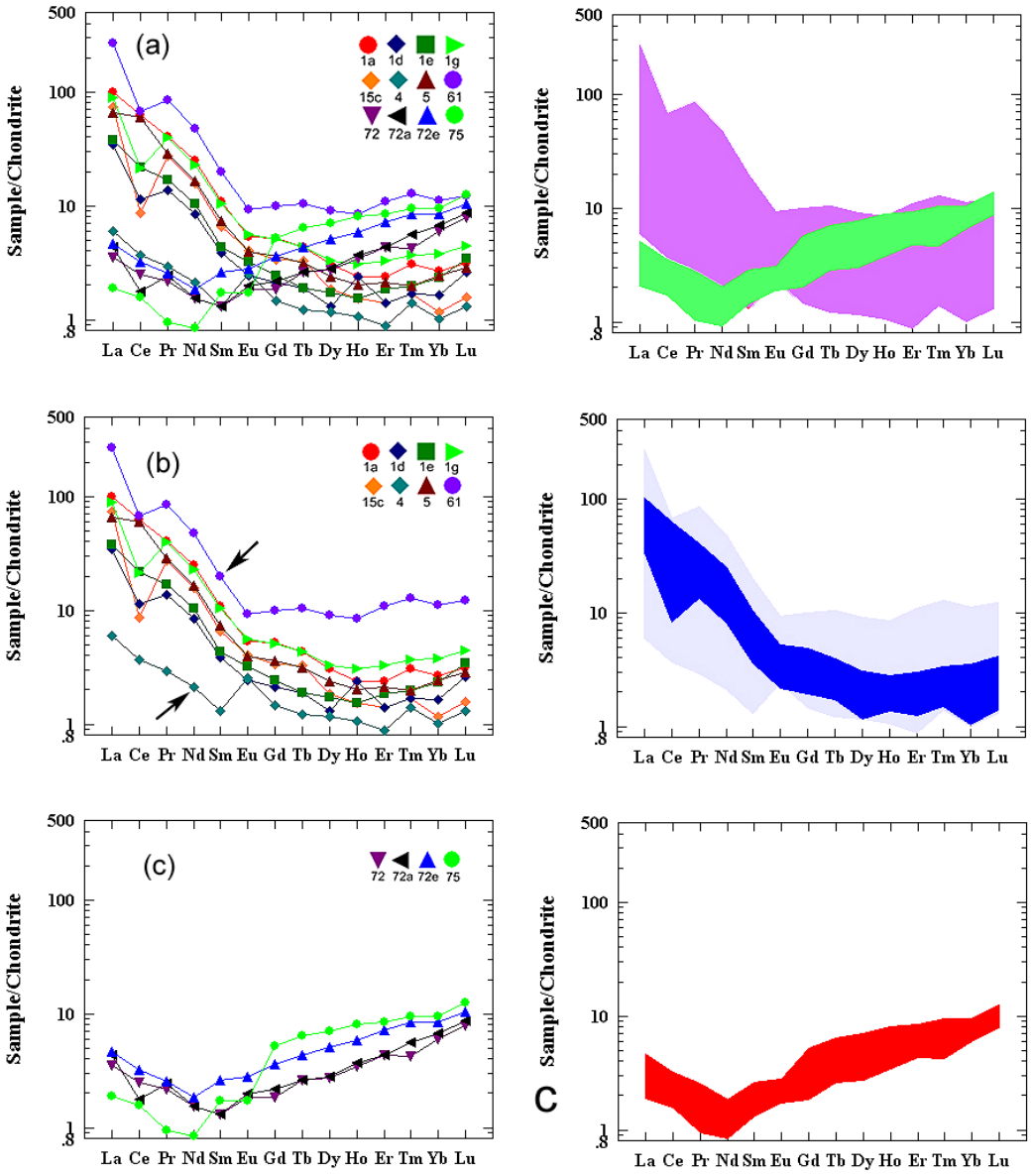

Figure 5.2: Chondrite normalized REE diagrams of the studied samples. a) Two groups together; the purple pattern represents group 1 and green pattern represents group 2; b) Chondrite-normalized REE pattern and concentrations of Group 1, dark colored pattern represents the chondrite normalized REE pattern of the group 1 samples, except 61 and 4; c) Chondrite-normalized REE pattern and concentrations of Group 2

formation mechanism of the tourmaline-rich rocks of Kerkenez granitoid should be different from those mentioned above. Unfortunately, tourmaline-breccia studies are scarce in the literature and they lack REE geochemical investigations, so no REE comparison could be made with the tourmaline-breccias from other locations.

5.4. Spider Diagrams

Chondrite-normalized spider diagrams indicate that both groups have similar spider-diagram patterns. Group 1 samples have similar patterns, but their trace-element concentrations are variable (Figure 5.3.a). Sample 61 is enriched especially in Th and U, and within the group some variations occur in Ce, K and Sr. Group 2 samples are nearly identical to one another, with similar trace-element concentrations and patterns (Figure 5.3.b). Group 2 samples have nearly the same spider-diagram patterns and the trace-element concentrations are also quite similar, the only variation is in Ce.

Figure 5.3.c shows that the spider diagrams of the two groups are quite similar to each other. Consequently, it can be concluded that the groups are cogenetic. Major concentration differences are in Ba, Th, U, Nb, Ce, on the other hand, the Ti, Tb, Y, Cr, Mn, Ni, Zn and Ta concentrations of the two groups are almost the same. Group 1 samples have higher trace element concentrations than Group 2. This may be due to the mobilization of trace elements by later faulting and deformation or to the formation of opaque minerals, as indicated by the presence of tourmaline porphyroclasts and abundant opaque phases within the Group 2 samples.

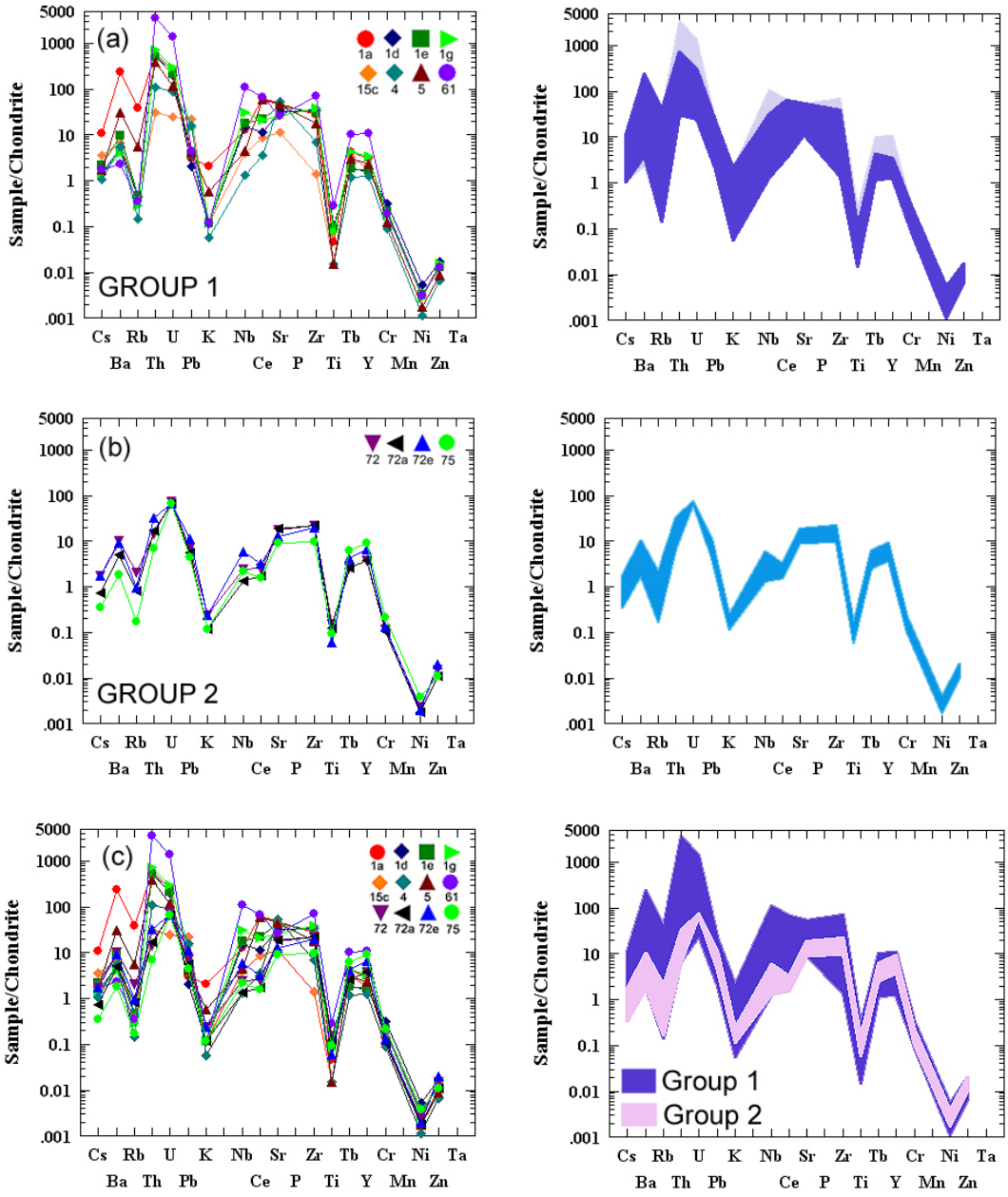

Figure 5.3: Chondrite-normalized spider diagrams of the studied samples. a) Group 1, the dark colored pattern represents the chondrite normalized pattern of the group 1 samples except 61; b) Group 2; c) two groups together; the blue pattern represents group 1 and the pink pattern represents group 2.

CHAPTER 6

DISCUSSION ON THE FORMATION OF THE QUARTZ-TOURMALINE ROCKS

In the last twenty years, tourmalines have been the subject of many studies. Tourmalines are natural laboratories which can 'record' the environment of formation, and monitor the physical and chemical changes in the environment and associated fluids (Henry and Dutrow, 1996). Although there have been many studies on tourmalines, tourmaline-breccia studies have not been plentiful. There are limited numbers of tourmaline-breccias worldwide. Many tourmaline-breccias are related to ore deposits, mainly of sulphides, tin and gold (Raith et al., 2004). Thus studying tourmaline-breccias and quartz-tourmaline rocks in the Kerkenez Granitoid is extremely important in order to understand the genesis and evolution of these enigmatic rocks, and to emphasize the importance of tourmaline in petrological studies.

Kerkenez Granitoid is the host rock of quartz-tourmaline-rich rocks. Petrographical studies show that none of the granitoids (HB and AFM) contain tourmaline or any other boron-rich mineral. If required physical and chemical conditions are not met, boron prefers to be in the melt stage and, consequently boron bearing minerals cannot crystallize from the melt (London et al., 1996). In the present case, boron-rich fluids were expeled into the wall rock and produced extensive tourmalinization. If this was the case for the Kerkenez Granitoid, at least some tourmalinization or tourmaline veins should be present within the contact zone of the Kerkenez Granitoid and the intruded metamorphic units. But there is no reported tourmalinization in the area. Therefore, petrography and field observations together suggest that the Kerkenez Granitoid was not enriched in boron during its emplacement into the CAO and CAM and cannot be the direct source of the tourmalines.

The studied rocks are characterized by cataclastic-brecciated textures and dark color due to tourmaline cementation. Local jigsaw-puzzle textures and mineral fillings indicate fluid-assisted fracturing associated with tectonic movements (Lorilleux et al., 2002). Therefore, the presence of jigsaw-puzzle textures with non-oriented quartz fragments, the angular and weakly rounded character of the rock-mineral fragments, a paucity of corrosion and intensive tourmaline cementation in the Kerkenez Granitoid indicate that the breccias formed by fluid-assisted brecciation which was associated with tectonic movements. The presence of angular fragments show that, the movements were not sufficient to round them and the lack of well-rounded fragments and corrosion indicates that the brecciation has a mechanical origin rather than a chemical origin. The presence of flow-like features indicates cataclastic flow and/or high fluid activity which reflect the cohesive nature of the breccias. Immature breccias have a low percentage of matrix and contain weakly corroded and/or abraded and slightly rotated fragments. As the breccia evolved to more mature stage, an increase in rotation of grains, corrosion, and/or abrasion occurred and a matrix component developed (Laznicka, 1988). In that sense, the Kerkenez tourmaline-breccias can be considered as immature fluid-assisted tectonic breccias. Breccias with higher matrix content, and sub-rounded quartz and tourmaline fragments, can be defined as mature breccias that evolved to higher maturities by reactivation of faults during new tectonic movements and brecciation periods. Consequently, it can be concluded that tectonic movement and associated brecciation in the Kerkenez Granitoid was polyepisodic.

The presence of tourmaline-breccia fragments in the Eocene sandstones and conglomerates indicates that brecciation took place within a time range between Late Cretaceous and Eocene.

Petrographical investigations revealed the presence of at least three different periods of deformation. D1, the first deformation, was responsible for the cataclastic deformation and associated brecciation. D1 is believed to have been related to a sudden, major faulting event, which broke, fractured and granulated the host granitoid rocks. Tourmaline-breccia zones and tourmalinized faults have trends similar to the regional structural trend (NE-SW) (Dirik and

Göncüoğlu, 1996), possibly indicating that cataclastic deformation (D1) was related to regional tectonic events. Cataclastic deformation was followed by boron-rich fluid infiltration into these deformed weak zones. This fluid emplacement was most probably explosive because boron rich fluids also produced some deformation and brecciation within the studied rocks by dislocating grains and producing local jigsaw-puzzle textures, either by fluid pressure or volume increase via tourmaline crystallization.

The host-rock granitoid includes significant amounts of feldspar, hornblende and biotite, but these minerals are generally absent in the studied rocks. Although tourmaline-breccias include some granitic minerals and rock fragments, these are entirely missing in the quartz-tourmaline rocks. This is thought to be related to intensive tourmalinization; boron-rich fluids attacked feldspars and mafic minerals and replaced these minerals with tourmaline, so the process resulted in a rock which comprises only quartz and tourmaline (Deer et al., 1996). Unfortunately, as suggested by London et al. (1996), replacement textures have not been observed. Not only replacement textures but also cataclastic textures have been overprinted in the quartz-tourmaline rocks. These rocks generally lack a brecciated or cataclastic texture, but the presence of deformed and recrystallized quartz together with new, undeformed quartz show that quartz-tourmaline rocks and tourmaline-breccias are genetically similar. The quartz-tourmaline rocks are probably the intensely tourmalinized equivalents of the tourmaline-breccias. The major difference is undoubtedly the amount of fluid-rock interaction. The quartz-tourmaline rocks likely formed in an environment of higher fluid activity. Subsequent deformation (D2) is represented by more grain-size reduction, increase in the matrix component, and the presence of tourmaline porphyroclasts. The last deformation (D3) thought to have been associated with younger faulting activity urelated to tourmaline-breccia formation.

Petrographic investigations also show that the tourmalines have different modes of occurrence, and that there are three optically different tourmaline generations in the studied rocks. Simply, they can be differentiated from one another as a blue pleochroic (oldest) generation, a blue-green pleochroic (intermediate)

generation and a green-light green pleochroic (youngest) tourmaline generation. Microprobe analyses reveal that optically different groups also differ from one another in terms of chemical composition, and a gradual change in composition has been observed within these three tourmaline groups. The general progression of the three generations implies that fluids were becoming successively enriched in Na, Al and Li and depleted in Fe and Mg. In addition to this Mg/(Mg+Fe) and Na/(Na+Ca) ratios indicate that the tourmaline-crystallizing boron rich fluids evolved with time. Therefore, the fluid composition must have changed at least three times during the formation of tourmaline-breccias. The Ca-Fe(t)-Mg diagram of Henry and Guidotti (1985) (Figure 4.10) shows that all tourmaline generations plot in the Li-poor granitoids and associated pegmatites field. In the ternary Al-$Al_{50}Fe(tot)_{50}$-$Al_{50}Mg_{50}$ plot (Henry and Guidotti, 1985) (Figure 4.11), it was found that, the tourmalines developed in environments characterized by Fe-rich quartz–tourmaline rocks, calc-silicate rocks, and metapelites, hydrothermally altered granites and Li-poor granitic rocks, and associated pegmatites and aplites.

Geological, petrological and geochemical relations indicate that the tourmaline occurrences have a magmatic origin and that tourmaline forming boron-rich fluids were derived by magmatic-hydrothermal processes. Here the word ‘hydrothermal’ indicates only that tourmaline crystallized from some sort of fluid as opposed to magma. However this yields no distinctions regarding the ultimate origins of the fluids or the tourmaline forming components (London and Manning, 1995). According to London and Manning (1995), quartz-tourmaline veins and massive tourmaline-breccias within granitic bodies reflect a hydrothermal origin rather than a magmatic origin. Accordingly, it can be concluded that the studied tourmalines were crystallized from fluids expelled from a deep seated but as yet unexposed evolving magma. Alternatively, they may represent the pegmatitic rest phase of a crystallized magma chamber. The compositional differences in tourmaline groups reflect the evolution history of the magma and associated fluids.

The whole-rock geochemistry of the samples shows that major-oxide concentrations are variable, and small variations occur due to the presence of

different granitic minerals. On the basis of REE concentrations and patterns, the studied rocks can be differentiated into two groups. The first group has higher ΣREEs, is enriched in LREEs and has a flat, depleted chondrite-normalized HREE pattern (Figure 5.2.a). The second group is depleted in LREEs relative to HREEs and has lower concentrations of ΣREEs. The two groups display very different (nearly opposite) chondrite-normalized REE patterns. Group 1 more or less represents quartz-tourmaline rocks and Group 2 is characterized by more brecciated texture, high opaque-mineral content and higher hydrothermal activity. Spider diagrams for the two groups are quite similar to one another; the major difference is the trace element concentrations. Group 1 has higher trace and rare-earth element concentrations than Group 2. Consequently, it can be suggested that the two groups are cogenetic, but discrete opaque mineral phases and/or later deformation with new hydrothermal activity, modified the REE pattern of Group 2 and produced some mobility.

6.1. Formation of Tourmaline-Breccias

The Kerkenez Granitoid is believed to have solidified and crystallized before tourmaline-breccia formation. This is indicated by cataclastic deformation and the resultant angular nature of the clasts in the breccia. The source of boron and the magma is enigmatic, and more studies should be performed in order to completely understand the source of the boron rich magma and the fluid.

Different scenarios can be proposed for the formation of the tourmaline-breccias:

Model 1: The source of the boron rich fluids may have been fractionating fluid-rich rest magma of the Kerkenez Granitoid. Regional tectonic movements produced cataclastic deformation and reduced the pressure on the rest magma. Pressure release produced further melting and boron-rich fractionated rest magma mixed with the newly formed one and obtained the Fe, Mg and other elements required to crystallize tourmaline. Crystallization of tourmaline and other minerals (?) within the magma chamber increased fluid pressures and fluids explosively entered the already cataclastically deformed weak zones,

faults and fractures, and crystallized tourmaline and quartz while moving through these open spaces.

Model 2: Regional tectonic movements produced cataclastic deformation and reduced the pressure from the rest magma. A major fault reached down to the rest magma of the Kerkenez Granitoid and caused expulsion of accumulating fluids and gases from the magma into the pre-existing faults and fractures within the Kerkenez Granitoid. Fluid pressures also caused new fracturing and fracture propagations, and veins and vein networks developed.

Model 3: Regional tectonic movements produced fault zones and cataclastic deformation within Kerkenez Granitoid. A new boron-rich magma (most probably pegmatitic) intruded the already solidified and crystallized Kerkenez Granitoid. Regional tectonic movements together with extension (due to magma emplacement and fluid overpressures) produced sudden faulting and fracturing within the already cataclastically deformed Kerkenez Granitoid. Brecciation took place by faulting and fluids explosively expelled from high-pressure regime into a low pressure regime (from the magma to the faults and fractures within the host-rock granitoid). Boron-rich fluids filled the newly formed open spaces and deposited tourmaline and quartz.

Model 4: A boron-rich, highly fractionated pegmatitic magma intruded the Kerkenez Granitoid and mixed with the rest part of the Kerkenez Granitoid. Boron-rich fluids took the Fe, Mg and other elements required for tourmaline crystallization and invaded the Kerkenez Granitoid via the same mechanism proposed in model 2.

Although different scenarios are here proposed for the formation of tourmaline-breccias in the Kerkenez Granitoid, they are more-or-less similar to one another. Moreover, the fault controlled nature of the tourmaline-breccia zones indicates that fluids penetrate into the Kerkenez Granitoid by using pre-existing fault zones. The major difference is the source of the boron rich magma, faulting and deformation mechanisms. Unfortunately, at this stage it is difficult to determine the origin of the magma and, especially the source of boron. Moreover, in the literature, most of the authors hesitate to suggest a source for the boron.

Therefore, the origin of the magma and the source of the boron left unanswered this study.

The formation of tourmalines within the Kerkenez Granitoid requires infiltration of enormous volumes of boron-rich fluids. The presence of such huge volumes of fluids can be explained by the composition of the magma. High concentrations of boron in granites have important effects. These effects can be summarized as follows:

1) The interval of magmatic crystallization can be extended into lower temperatures, as low as 450°C, and the viscosity of the magma decreases. (London et al. 1989, 1994, 1996; London and Manning, 1996)

2) The solubility of the melt and H_2O increase and forestall aqueous water saturation, making continuous supercritical fluid transition from magmatic to hydrothermal regimes possible. (London et al. 1989; London and Manning, 1995).

As a result, high boron contents allow intrusion of the magma to shallower depths without significant crystallization and, because of the high volatile contents, magma can produce high fluid pressures in the host rocks (London et al. 1989, 1994, 1995). Presence of a magmatic source, cataclastic deformation, intense faulting and fracturing, in the Kerkenez Granitoid indicate that, tourmaline crystallization occurred at shallow depths within the continental crust.

Intrusion to shallow levels and fluid infiltrations into the host rock can be explained by the plutonic apex concept. Finger-like extrusions from a large underlying silicic magma chamber, cylindrical intrusions, small diameter stocks of plutonic rocks or small cupolas connected to large underlying batholiths that are emplaced to a few kilometers depth are generally known as plutonic apexes (Titley and Beane., 1981; Shinohara et al., 1995; Tosdal and Richards, 2001; Guillou-Frottier and Burov, 2003) (Figure 6.1.a). Concentration of fractures and faults around plutonic apexes allow mineral-enriched hydrothermal and magmatic fluids to circulate and exchange heat and mass with the host rock

(Guillou-Frottier and Burov, 2003). Additionally, the presence of brittle deformation can be explained by the relatively small size of the intrusion. According to Guillou-Frottier and Burov (2003), the small diameters of the plutonic apexes provide lateral cooling from the host rocks and can enable brittle deformation around and above the apex. Figure 6.1.b-c shows the deformation around the apex in different rheological contrasts. The most likely mechanism for the Kerkenez Granitoid is shown in Figure 6.1.c, in which intensive fracturing and faulting take place above and around the apex.

Field and petrographical studies show that boron-rich fluids were introduced explosively into the Kerkenez Granitoid. This type of fluid emplacement requires accumulations of fluid overpressures. Fluid overpressure can develop by a combination of two processes (Boorman et al., 2003): 1) Compaction of the crystal pile, such that any interstitial fluid supports a lithostatic load in excess of the hydrostatic pressure on the fluid, 2) Crystallization overpressure and fluid separating from an interstitial liquid which cannot escape from the crystal pile as fast as it is being generated.

When silicate minerals crystallize, fluids begin to accumulate and exert an increasing pressure on the system. If the granite body is emplaced at a depth where the confining pressure is never exceeded by the fluid pressure (or pressure is low), then the fluids will eventually be dissipated by diffusion into the surrounding rocks, giving rise to intensive alteration. If the granite body is emplaced at shallower levels, then the fluid pressure may exceed the confining pressure and the tensile strength of the rock, giving rise to fracture propagation and fluid release (Halls, 1987). In that sense, high fluid pressures may have accumulated by the upwelling and crystallization of the magma, and crystallization of anhydrous minerals may have increased the fluid content so that fluids began to exert higher pressures onto the roof (Kerkenez Granitoid). Generally a tourmaline-breccia pipe occurs in such a system (Figure 6.1.b) because fluid pressures localize at one point within the intact roof rock and fluids explosively invade the roof (Guillou-Frottier and Burov, 2003). This is thought to be the case for most of the granitoid-hosted tourmaline-breccias.

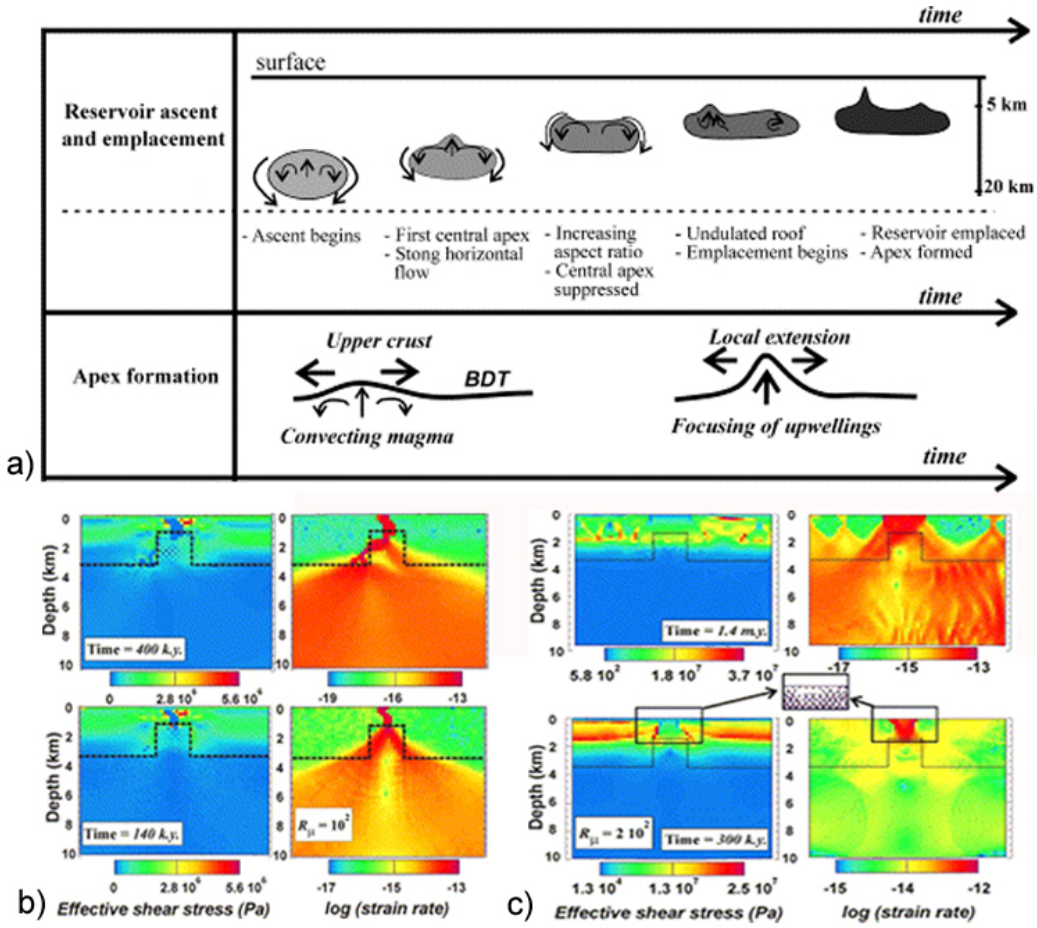

Figure 6.1: a) Scenario for successive processes promoting the genesis of plutonic apexes. b) Experiment with a single predefined apex, and with a rheological contrast of 10^2. A single fracturing event is obtained. The faulted zone connects the center of the apex summit to the surface. c) Experiment with a rheological contrast of 2×10^2. A network of potential fractures is obtained around the edges of the apex. Distal faults are obtained in the two first kilometers of the crust, more than 1.0 m.y. after the first fracturing event. Vertical and horizontal scales are identical and the dashed line shows the location of the apex margins in Figures 6b and c (after Guillou-Frottier and Burov, 2003).

But neither the geology nor the geomorphology of the study area suggest the presence of a breccia pipe like structure. In contast, the studied rocks occur as an elongated zone parallel to the regional faults. Therefore, the system may have been disturbed by another process.

This process is thought to be tectonic activity in the study area. Tectonic movements produced faults and cataclastic deformation within the Kerkenez

Granitoid. Deformation and faulting lowered the tensile strength of the granitoid and released the confining pressure on the accumulating fluids. So at one point (maybe a sudden major faulting event), the pressure equilibrium was disturbed, and the fluid overpressures surpassed the confining pressure such that the fluids explosively infiltrated into the weak zones of the Kerkenez Granitoid. According to Ridley (1993), shear zones can act like conduits for focused flow of overpressured fluids and at each seismic event, fluids move from high-to low-pressure areas and slow down in the strongly fractured low- pressure regimes.

An abundance of tourmaline veins and vein networks indicate that fluids also produced some fracturing and deformation within the host rock. A slight increase of fluid overpressures can motivate fracture formation in the isolated fracture domains. Fracture formation was followed by a drop in pressure and one domain interconnects with its nearest neighbor and fluids penetrate and flow through the newly formed parts (Helgeson, 1992). Such a scenario would have led to fracturing and fracture propagation within the solidified Kerkenez Granitoid.

Flow along negative temperature gradients from the batholith into the host rock tends to precipitate tourmaline from boron bearing fluids (Norton and Dutrow, 2001). Consequently, infiltration of boron-rich fluids into low-pressure and low-temperature areas within the brecciated Kerkenez Granitoid triggered crystallization of tourmaline within fractures, fault zones and open spaces, and tourmaline crystallized within the cataclasites of Kerkenez Granitoid.

As discussed earlier, cross cutting relationships and the compositions of the tourmalines indicate that tourmaline generation occurred in different periods. Group A and B tourmalines are chemically similar to each other, but Group C tourmalines are different and represent more fractionated boron-rich fluid activity. This situation can be explained by the reactivation of the faults. Hydrothermal fluids injected into faults and fractures can seal the faults by new mineral crystallization and produce new fluid pressure accumulations which ultimately lead to reactivation of the faults (Clark and James, 2003).

After crystallization seals the fractures, internal fluid pressures increase in the volatile reservoir with time, and again reach the point at which failure and reactivation of faults can occur. The weak zone occupied by the original vein is reopened and the fracture is able to propagate to a higher structural levels and refilling of the veins can take place (Halls, 1994). In Kerkenez Granitoid, this process appears to be has been repeated several times until internal fluid pressures finally declined or stress conditions changed. These stages of opening, sealing and reopening of veins produced different parageneses of tourmaline at different times. Sealing-opening periods and abrupt changes in the physical and chemical conditions prevented continuous fluid flow in the fractures. This is marked by the lack of either intense alteration (except tourmalinization) within the host rock or complex zonation in tourmalines. Intensive alteration is absent at the present level of exposure, but it may be present within deeper parts of the pluton. This is most probably due to the crystallized and resistant character of the Kerkenez Granitoid and sudden-rapid formation of faulting, fracturing and tourmaline crystallization.

As a result, tourmaline precipitation not only deformed and enlarged the deformation zones but also sealed them. This situation resulted in the isolation and further fractionation of the magma. New faulting and fracturing events took place by reactivation of the faults due to new fluid overpressures and/or regional tectonic movements. Mature breccias formed during these periods. Slickensides found on fault surfaces may have formed during these events, or represent younger faulting activity in the study area.

The relative temperatures of tourmaline-crystallizing fluids can be found by using mineral paragenese. The presence of albites together with tourmalines in the studied samples indicates a lower limit for the fluid temperatures of 180-200°C. The upper limit is more problematic, but equilibrium of tourmaline and epidote suggests a temperature range of 400-500°C (pers. comm., G. Topuz 2004). Figure 6.2 shows that a granitic magma can reach maximum fluid-pressure levels in the pegmatitic stage and pressures decrease gradually during the hydrothermal stage. Therefore, the proposed deformation mechanism, tourmaline mineral chemistry and high boron content (marked by high

tourmaline crystallization) suggest that intruding magma or rest magma was in a pegmatitic stage. Late hydrothermal tourmalines (light green tourmalines concentrated along fractures as radial acicular crystals) are thought to have crystallized during a hydrothermal stage with low fluid pressures and without new violent faulting and fracturing events.

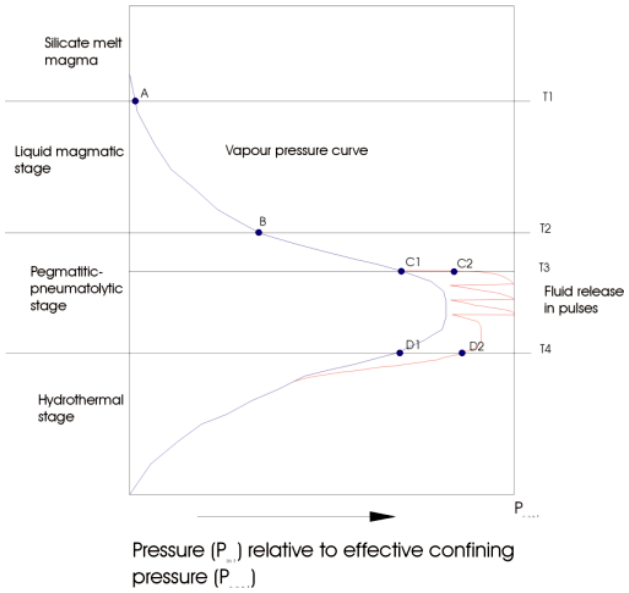

Figure 6.2: The evolution of vapour pressure relative to confining pressure and declining temperature in a crystallising volatile-rich granite. The path B-C1-D1 is that followed by a plutonic body in which the confining pressure remains greater than the evolved vapour pressure. Deuteric alteration will occur, pervasively altering the host rock, but the fluids will eventually be dissipated by diffusion. The path B-C2-D2 is that taken when the granite body is emplaced at shallower levels and the fluids are released in pulses to form pneumatolytic veins of greisen type (after Halls, 1994).

Tourmaline veins represent fractures that were filled with boron-rich fluids. Fluids not only filled the pre-existing fractures, but also caused enlargement and propagation thereof. New fractures also developed and interconnected to produce vein networks within the Kerkenez Granitoid. Tourmaline-breccias are the cataclastically deformed rocks which lie closer to faults and simply formed by penetration of boron rich fluids into fault zones and crystallization of tourmaline within the matrix. Quartz-tourmaline rocks are enigmatic, as

suggested by London and Manning (1995), but general characteristics indicate that they formed in an environment represented by a high fluid/rock ratio with high tourmalinization. High fluid activity and paucity of host-rock fragments indicate that these rocks formed in larger open spaces within the Kerkenez Granitoid.

In light of these data; from among the four proposed models, model 3 appears to be the most realistic. Further work might include fluid-inclusion and isotope studies. Fluid-inclusion studies should be performed in order to find the exact homogenization temperatures and the nature of the fluids responsible for tourmaline crystallization. Boron and oxygen isotopic studies might reveal the source and the nature, not only of the magma, but also the boron.

CHAPTER 7

CONCLUSIONS

Tourmaline-breccia formation and chronology can be summarized as follows:

1) The Kerkenez Granitoid was emplaced into the CACC during the Late Cretaceous.

2.1) A new highly evolved fluid rich magma was emplaced into the Kerkenez Granitoid. Emplacement of the magma created an extensional regime; upwelling and crystallization lead to separation of the interstitial fluid and an increase in fluid overpresure.

2.2.) Fluids accumulated in the top part of the highly fractionated rest magma of the Kerkenez Granitoid.

3) Tectonic movements produced cataclastic deformation and most probably sudden, major faulting (D1).

4) Faulting released the pressure on the fluid. Faulting and fracturing created a low-pressure regime in the host rock. Impermeable granitoid turned into a relatively permeable unit and boron-rich fluids were explosively expelled into the low-pressure regime (the faulted and fractured Kerkenez Granitoid) from a high pressure regime (magma). Infiltration of boron-rich fluids triggered fracture formation and propagation.

5) Pressure of degassing and volatiles, together with crystallization of tourmalines, enlarged the main deformation zone and opened spaces to boron-rich fluids, and these fluids caused further brecciation and fracture propagation. Fractures connected with each other, producing tourmaline veins and vein networks.

6) The boron-rich hydrothermal fluids which were injected into faults and fractures crystallized quartz and tourmaline-rich matrix. On the basis of their optical properties, tourmalines can be divided into three groups. The oldest group (Group A) consists of tourmalines with bright dark blue-blue-green pleochroism. The intermediate group (Group B) is represented by tourmalines having light blue-green-brown pleochroism and the youngest group (Group C) of tourmalines is characterized by pale green pleochroism. Group A has low Na/(Na+Ca) ratios which are less than 0.5. As a result of the Ca abundance in their X-sites, Group A tourmalines are found to be a member of calcic tourmalines and are named as feruvite. Group B tourmalines have Na/(Na+Ca) ratios between 0.53-0.86 and they are named as schorl. Operation of the same exchange vectors and chemical similarity of Group A and B tourmalines indicate that faults reactivated after a short time and then Group B tourmalines formed or these two groups of tourmalines formed contemporaneously during the first faulting event.

7) Crystallization of tourmalines and quartz sealed the fractures and fault zones; therefore new pressure equilibrium was reached.

8) Sealing of the faults and joints isolated the magma and allowed more fractionation and new fluid formation via further crystallization.

9) Further upwelling-crystallization of magma and the sealing of the faults by tourmaline crystallization allowed further build-up of fluid pressure. Regional tectonic activity and/or increasing fluid overpressures led to reactivation of the faults and produced further episodes of brecciation (D2) and led to Group C tourmaline crystallization. The distinct, more-evolved composition of Group C tourmalines suggests the isolation and fractionation of the magma. These tourmalines are characterized by their high X_{vac} and low Ca contents, they have very high Na/(Na+Ca) ratios (0.89-0.99). The gradual change in the chemical compositions of the different three tourmaline generations implies that, fluids giving way to their crystallization were generally undergoing fractionation and becoming successively enriched in Na, Al and Li, and depleted in Ca and Mg.

General chemical characteristics of tourmaline groups indicate internal evolution and differentiation of the magmatic source and the tourmalines.

10) Fluid pressures lowered after the second event (D2). Confining pressure and tensile strength of the host rock surpassed the fluid pressure and prevented any further violent fluid emplacement. Hydrothermal activity continued after formation of the tourmaline-breccias and deformation (D2) by passive, open-fissure filling. This is reflected by the presence of hydrothermal tourmalines, epidotes and cross-cutting epidote, quartz and calcite veins.

11) There is no evidence of tourmalinization in the Eocene sedimentary rocks, and the presence of tourmaline-breccia clasts within the Eocene sandstones indicate that tourmalinization and brecciation within the Kerkenez Granitoid occured between Post-Late Cretaceous and Eocene.

REFERENCES

Abraham, K., Mielke, H., Povondra, P., 1972. On the enrichment of tourmaline in metamorphic sediments of the Arzberg Series, W. Germany (NE Bavaria). *Neues Jahrb Mineral Monatsh*, **5**, 209-219.

Akıman, O., Erler, A., Göncüoglu, M.C., Güleç, N., Geven, A., Türeli, T.K., Kadıoglu, Y.K., 1993. Geochemical characteristics of the granitoids along the western margin of the Central Anatolian Crystalline Complex and their tectonic implications. *Geol. Jour*., **28**, 371-382.

Appel, P.W.U., 1985. Stratabound tourmaline in the Archaean Malene supracrustal belt, West Greenland. *Can J. Earth Sci*., **22**: 1485-1491.

Appel, P.W.U., 1995. Tourmalinites in the 3800 Ma old Isua supra-crustal belt, West Greenland. *Precambrian Res*., **72**, 227-234.

Appleby, A.M., Williams, P.J., 1988. Epigenetic tourmalinite in the aureole of the Leinster batholith, SE Ireland. *Mineral. Deposita*, **23**, 247-255.

Aydın, N., Göncüoğlu, M.C., Erler, E., 1998. Latest Cretaceous magmatism in the Central Anatolian Crystalline Complex: brief review of field, petrographic and geochemical features. *Turkish Journal of Earth Sciences*., **7**, 259-268.

Aydın, N., Önen, P., 1998. Field, Petrographic and Geochemical Features of the Baranadağ Quartz Monzonite of the Central Anatolian Granitoids, Turkey., *Turkish Journal of Earth Sciences***, 8**, 113-123.

Badham, J.P.N., 1980. Late magmatic phenomena in the Cornish Batholith-useful field guides for tin mineralisation. *Proceedings of the Ussher Society*, **5**, 44-53.

Bayhan, H., 1986. İç Anadolu granitoyid kuşağındaki Çelebi sokulumunun jeokimyası ve kökensel yorumu. *Jeol. Mühendis*., **29**, 27– 36.

Bayhan, H., 1989. Petrographical and chemical-mineralogical characteristics of Keskin pluton. *Yerbilimleri,* **15**, 29-36.

Bloodaxe, E.S., Hughes, J.M., Dyar, M.D., Grew, E.S., Guidotti, C.V., 1999. Linking structure and chemistry in the Schorl-Dravite series. *American Mineralogist*, **84 (5–6)**, 922–928.

Boorman, S.L., McGuire, J.B., Boudreau, A.E., Kruger, F.J., 2003. Fluid overpressure in layered intrusions: formation of a breccia in the Eastern Bushveld Complex, Republic of South Africa. *Mineralium Deposita*, **38**, 356–369.

Boztuğ, D., 1995. Kırsehir blogundaki Yozgat batoliti dogu kesiminin (Sorgun güneyi) petrografisi, ana element jeokimyası ve petrojenezi. *İstanbul Üniversitesi, Yerbilimleri,* **9, 1-2**, 1-20.

Boztuğ, D., 2000. S-I-A intrusive associations: geodynamic significance of synchronism between metamorphism and magmatism in Central Anatolia, Turkey, In: Bozkurt, E., Winchester, J., A., Piper, J., D., A., (eds), Tectonics and Magmatism in Turkey and the Surrounding Area. *Geological Society of London, Special Publications*, **173**, 441-458.

Burns, R.G., McDonald, D.J., Hawthorne, F., 1994. The crystal chemistry of manganese-bearing elbaite. *Canadian Mineralogist*, **32**, 31–41.

Charoy, B., 1982. Tourmalinization in Cornwall, England. In: Evans AM (ed) Metalization Associated with Acid Magmatism. Wiley, Chichester, UK, 63-70.

Clark, C., James, P., 2003. Hydrothermal brecciation due to fluid pressure fluctuations: examples from the Olary Domain, South Australia. *Tectonophysics*, **366**, 187– 206.

Deer, W.A.., Howie, R.A., Zussman, J., 1996. An introduction to the Rocks Forming Minerals (2nd ed.). Longman, London, 696 p.

Dirik, K., Göncüoğlu, M.C., 1996. Neotectonic characteristics of Central Anatolia. *International Geology Review*, **38**, 807-817.

Douville, E., Bienvenu, p., Charlou,J.L., Donval, J.P., Fouquet, Y., Appriou, P., Gamo, T., 1999. Yttrium and rare earth elements in fluids from various deep-sea hydrothermal systems. *Geochim. Cosmochim. Acta*, **63**, 627–643.

Dutrow, B., Henry, D.J., 2000. Complexly zoned fibrous tourmaline: A record of evolving magmatic and hydrothermal fluids. *Canadian Mineralogist*, **38**, 131-143.

Erkan, Y., Ataman, G., 1981. Orta Anadolu Masifi (Kırşehir yöresi) metamorphizma yaşı üzerine K-Ar yöntemi ile bir inceleme. *Yerbilimleri*, **8**, 27-30.

Erler, A., Akıman, O., Unan, C., Dalkılıç, F., Dalkılıc, B., Geven, A., Önen, P., 1991. Petrology and geochemistry of the magmatic rocks of the Kırsehir Massif at Kaman (Kırşehir) and Yozgat. *Doga, Turk. Jour. Eng. and Env. Sci.,* **15**, 76-100.

Erler, A., Bayhan, H., 1995. General evaluation and problems of the Central Anatolian granitoids. *Yerbilimleri*, **17**, 49-67.

Erler, A., Göncüoğlu, M.C., 1996. Geologic and tectonic setting of the Yozgat Batholith, Northern Central Anatolian Crystalline Complex, Turkey. *International Geology Review*, **38**, 714-726.

Ethier, V.G., Campbell, F.A., 1977. Tourmaline concentrations in Proterozoic sediments of the southern Cordillera of Canada and their economic significance. *Can. J. Earth Sci.*, **14**, 2348-2363.

Farmer, C.B., Halls, C., 1993. Paragenetic evolution of cassiterite-bearing lodes at South Crofty Mine, Cornwall, UK. In: Maurice, Y.T. Ed., Proceedings of the Eighth Quadrennial IOAGOD Symposium, 1990. E. Schweizerbartische Verlagsbuchhandlung, Stuttgart, 365–381.

Floyd, P.A., Göncüoğlu, M.C., Winchester, J.A., Yalınız, M.K., 2000. Geochemical character and tectonic environment of Neotethyan ophiolitic fragments and metabasites in the Central Anatolian Crystalline Complex, Turkey. In: Bozkurt, E., Winchester, J., A., Piper, J., D., A., (eds), Tectonics and Magmatism in Turkey and the Surrounding Area. *Geological Society of London, Special Publications*, **173**, 183-202.

Floyd, P.A., Yalınız, M.K., Göncüoğlu, M.C., 1998. Geochemistry and petrogenesis of intrusive and extrusive ophiolitic plagiogranites, Central Anatolian Crystalline Complex, Turkey. *Lithos*, **42**, 225-242.

Frimmel, H.E., Jiang, S.Y., 2001. Marine evaporites from an oceanic island in the Neoproterozoic Adamastor ocean. *Precambrian Research* **105**, 57–71.

Fuchs, Y., Lagache, M., 1994. La transformation chlorite-tourmaline en milieu hydrothermal, exemples naturels et approche experimentale. *CR Acad. Sci. Paris*, **319**, 907–913.

Gallagher, V., 1988. Coupled substitutions in schorl-dravite tourmaline: New evidence from SE Ireland. *Mineralogical Magazine*, **52**, 637-650.

Gençalioğlu-Kusçu, G., Floyd, P.A., 2001. Mineral compositional and textural evidence for magma mingling in the Saraykent volcanics. *Lithos*, **56**, 207–230.

Gençalioğlu-Kusçu, G., Floyd, P.A., 2002. Geochemical correlations between effusive and explosive silicic volcanics in the Saraykent region (Yozgat), Central Anatolia, Turkey. *Geological Journal.*, **37**, 143–165.

Göncüoğlu, M.C., 1977. Geologie des Westlichen Niğde Massivs: University of Bonn, Ph.D. Thesis (unpublished).

Göncüoğlu, M.C., 1981. Niğde Masifinde viridin-gnaysın kökeni. *Geological Society of Turkey Bulletin*, **24**, 45-51.

Göncüoğlu, M.C., 1982. Niğde Masifi paragnayslarında zirkon U/Pb yaşları. *Geological Society of Turkey Bulletin*, **25**, 61-66.

Göncüoğlu, M.C., 1985. Niğde masifi batı yarısının jeolojisi. *MTA Rapor*, No: **7856**, 156 p.

Göncüoğlu, M.C., 1986. Geochronologic data from the southern part (Niğde area) of the Central Anatolian Massif. *MTA Dergisi*, **105/106**, 83-96.

Göncüoğlu, M.C., and Türeli, T.K., 1994. Alpine Collisional-Type Granitoids from western Central Anatolian Crystaline Complex, Turkey. *Journal of Kocaeli University*, **1**, 39-46.

Göncüoğlu, M.C., Dirik, K., Erler, A., Yalınız, M.K., 1994. Orta Anadolu Masifinin Doğu Bölümünün Jeolojisi Bölüm 4, Orta Anadolu Masifinin Sivas Baseni ile ilişkisi. *TPAO Rep*., No. **3535**, 135 p, (unpublished).

Göncüoğlu, M.C., Dirik, K., Kozlu, H., 1996-1997. General characteristics of pre-Alpine and Alpine Terranes in Turkey: Explanatory notes to the terrane map of Turkey: Annales Geologique de Pays Hellenique, **37**, *Geol.Soc Greece*, 515-536.

Göncüoğlu, M.C., Erler, A., Toprak, G.M.V., Olgun, E., Yalınız, M.K., Kusçu, İ., Köksal, S., Dirik, K., 1993. Orta Anadolu Masifi'nin orta bölümünün jeolojisi, Bölüm 3, Orta Kızılırmak Tersiyer baseninin jeolojik evrimi. *TPAO Rep.*, No. **3313**, 104 p, (unpublished).

Göncüoğlu, M.C., Erler, A., Toprak, V., Yalınız, M.K., Olgun, E., Rojay, B. 1992. Orta Anadolu Masifi'nin batı bolumunun jeolojisi, Bolum 2: Orta Kesim. *TPAO Rep.*, No: **3155**, 76 p, (unpublished).

Göncüoğlu, M.C., Toprak, V., Kuşcu, İ., Erler, A., Olgun, E., 1991. Orta Anadolu Masifi'nin batı bölümünün jeolojisi, Bölüm 1, Güney Kesim. *TPAO Rep*., No. **2909**, 140 p, (unpublished).

Göncüoğlu, M.C., Turhan, N., Şentürk, K., Özcan, A., Uysal, S., Yalınız, M.K., 2000. A geotraverse across northwestern Turkey: tectonic units of the Sakarya region and their tectonic evolution. In: Bozkurt, E., Winchester, J., A., Piper, J., D., A., (eds), Tectonics and Magmatism in Turkey and the Surrounding Area. *Geological Society of London, Special Publications*, **173**, 139-161.

Göncüoğlu, M.C., Türeli, T.K., 1993. Petrology and geodynamic interpretation of plagiogranites from Central Anatolian ophiolites. *Turkish Journal of Earth Sciences.*, **2**, 195-203.

Grice, J.D., Robinson G.W., 1989. Feruvite, a new member of the tourmaline group, and its crystal structure. *Canadian Mineralogist,* **27**, 199-203.

Guillou-Frottier, L., Burov, A., 2003. The development and fracturing of plutonic apexes:implications for porphyry ore deposits. *Earth and Planetary Science Letters*, **214**, 341-356.

Güleç, N., 1994. Rb-Sr Isotope data from the Ağaçören Granitoid (East of Tuz Gölü): Geochronological and genetical implications. *Turkish Journal of Earth Sciences.*, **3**, 39-43.

Halls, C., 1987. A mechanistic approach to the paragenetic interpretation of mineral lodes in Cornwall. *Proceedings of the Ussher Society*, **6**, 548-554.

Halls, C., 1994. Energy and mechanism in the magmato-hydrothermal evolution of the Cornubian Batholith - a review. In: Seltmann, R., Kampf, H., Moller, P. (eds) Metallogeny of collisional orogens, *Czech Geological Survey*, Prague, 274-294.

Hawthorne, F.C., 1996. Structural mechanisms for light element variations in tourmaline. *Canadian Mineralogist*, **34 (1)**, 123–132.

Hawthorne, F.C., McDonald, D.J., Burns, P.C., 1993. Reassignment of cation site occupancies in tourmaline: Al-Mg disorder in the crystal structure of dravite. *American Mineralogist*, **78**, 265-270.

Hawthorne, F.J. and Henry, D.J. (1999) Classification of the minerals of the tourmaline group. *European Journal of Mineralogy*, **11**, 201-216.

Helgeson H.C., 1992. Effects of complex formation in flowing fluids on the hydrothermal solubilities of minerals as a function of fluid pressure and temperature in the critical and supercritical regions of the system-H_2O. *Geochim. Cosmochim. Acta,* **56,** 3191–3207.

Henry, D.J., Dutrow, B.L., 1996. Metamorphic tourmaline and its petrologic applications. In: Grew, E.S., Anovitz, L.M., (Eds.), Boron: Mineralogy, Petrology, and Geochemistry, *Reviews in Mineralogy*, **33**, 503–557.

Henry, D.J., Guidotti, C.V., 1985. Tourmaline as a petrogenetic indicator mineral: an example from the staurolite- grade metapelites of NW Maine. A*merican Mineralogist*, **70**, 1-15.

İlbeyli, N., Pearce, J.A., Thirlwall, M.F., Mitchell, J.G., 2004. Petrogenesis of collision-related plutonics in Central Anatolia, Turkey. *Lithos,* **72**, 163-182.

Jiang, S.Y., Palmer, M.R., Christopher, J.Y., 2002. Chemical and boron isotopic compositions of tourmaline from the Archean Big Bell and Mount Gibson gold

deposits, Murchison Province, Yilgarn Craton, Western Australia. *Chemical Geology,* **188**, 229– 247.

Kadıoğlu, Y.K., Güleç, N., 1996. Mafic microgranular enclaves and interaction between felsic and mafic magmas in the Ağaçören Intrusive Suite: Evidence from petrographic features and mineral chemistry. *International Geology. Review*, **38**, 854-867.

Kadıoğlu, Y.K., Güleç, N., 1999. Types and genesis of the enclaves in Central Anatolian Granitoids. *Geological Journal*, **34**, 243-256.

Karayigit, A.I., Eris, E., Cicioglu, E., 1996. Coal geology, chemical and petrographical characteristics and implications for coalbed methane development of subbituminous coals from the Sorgun and Suluova basins, Turkey. In: Gayer, R.A., Harris, I., (Eds.), Coalbed Methane and Coal Geology. *Geol. Soc. Spec. Publ.*, **109**, 325–338.

Karayigit, A.I., Gayer, R.A., Cicioglu, E., Eris, E., 1997. Mineralogy and petrography of the two lower Eocene lacustrine coals, Sorgun and Suluova, *Turkey. Int. J. Coal Geol*., **34**, 115–130.

Keller, P., Roda, E., Pesquera, A., Fontan, F., 1999. Chemistry, paragenesis and significance of tourmaline in pegmatites of the Southern Tin Belt, central Namibia. *Chemical Geology.*, **158**, 203–225.

Ketin, İ., 1963. 1/500.000 Scale Geological Map of Turkey, Kayseri Sheet. Mineral Research and Exploration Institute of Turkey.

Ketin, İ., 1966. Tectonic units of Anatolia (Asia Minor). *Mineral Research and Exploration Institute of Turkey Bulletin*, **66**, 23–34.

Klinkhammer, G., German, C.R., Elderfield, H., Greaves, M.H., Mitra, A., 1994. Rare earth elements in hydrothermal fluids and plume particulates by inductively coupled plasma mass spectrometry. *Mar. Chem.*, **45**, 179–186.

Laznicka, P., 1988. Breccias and coarse fragmentites. Petrology, Environments, Associations, Ores. Elsevier, 832 p.

London, D., Manning, D.A.C., 1995. Chemical variation and significance of tourmaline from Southwest England. *Economic Geology,* **90**, 495–519.

London, D., Morgan, G.B, Hervig, R.L., 1989. Vapor-undersaturated experiments in the system macusanite-H2O at 200 MPa, and the internal differentiation of granitic pegmatites. *Canadian Mineralogist.*, **28**, 771-786.

London, D., Morgan, G.B., Wolf, D., 1996. Boron in granitic rocks and their contact aureoles. In: Grew, E.S., Anovitz, L.M., (Eds) Boron. Mineralogy, petrology and geochemistry. The *Mineralogical Society of America, Washington, DC, Rev. Mineral.* **33**, 299–330.

London, D., Wolf, M.B., Morgan, G.B., 1994. Boron saturation in granitic magmas: tourmaline-biotite-cordierite equilibria. *Geol. Soc. Am. Prog. Abstr.*, **26,** A516.

Lorilleux, G., Jebrak, M., Cuney, M., Baudemont, D., 2002. Polyphase hydrothermal breccias associated with unconformity-related uranium mineralisation (Canada): from fractal analysis to structural significance. *J. Structural Geology.,* **24**, 323– 338.

Lottermoser, B.G., 1989. REE behavior associated with strata-bound scheelite mineralization (Broken Hill, Australia). *Chemical Geology.* **78**, 119–134.

Lünel, A.T., 1985. An approach to the naming, origin and age of Baranadag monzonite of Kırsehir intrusive Suite. *METU J. Pure and Appl., Sci.*, **18**, 385-404.

Lünel, A.T., Akıman, O., 1984. Pseudoleucite from Hamitköy area, Kaman, Kırşehir occurrence and its use as a pressure indicator. *Mineral Research & Exploration Unit*, **103-04**, 29-35.

Lynch, G., Ortega, J., 1997. Hydrothermal alteration and tourmaline-albite equilibria at the Coxheat porphyry Cu–Mo–Au deposit, Nova Scotia. *Canadian Mineralogist*, **35 (1)**, 79–94.

Manning, D.A.C., 1982. Chemical and morphological variation in tourmalines from the Hub Kapong batholith of peninsular Thailand. *Mineralogical Magazine,* **45**, 139–147.

McLennan, S.M., 1989. Rare earth elements in sedimentary rocks: influence of provenance and sedimentary processes. In: Lipin, B.R., McKay, G.A., (Eds). *Geochemistry and Mineralogy of Rare Earth Elements, The Mineralogical Society of America, Washington, DC, Rev. Mineral.* **vol. 21**, 169–200.

Michard, A., 1989. Rare earth element systematics in hydrothermal fluids. *Geochim. Cosmochim. Acta*, **54,** 745–750.

Mittwede, S. K., Helvaci, C., Karamaderesi, I. H., Kun, N. and Candan, O., 1992. Modes and implications of tourmaline occurrence in the Menderes Massif, Western Anatolia, Turkiye. *Geosound*, **20**, 179-190.

Norton, D.l., Dutrow, B.L., 2001. Complex behavior of magma–hydrothermal processes: Role of supercritical fluid Complex behavior of magma–hydrothermal processes: Role of supercritical fluid. *Geochimica et Cosmochimica Acta,* **65-21**, 4009–4017.

Peng, Q.M., Palmer, M.R., 1995. The Palaeoproterozoic boron deposits in eastern Lianing, China: a metamorphosed evaporite. *Precambrian Res*., **72**, 185–197.

Pesquera, A., Velasco, F., 1997. Mineralogy, geochemistry and geological significance of tourmaline-rich rocks from the Paleozoic Cinco Villas Massif (western Pyrenees, Spain). *Contrib. Mineral Petrol.,* **129**, 53–74

Plimer, I.R., 1986. Tourmalinites from the Golden Dike dome, northern *Australia. Mineral. Deposita*, **21**, 225–239.

Pouchou, J.L., Pichoir, F., 1984. A new model for quantitative analyses: I. Application to the analysis of homogeneous samples. *La Recherche Aérospatiale,* **3**, 13–38.

Pouchou, J.L., Pichoir, F., 1985. "PAP" (ϕ–ρ–Z) correction procedure for improved quantitative microanalysis. In: Armstrong, J.T., (Ed), 1985. *Microbeam Anal.*, 104–106.

Raith, J.G., Riemer, N., Meisel, S.T., 2004. Boron metasomatism and behaviour of rare earth elements during formation of tourmaline rocks in the eastern Arunta Inlier, central Australia. *Contrib. Mineral. Petrol.,* **147**, 91–109.

Ridley, J.,1993. The relations between mean rock stress and fluid flow in the crust: with reference to vein- and lode-style gold deposits. *Ore Geology Reviews,* **8**, 23–37.

Roda-Robles, E., Pesquera, A., Gil, P.P, Torres-Ruiz, J.,Fontan, F., 2004. Tourmaline from the rare-element Pinilla pegmatite, (Central Iberian Zone, Zamora, Spain): chemical variation and implications for pegmatitic evolution. *Mineralogy and Petrology*, **81**, 249–263

Rosenberg, P., Foit, F., Ekambaran, V., 1986. Synthesis and characterization of tourmaline in the system Na_2O–MgO–Al_2O_3–SiO_2–B_2O_3–H_2O. *American Mineralogist,* **71**, 971–976.

Ruiz, J.T., Pesquera, A., Gil-Crespo, P., Velilla, N., 2003. Origin and petrogenetic implications of tourmaline-rich rocks in the Sierra Nevada (Betic Cordillera, southeastern Spain). *Chemical Geology*, **197**, 55– 86.

Şengör, A.M.C., Yılmaz, Y., 1981. Tethyan evolution of Turkey: A plate tectonic approach. *Tectonophysics*, **75**, 181-241.

Seymen, Ü., 1981. Kaman (Kırşehir) dolayında Kırşehir Masifinin stratigrafisi ve metamorfizması. *Geological Society of Turkey Bulletin*, **24**, 101-108.

Shinohara, H., Kazahaya, K., Lowenstern, J.B., 1995. Volatile transport in a convecting magma column: implications for porphyry Mo mineralization, *Geology*, **23**, 1091-1094.

Sillitoe, R.H. and Sawkins, F.J., 1971. Geologic, mineralogic and fluid inclusion studies relating to the origin of the copper-bearing tourmaline-breccia pipes, Chile. *Economic Geology.* **66**, 1028–1041.

Skewes, M.A., Holmgren, C., Stern, C.R., 2003. The Donoso copper-rich, tourmaline-bearing breccia pipe in central Chile: petrologic, fluid inclusion and stable isotope evidence for an origin from magmatic fluids. *Mineralium Deposita*, **38**, 2–21.

Slack, J.F., 1993. Models for tourmalinite formation in the Middle Proterozoic Belt and Purcell supergroups (Rocky Mountains) and their exploration significance. *Current Res., Canada Geol. Survey,* **93-1E**, 33–40.

Slack, J.F., 1996. Tourmaline associations with hydrothermal ore deposits. In: Grew, E.S., Anovitz, L.N., (Eds.), Boron: Mineralogy, Petrology and Geochemistry. *Rev. Mineral*., **33**, 559–643.

Slack, J.F., Coad, P.R., 1989. Multiple hydrothermal and metamorphic events in the Kidd Creek volcanogenic massive sulfide deposit, Timmins, Ontario: Evidence from tourmalines and chlorites. *Can. J. Earth Sci., **26**, 694-7*15.

Slack, J.F., Herriman, N., Barnes, R.G., Plimer, I.R., 1984. Stratiform tourmalinites in metamorphic terranes and their geologic significance. *Geology*, **12**, 713-716.

Smith, M.P., Yardley, B.W.D., 1996. The boron isotopic composition of tourmaline as a guide to fluid processes in the southwestern England orefield: an ion microprobe study. *Geochim. Cosmochim. Acta*, **60**, 1415–1427.

Steven, N.M., Moore, J.M., 1995. Tourmalinite mineralization in the Late Proterozoic Kuiseb Formation of the Damara Orogen, central Namibia: evidence for a replacement origin. *Economic Geology.,* **90**, 1017–1098.

Streckeisen, A.L. and LeMaitre, R.W., 1979. A chemical approximation to the modal QAPF classification of the igneous rocks, *N. Jb. Min. Abh*., **136**, 169-206.

Tatar, S., Boztuğ, D., 1998. Fractional crystallization and magma mingling/mixing processes in the monzonitic association in the SW Part of the Composite Yozgat Batholith (Sefaatli–Yerköy, SW Yozgat). *Turkish Journal of Earth Sciences*, **7**, 215–230.

Taylor, B.E., Slack, J.F., 1984. Tourmalines from Appalachian-Caledonian massive sulfide deposits: textural, chemical and isotopic relationships. *Economic Geology*, **79**, 1703-1726.

Titley, S.R., Beane, R.E., 1981. Porphyry copper deposits, *Econ. Geol.*, 75th anniversary vol., 214–235.

Toksoy, F., 1998. Petrography and mineralogy of the vermiculitized phlogopitic metagabbro from the Kurançalı Area (Kırşehir-Central Anatolia). M.Sc Thesis, Middle East Tech. University., Ankara, 175p, (unpublished).

Torres-Ruiz, J., Pesquera, A., Gil-Crespo, P.P., and Casas, J. (1996) Tourmalinites and Sn-Li mineralization in the Valdeflores area (Caiceres, Spain). *Mineralogy and Petrology*, **56**, 209-223.

Tosdal, R.M., Richards, J.P., 2001. Magmatic and structural controls on the development of porphyry Cu-Mo-Au deposits, in: J.P. Richards, R.M. Tosdal (Eds.), Structural Controls on Ore Genesis, Society of Economic Geologists, *Rev. Econ. Geol*., **2001**, 14, 157-181.

Trumbull, R., B., Chaussidonr, M., 1999. Chemical and boron isotopic composition of magmatic and hydrothermal tourmalines from the Sinceni granite–pegmatite system in Swaziland . *Chemical Geology*, **153**, 125–137.

Warnaars, F.W., Holmgren C., Barassi, S., 1984. Porphyry copper and tourmaline-breccias at Los Bronces–Rio Blanco, Chile. *Economic Geology*, **80,** 1544–1565.

Whitney, D.L., Dilek, Y., 2001. Metamorphic and Tectonic Evolution of the Hırkadağ Block, Central Anatolian Crystalline Complex. *Turkish Journal of Earth Sciences.*, **10**, 1-15.

Williamson, B.J., Spratt, J., Adams, J.T., Stanley, C.J. (2000) Geochemical constraints from zoned hydrothermal tourmalines on fluid evolution and Sn mineralization: an example from Fault Breccias at Roche, SW England. *Journal of Petrology*, **41**, 1439-1453.

Yalınız, K., Göncüoğlu, M.C., 1999. Clinopyroxene Compositions of the Isotropic Gabbros From the Sarıkaraman Ophiolite: New Evidence on Supra-Subduction Zone Type Magma Genesis in Central Anatolia. *Turkish Journal of Earth Sciences*, **8**, 103-111.

Yalınız, K., Parlak, O., Özkan-Altıner, S., Göncüoğlu M.C., 1997. Formation and emplacement ages of supra-subduction-type ophiolites in Central Anatolia; Sarıkaraman Ophiolite, Central Turkey. *Çukurova Universitesinde Jeoloji Mühendisliği Eğitiminin 20.Yıl Simpozyumu, Adana, 30 April-3 May 1997, Abstracts*, 61-62.

Yalınız, M.K., Göncüoğlu, M.C., 1998. General geological characteristics and the distribution of the Central Anatolian Ophiolites. *H. Ü. Yerbilimleri Dergisi,* **20**, 19-30.

Yardımcılar, C., 1995. Petrography and geochemistry of the Kerkenez granitoid, (Sorgun-Yozgat), Grad. Thesis, Middle East Tech. University., Ankara, 54 p, (unpublished).

Yavuz, F., Gultekin, A.H., Karakaya, M.C., 2002. CLASTOUR: a computer program for classification of the minerals of the tourmaline groups. *Computers & Geosciences*, **28**, 1017–1036.